Preparation and characterisation of fragrance oil microcapsules: how does shell thickness influence mechanical strength

Author: Ling He

Supervisor: Dr. Olivier Cayre

Submitted in accordance with the requirements for the degree of Master of Philosophy

School of Chemical and Process Engineering

The University of Leeds

September 2022

Intellectual Property and Publication Statements

The candidate confirms that the work submitted is her own, except where work which has formed part of jointly authored publications has been included. The contribution of the candidate and the other authors to this work has been explicitly indicated below. The candidate confirms that appropriate credit has been given within the thesis where reference has been made to the work of others.

Chapter 4.3 Core material selection via microcapsule morphology prediction is based on work from jointly authored publications. The title of the publication is *The effect of surfactant chain length on the morphology of poly(methylmethacrylate) microcapsules for fragrance oil encapsulation*, published on Journal of Colloid and Interface Science 484 (2016). The authors are Alison Louise Tasker, James Paul Hitchcock, Ling He, Elaine Alice Baxter, Simon Biggs, Olivier Jean Cayre.

In the publications, section 3.2 *Encapsulating fragrance oils using C16TAB stabilised microcapsules* is directly attributable to you; and the rest part including comparing capsule morphology predictions with PMMA-hexadecane microcapsules for different stabilizers are contributed by the other authors of work.

Acknowledgements

I would like to express my deepest gratitude to my supervisor Dr Olivier Cayre, who provided continuous guidance, support, advice and encouragement throughout the whole period of the research. Gratitude also extends to my industrial supervisor Elaine Baxter from P&G, who has been approachable and enthusiastic at the outset, and Professor Simon Biggs, who was the supervisor in my first year and provided his valuable support and guidance for starting the research.

I would also like to thank my colleagues in the same research group, especially those who worked on the same P&G-funded project, namely James Hitchcock, Alison Tasker, and Kirsty Stark. This research has been carried out as a part of teamwork. I benefit a lot from their knowledge and ideas.

I would like to acknowledge Professor Zhibing Zhang and his team at the University of Birmingham. A big part of this research was conducted in his lab using the micromanipulator. His knowledge and guidance helped me a lot, as well as the kindly support from his team.

Not to mention the many other people who helped me to carry out all the characterisation techniques. Their help helped me greatly in conducting the research.

I'd also like to use this opportunity to acknowledge the funding from EPSRC; without this, the study won't be possible.

Finally, I'd like to thank my son Ryan, who is part of my motivation to complete this work. He accompanied and supported me in the past years, and I hope he will be proud of me by completing this work.

Abstract

This study aims to achieve long-term retention of the volatile, small molecular fragrance oil molecules by focusing on the preparation of silver shell fragrance oil core microcapsules. A three-step method of preparing such microcapsules was developed in this study. Firstly the polymer shell oil core microcapsules were prepared. Then the negatively charged Au NPs were adsorbed on the polymer capsule surface via electrostatic attraction as the catalyst. Finally, the silver shell was grown on the polymer capsule surface via the electroless plating method.

The morphologies of the microcapsules and Au NPs were observed using Scanning Electron Microscopy (SEM) and Transmission Electron Microscopy (TEM), respectively. The retention/release of the oil core was analysed using Gas Chromatography (GC). The factors which influenced the morphology of the polymer capsules and the polymer shell thickness, including interfacial tensions between oil, polymer and aqueous phases and core/shell ratio, were discussed. The adsorption density of Au NPs on the polymer capsule surface was studied by looking into the surfactant concentration and Au NPs concentration. Variables that affected the silver shell thickness, such as Au NPs adsorption density and the silver salt concentration, were also investigated.

The mechanical strength of the microcapsules was analysed using the micromanipulation technique. The relationship between the shell thickness and the capsules' mechanical strength was explored.

Table of Contents

Lists of tables

List of illustrations

Abbreviations

AFM	Atomic Force Microscopy
APTMS	(3-aminopropyl)trimethoxysilane
A/V	Surface-to-volume
BSE	Back scattered electrons
CMC	Critical micelle concentration
CTAB	Cetyl trimethylammonium bromide
DCM	Dichloromethane
DLS	Dynamic Light Scattering
DMAB	Dimethylamine borane
EDS	Energy Dispersive X-ray Spectroscopy
EDX	Energy Dispersive X-ray
ELP	Electroless plating
FEGSEM	Field emission gun scanning electron microscopy
FEGTEM	Field Emission Gun Transmission Electron Microscopy
FIBSEM	Focused Ion Beam Scanning Electron Microscopy
GC	Gas Chromatography
HCHO	Formaldehyde
HS	Hexylsalicylate

L-b-L	Layer by layer
MPPMS	3-mercaptopropyltriethoxysilane
NPs	Nanoparticles
O/W	oil in water
PAH	Poly(allylamine hydrochloride)
PCL	Polycaprolactone
PDMS	Polydimethylsiloxan
PEMA	Poly(ethyl methacrylate)
PET	Poly(ethylene terephthalate)
PIBMA	Poly(isobutyl methacrylate)
PLGA	Poly(DL-lactide-co-glycolide)
PMMA	Poly(methyl methacrylate)
PS	Polystyrene
PTHF	Poly(tetrahydrofuran)
PU	Polyurethane
PVP	Poly(vinylpyrrolidinone)
SC	Stearyl trimethyl ammomium chloride
SE	Secondary electrons
SEM	Scanning Electron Microscopy
SPR	surface plasmon resonance

TEM	Transmission Electron Microscopy
Tg	Glass transition temperature
TGA	Thermogravimetric analysis
XRD	X-ray Diffraction
UV-Vis	Ultraviolet–visible
ZP	Zeta potential

Chpater 1 Introduction

1.1 Overview and motivation

Fragrance oil has been used in lots of applications, especially perfume. The challenge is the rapid release of low vapour pressure fragrance oil particles in a liquid environment that dissolves fragrance oil.

Microencapsulation is a technique that enables the protection of active materials by enveloping them inside one or more layers of coating. The coated particles, thus formed, usually fall into the micron size range and are therefore termed microcapsules (Dubey et al., 2009, Ghosh, 2006, Green, 1957). This technique provides protection to unstable or sensitive active ingredients from their external environment, preventing unwanted reactions, such as oxidation, from taking place (Champagne and Fustier, 2007, Desai and Park, 2005); separates incompatible components within a formulation, or masking odour and/or taste (Bhandari et al., 1999, Jain et al., 1997); and improves the handling process, for example, a safe handling process of some toxic ingredients in pesticide formulations (Tsuji, 2001, Scher et al., 1998). The enveloped active material can be liquid, solid or gaseous, and it can be released under certain conditions through various triggers, such as pH, ionic strength, rupture force, or temperature (Pena et al., 2012, Yow and Routh, 2006, Gouin, 2004). The release rate can be controlled via the careful design of the capsule shell tailored to a preferred mechanism of release.

Since the first industrial usage of microcapsules in carbonless copy paper by Green and Lowell (1957), microencapsulation has stimulated great interest in diverse applications such as pharmaceutical formulations (Wischke and

Schwendeman, 2008, Lam et al., 2001), pesticides (Dowler et al., 1999, Scher et al., 1998), cosmetics (Im et al., 2005, Lapidot et al., 2003), fragrances (Specos et al., 2010, Rodrigues et al., 2009), and dyes (Monllor et al., 2007, Sukhorukov et al., 2000). Although the technique is widely used in various applications, the encapsulation of small molecules and volatile active liquids without leakage before application still remains a challenge due to the relatively poor barrier properties of polymer membranes (Patchan et al., 2012, Madene et al., 2006, Evans, 1970).

Active components with small molecules, such as toluene and fragrance oil, permeate most of the polymeric shells through the pores pre-existing. The large free volume within the polymer also provides a low resistance pathway to the rapid diffusion of small molecules (Patchan et al., 2012, Madene et al., 2006, Brannonpeppas, 1993, Evans, 1970). Compared to the polymer membrane, the metal membrane provides a higher resistance to the rapid diffusion of gas molecules and small organic molecules because of its closed-packed structure, which results in a longer diffusion path for gases or small molecules. The diffusion of gas or small molecules can also occur through various defects. Therefore, coating a continuous layer of metal-membrane on the polymer shell of microcapsules provides vastly improved barrier properties to avoid the evaporation of volatile core content and hence they have a longer shelf life than the polymer-based microcapsules (Patchan et al., 2012, Wang et al., 2005, Prins and Hermans, 1959). Silver, as an inorganic compound, provides a better barrier to small molecules than polymers. Meanwhile, it has been widely used in food, medicine/clinic, cosmetic and personal care products due to its safety to use within the human body and its powerful antimicrobial properties(Pandey et al.,

2020, Hancu et al., 2013, Padmavathy and Vijayaraghavan, 2008, Delaney et al.,

2008). Silver was selected as the metal coating of the polymer shell fragrance oil

core microcapsules in this study.

Diffusion of the core content from the microcapsules also relates to the capsules'

surface area and shell thickness. Fick's law of diffusion can be used to describe

the change in concentration in the continuous phase over a specified time. Fick's

first law states that flux is directly proportional to the concentration gradient. The

rate of flow of the core content through an area (d_q/d_t per surface area) is the flux,

and the proportionality constant D is the diffusion coefficient, which unit is area

per time. Assuming the diffusion coefficient is independent of temperature and

pressure, the change of the core content through the shell surface area over a

specified time is described in equation 1.1-1 (Anthony and Berland, 2013,

Enderle, 2012, Ferrando, 2006).

$$\frac{d_q}{d_t} = -DA\frac{d_c}{d_x} \qquad \text{Equation 1.1-1}$$

where

q = quantity of core content molecules
t = time
A = shell surface area
c = concentration
D = diffusion coefficient
d_x = shell thickness
$\frac{d_c}{d_x}$ = concentration gradient

From equation 1.1-1, it can be seen that the release of the core content can be

predicted and controlled through a series of parameters involved in the fabrication

process, such as the surface area and shell thickness of the capsules, the concentration of core and different types of shell materials. The larger surface area of microcapsules can be achieved by reducing their particle size as a result of increasing the diffusion rate of core content. Increasing the shell thickness also reduces the release.

The core content in microcapsules can be released through various mechanisms according to different purposes in an application. In the rupture release mechanism, the active ingredient was released from capsules by external mechanical forces. The force needed to break the capsules depends on the mechanical properties of the shell, such as microcapsule diameter, deformation characteristics at compression, rupture stress, *etc.*

1.2   Aims and objectives

In perfume application, the challenge remains to efficiently encapsulate low vapour pressure fragrant oil with no release in a continuous phase that dissolves the oil. A continuous layer of metallic coating on the polymer shell of the microcapsule is expected to improve the resistance of the shell to the leakage of core content, the fragrance oil. Gold shell hexylsalicylate (HS) core microcapsules have been successfully prepared in our research group, and full retention of the core content over 30 days has been demonstrated via the Gas Chromatography (GC) technique.

This study aims to achieve long-term retention of the volatile, small molecular fragrance oil particles by focusing on the preparation of silver shell hexyl salicylate core microcapsules using Au NPs as the catalyst. The retention/release of the oil core was analysed using GC.

The factors which influenced microcapsule formation and the shell thickness were studied, and the relationship between the shell thickness and the capsule mechanical strength was also investigated. The research results will estimate the delayed release of the core content via shell breakage under mechanical force.

1.3 Outline and the structure of the thesis

A three-step method of preparing silver shell fragrance oil core microcapsules was developed in this study. The process of the method is shown in Figure 1.3-1 and Figure 1.3-2.
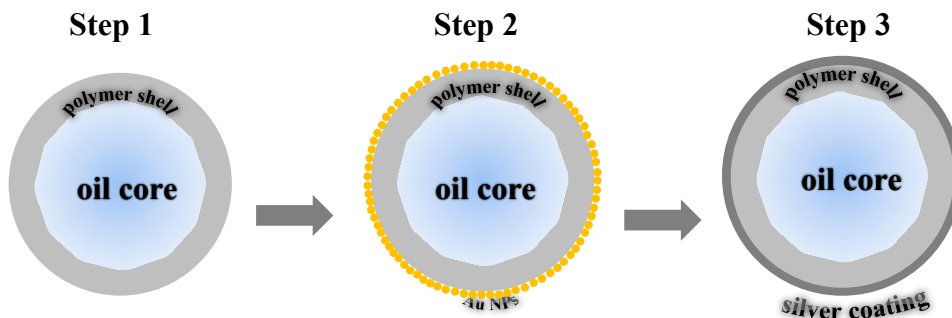
Figure 1.3-1 Schematics of a three-step method for preparing a silver shell oil core microcapsule: step 1: polymer shell oil core microcapsule formation; step 2: Au NPs adsorption on polymer capsule surface as a catalyst; step 3: silver shell microcapsule formation via electroless plating
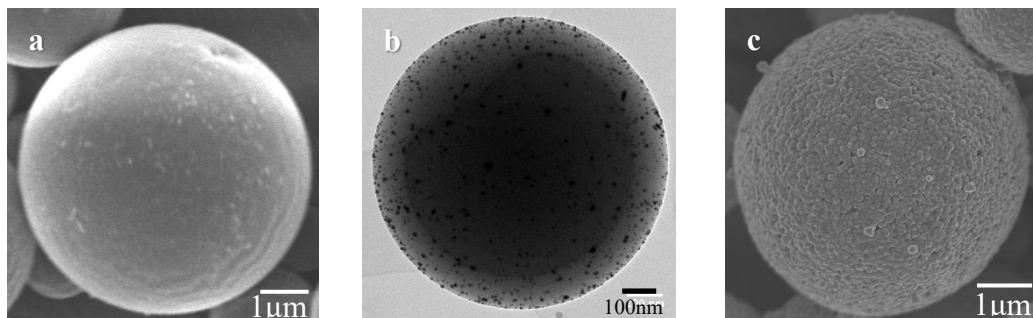
Figure 1.3-2 Electron microscopy micrographs of capsules in different stages. a: PEMA shell microcapsule observed via SEM; b: Au NPs adsorbed PEMA microcapsules observed via TEM (a smaller size capsule was present in b to give a full overview of Au NPs adsorbed capsule. 1µm capsule is too big to be pictured as one under TEM); c: silver shell microcapsules observed via SEM

In Chapters 1-3, an introduction, background literature review, and research methodologies were presented, respectively. Chapters 4 - 6 focused on the three-step method of preparing silver shell fragrance oil core microcapsules and corresponding systematic studies on the variables of the research.

In Chapter 4, the detailed preparation method of the polymer shell and oil core microcapsules was discussed. A model capsule of PEMA shell toluene core was firstly prepared. Then the PMMA shell fragrance oil core (hexylsalicylate, cyclamen aldehyde, dihydromyrcenol, respectively) microcapsule was prepared for the morphology study. The influence of the interfacial tensions between oil, polymer and aqueous phases on the microcapsule morphology was investigated. The influence of core/shell ratio on the oil core retention and polymer shell thickness was also discussed.

In Chapter 5, a method of preparation of electrostatic stabilised Au NPs in aqueous suspension and the process of Au NPs adsorption on polymer capsule surface were explained. The influence of the cationic surfactant $C_{16}TAB$, which was used to stabilise the polymer capsule, on the Au NPs adsorption was studied. The effect of the Au NPs concentration on the adsorption density was analysed via both Ultraviolet-visible (UV-Vis) spectroscopy and thermal gravimetric analysis (TGA).

In Chapter 6, silver shell microcapsules were prepared based on PMMA shell hexylsalicylate core capsules using the electroless plating method. The influence of Au NPs adsorption density and the silver salt concentration on the silver shell thickness was evaluated. The factors affecting the silver shell microcapsules'

mechanical strength, including capsule diameter, polymer shell thickness and silver shell thickness, were investigated.

In Chapter 7, the whole research was concluded, and future work was considered.

Chpater 2 Literature review

2.1 Microcapsules

Microcapsules are a type of micro-sized vessel, package or container, in which solid, liquid or gaseous active ingredients are enclosed by a polymer wall. The capsules release their contents at controlled rates under specific conditions. The active ingredients are denominated as the 'core' 'fill' or 'internal phase', whereas the second encapsulant material is termed variously as the 'shell', 'wall', 'coating' or 'membrane' (Zhao and Zhang, 2011, Dubey et al., 2009, Ghosh, 2006, Gibbs et al., 1999, Jain et al., 1997).

2.1.1 Applications

Microcapsules have been widely used in a variety of applications, especially in the medicine, pharmaceutical and cosmetics industries, since such microcapsules may be used as carriers to protect sensitive compounds from undesired conditions giving effective controlled release of the active agent. The most successful examples include carbonless copy paper, scratch-n-sniff fragrance samples and the encapsulation of pesticides, herbicides and pharmaceuticals.

Microcapsules are able to provide sustained-release insecticides and herbicides (Boehm et al., 2003, Scher et al., 1998); to enhance the various qualities of ingredients such as colour, taste, stability and shelf life in the food industry (Klaypradit and Huang, 2008, Champagne and Fustier, 2007, Gharsallaoui et al., 2007); to protect unstable or sensitive active components, such as some vitamins, against degradation by light or oxygen (Desai and Park, 2005); to decrease the rate of evaporation or the rate of transfer of the core in flavour oils (Bhandari et

al., 1999, Kim and Morr, 1996); to convert liquid components to free flowing powders, such as powdered fat (Jafari et al., 2008, Faldt and Bergenstahl, 1995); to improve a product performance by separating the reactive ingredients until the needed materials are released; to improve the handling process where, for example, some active ingredients in pesticide formulations are toxic; a safe handling process can be enabled by encapsulation (Tsuji, 2001, Tefft and Friend, 1993).

Among all the applications, the use of microcapsules provides a means for the pressure-activated release of fragrance oil will be focused on this project. Such control over the release was gained through careful design of the capsule shell tailored to a preferred mechanism of release. These functions can be achieved or optimised through appropriate choice of materials, synthetic methods, and other experimental parameters, such as the concentration of the reagents, or reaction temperature, *etc.*

2.1.2   Preparation methods

A number of methods have been developed and reported to achieve the fabrication of microcapsules. Generally, these methods can be divided into chemical methods: physico-chemical methods and physical-mechanical methods listed in Table 2.1-1 (Ghosh, 2006). Each method may produce the different characteristics of microcapsules, such as morphology of microcapsules, size and/or size distribution, core-shell ratio and shell thickness. All these factors have an influence on the release mechanism and release profile. Chemical and physico-chemical methods are most used due to their relatively easy process and low cost. These methods for the preparation of liquid-core-solid-shell structure microcapsules are discussed in the following sections.

Table 2.1-1 Different techniques in microcapsules synthesis

Chemical Methods	Physicochemical methods	Physical/Mechanical methods
• Interfacial polymerisation • *In-situ* polymerisation	• Coacervation / phase separation • Precipitation • Solvent evaporation /extraction • Layer-by-layer assembly • Sol-gel encapsulation	• Spray-drying • Multiple nozzle spraying • Fluid-bed coating • Centrifugal techniques • Vacuum encapsulation • Electrostatic encapsulation

2.1.2.1 Interfacial polymerisation for microencapsulation

This method has been widely used for the preparation of latex core-shell particles (Sommer et al., 1995, Jonsson et al., 1994) and inorganic core-shell particles (O'Sullivan et al., 2009, Obey and Vincent, 1994). Generally, interfacial polymerisation starts with an emulsion containing two immiscible phases, which are terms of the 'oil' phase and the 'water' phase. Two different monomers are dissolved respectively in each phase and react with each other at the interface. A thin film is created at the interface to form a shell of the microcapsules. The reaction rate decreases as the polymerisation reaction proceeds. This is because the formed film at the interface between the oil phase and the water phase becomes a barrier for the two reactants to meet at the interface, which results in the reduction of reaction rate until the reactants can not penetrate through the film where the encapsulation completes. The interfacial film (the shell of the microcapsule) is generally thin and sufficient reaction time is required for the

completion of the shell formation. The process of interfacial polymerisation is schematically illustrated in Figure 2.1-1 (Munin and Edwards-Lévy, 2011, Jang et al., 2007, Macritch.F, 1969).

| Monomers dissolved in aqueous (A) and organic phase (B) respectively | Monomers meet and react at interface of two immiscible phases | Polymerisation at interface and form a thin film | Continued polymerisation and shell formation |
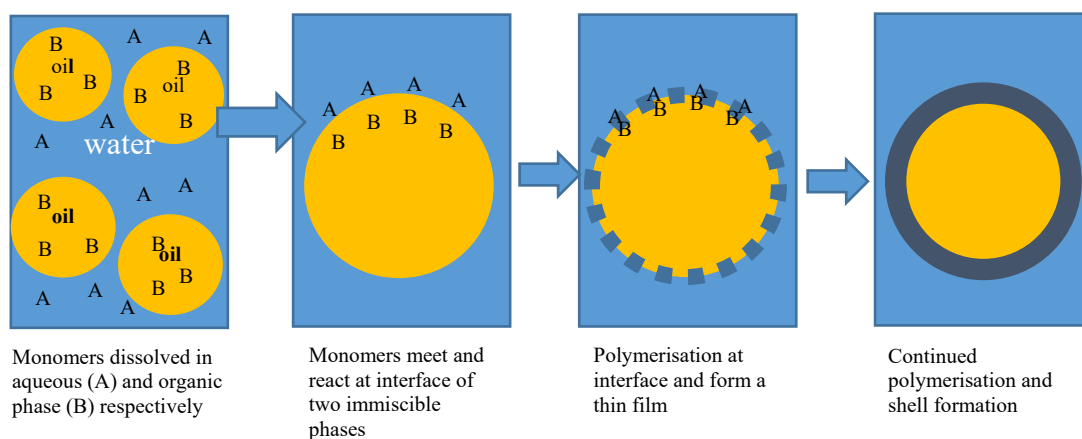
Figure 2.1-1 Schematic of the interfacial polymerisation process

In some studies, certain surfactants or polymers are employed in the continuous/dispersed phase to make the emulsion stable. Owing to the nature of this technique, some unreacted monomers might remain in the core, causing the problem of impurity.

2.1.2.2 In-situ polymerisation for microencapsulation

In-situ polymerisation is similar to interfacial polymerisation, but the polymer chain growth occurs in the continuous phase rather than at the interface described in the aforementioned interfacial polymerisation technique. The schematic of this process is shown in Figure 2.1-2. This method adopts the self-assembly approach and is suitable for biological applications as it involves no exposure to harsh solvents. The distinguishing characteristic of microcapsules prepared by in situ polymerisation is that no reactants are included in the core material (Brown et al.,

2003, Hentze and Kaler, 2003, Wong et al., 2002, Tiarks et al., 2001, Huang et al., 1999).

| continuous phase | | shell |
| organic phase | | solidification |

| Monomers dissolved in two immiscible phases respectively | Monomers diffused towards each other and polymer growth in continuous phase | Continued polymerisation and shell formation |
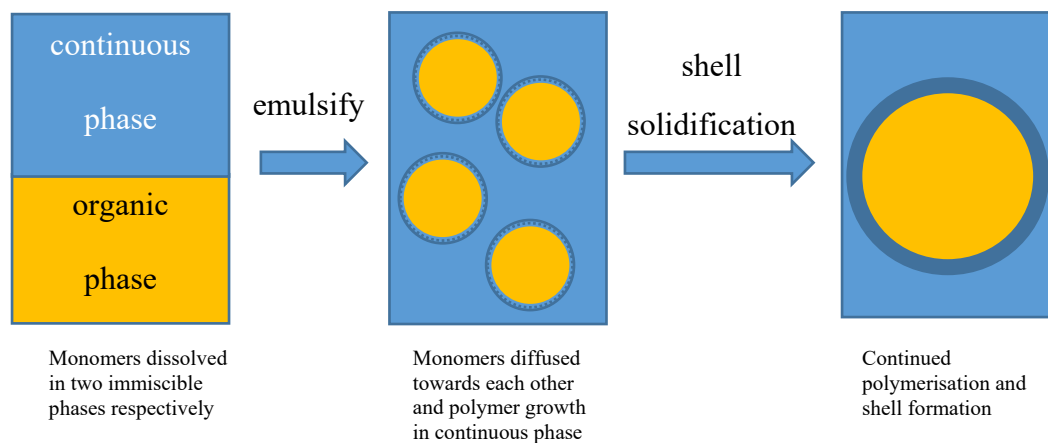
Figure 2.1-2 Schematic showing the in-situ polymerisation process

2.1.2.3 Coacervation and phase separation for microencapsulation

Coacervation is a physico-chemical, phase separation phenomenon. The term 'coacervation' was initially coined by Bungenberg and colleagues (Ghosh, 2006, Kruyt, 1949), and it involves a number of steps that are usually carried out under continuous agitation. This method starts with the preparation of a polymer solution. The core material is finely dispersed in the coating polymer solution. In coacervation processes, a suitable desolvating agent (coacervating agent) is gradually introduced to the mixture, depending on the nature of the polymer solution. Phase separation is induced by the introduction of the coacervating agent, *i.e.* changing temperature or pH of polymer solution, adding salt or non-solvent, using an oppositely charged polymer or cross-linking agent, etc. The polymer precipitates from the solution and deposits on the surface of the core

particles. Sometimes a further isolation step is needed to avoid aggregation. The whole process is illustrated in Figure 2.1-3.

| A mixture of polymer dispersion, good solvent, and poor solvent | After emulsification, polymer precipitate and coacervate | The coacervate spread around the active ingredient and form a layer | Solidification of the coacervate and shell formation |
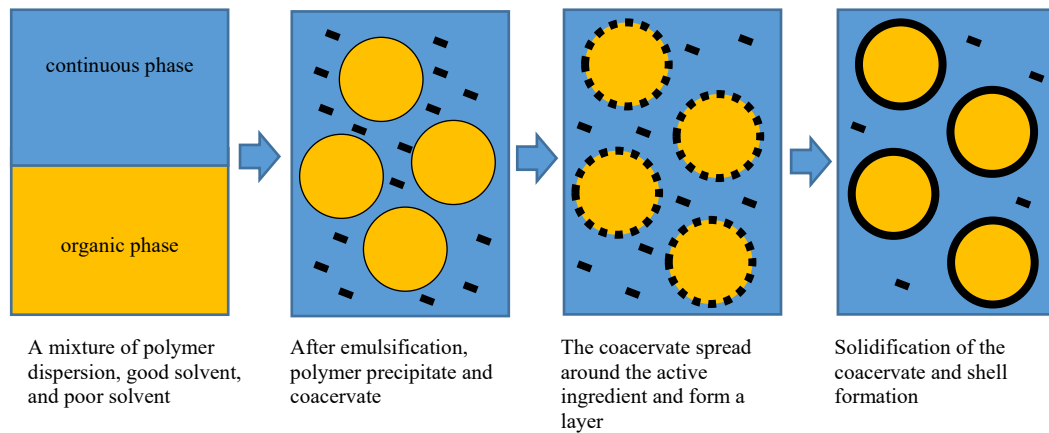
Figure 2.1-3 Schematic showing coacervation/phase separation microencapsulation

In this method, no impurities are included in the core material. Sometimes, an additional step is required (*e.g.* hardening agents) for solidification of the preformed shell (Andersson Trojer et al., 2013, Ghosh, 2006, Yow and Routh, 2006, Loxley and Vincent, 1998).

2.1.2.4 Layer by layer (L-b-L) assembly for microencapsulation

Layer by layer assembly is used to build up a polyelectrolyte layer onto a solid substrate (2D and 3D) through electrostatic deposition (Caruso et al., 1997). This method requires a sufficiently charged colloidal system and oppositely charged polymer particles. The polyelectrolyte-shell microcapsules are formed under the electrostatic attraction between oppositely charged particles. Multilayers of polyelectrolytes can be assembled on microcapsules using this method, with precise control of thickness. Physical and chemical properties of the surface can

be modified to fit into different applications. The illustration of process of L-b-L

process is illustrated in Figure 2.1-4 (Tarn et al., 2013, Ghosh, 2006, Yow and

Routh, 2006).
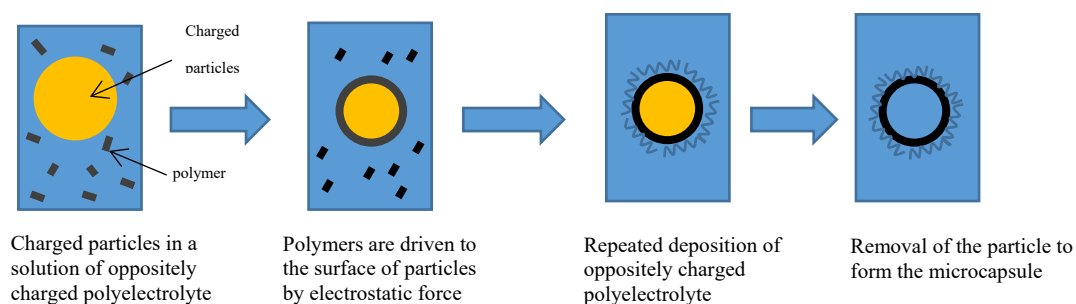
Figure 2.1-4 Schematic of L-b-L polyelectrolyte deposition

2.1.2.5 Solvent extraction/evaporation for microencapsulation

Solvent extraction/evaporation is another approach of phase separation and it

sometimes terms 'internal phase separation'. The method became popular due to

its straight-forward procedure. The polymer is firstly dissolved into volatile

organic solvent (s) to form a polymer solution. The core material is dissolved or

dispersed into this polymer solution. The resulting solution is then dispersed into

an aqueous solution, with continuous agitation. Surfactants are used to stabilise

the emulsion. The polymer precipitates and migrates towards the interface

between the discontinuous phase and the continuous phase to form the polymer

shell around the droplets. The formation of the polymer shell may be achieved by

either the removal of the solvent from the droplets or by solvent extraction with a

third liquid (Zhao et al., 2011, Mandal, 1999, Bodmeier et al., 1997). The process

of microencapsulation via solvent extraction/evaporation is illustrated in Figure

2.1-5. This method is most suitable for encapsulation of active ingredients in

liquid oil cores (Dowding et al., 2005, Dowding et al., 2004, Loxley and Vincent,

1998), as well as aqueous cores (Lorenceau et al., 2005, Atkin et al., 2004,

Zydowicz et al., 2002).

continuous phase			
organic phase			
Polymer dissolved in organic phase	After emulsification, polymer precipitates within the emulsion droplets	Precipitated polymers migrate to the interfacial and form a layer	Solidification of the shell and formation of the microcapsules
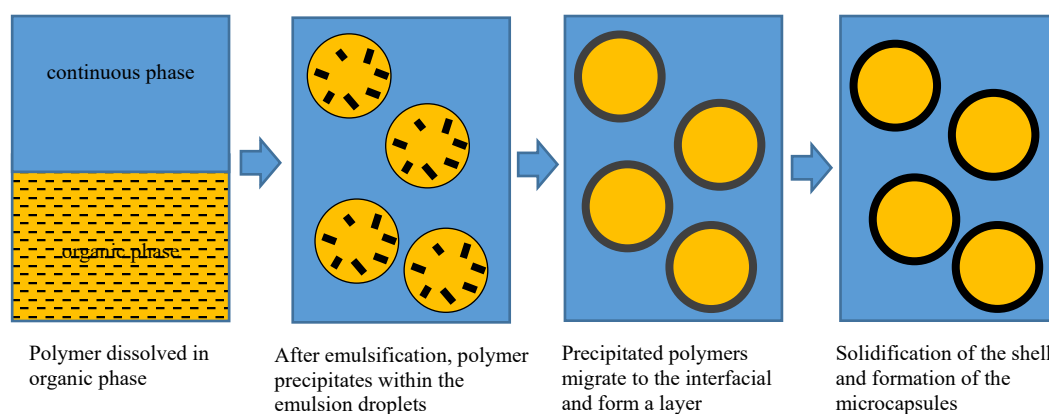
Figure 2.1-5 Schematic of the solvent evaporation procedure

This method is easy to use and feasible for industrial scale up. The release of core

material can be controlled in principle through various reaction parameters, such

as monitoring the particle size of microcapsules, controlling the concentration of

wall materials used for the microencapsulation and the thickness of the

microcapsules. Homogeneous shell thickness can be obtained through this

method.

Loxley and Vincent (1998) have utilised a solvent evaporation method to prepare

PMMA microcapsules containing oil core. It was found that the concentration of

PMMA in the oil phase has an effect on the size and the shell thickness of the

microcapsules. The types and the concentration of emulsifier also have impact on

the size and the morphology of the microcapsules. Increased amount of wall

materials used in the system reduces the release rate and dense polymer matrix

leads to hindrance of the release (Romero-Cano and Vincent, 2002). Dowding et al. (2004) also prepared polymer (polystyrene) shell oil core microcapsules using this technique. The release rate of the active ingredient was a function of the thickness of the polymeric shell and the thickness could be controlled by the amount of polymer dissolved in the oil phase. The diffusion rate of active ingredient through the pores was slower in thicker shell and greater amount of active ingredient was retained. Atkin et al. (2004) have revealed that different types of polymers such as PMMA, poly(isobutyl methacrylate) (PIBMA), and Poly(tetrahydrofuran)(PTHF) that were used as wall materials for the preparation of aqueous-core microcapsules had the different release behaviours. This because these polymers with different glass transition temperature (T_g) would produce the different morphology and shell structures of the microcapsules. Therefore, the design of shell structure is important for the controlled release of microcapsules in different applications.

2.1.3 Release mechanism

The controlled release of the active ingredient is one of the most important factors during the use of microcapsules in different applications. Depending on the purposes of the applications, various mechanisms have been employed in the alteration of the shell properties, such as (a) rupture release (Abderrahmen et al., 2011, Herrmann and Bodmeier, 1995), (b) shell-dissolution release (Yeo et al., 2005, Zhu et al., 2000, Ribeiro et al., 1999) and (c) diffusion-controlled release (Putney and Burke, 1998, Edelman et al., 1991).

(a) In the rupture release mechanism, the core ingredient is stored within the microcapsules until its sudden release upon rupture of the shell under external shear and/or stress. Two well-known examples of shell breakage are carbonless

copy paper and 'scratch-n-sniff' fragrance cards. In carbonless copy paper, a transparent dye precursor is previously encapsulated and coated on the back of the top paper, and isolated from the acidic coating on the surface of the lower paper. When writing on the paper, the force from tip of the ball pen compresses and ruptures the microcapsules, leading to the release of the dye precursor and darkening following exposure to the acidic coat. The similar mechanism is applied in 'scratch-n-sniff' fragrance cards: microcapsules, containing volatile perfume oil, are coated on the card. Under the stress of scratching, the polymer shell is broken and the perfume is released (Berger, 2007, Lacasse and Baumann, 2004, Karukstis and Van Hecke, 2003). This mechanism is suitable for providing full protection for the core content from the external environment and can afford little leakage prior to the breakage of the wall if the shell material is carefully designed. This mechanism requires a brittle solid shell and the release kinetics are determined by the mechanical strength of the shell.

(b) In the shell-dissolution release mechanism, the active ingredient that is incorporated inside microcapsules can be released due to the dissolution of the shell. The release trigger used depends on the applications. For instance, water is used as the release trigger for releasing enzymes, such as protease, in washing powder formulations to remove blood stains from fabrics. The enzymes are protected and stored in the water-soluble polymer (*e.g.* polyethylene glycol) microcapsules for safe handling purposes. The dissolution of the microcapsule shell in water at a certain stage of the washing cycle and the enzyme was released from microcapsules to help the removal of the bloodstains (Deshpande et al., 2006, Maurer, 2004, Bachtsi and Kiparissides, 1995). Heat is used as the release trigger for the release of the food powder for the preparation of hot drinks after

the addition of hot water. Lipids, fats and waxes are preferred as shell materials (Chu et al., 2001, Ichikawa and Fukumori, 2000). Many other release triggers, such as pH change (Dejugnat and Sukhorukov, 2004, Sukhorukov et al., 2001), enzyme attack (Park et al., 2014, Itoh et al., 2006, Shi and Caruso, 2001), photochemical reaction (Pastine et al., 2009, Volodkin et al., 2009), or electrical stimuli (Yoshida et al., 2004, Yoshida et al., 2002), may be used, depending on the application.

(c) In the diffusion-controlled release mechanism, the sustained release of the core content is required over an extended period of time. This mode of the release mechanism is widely used in drug delivery, fragrance and pharmaceutical formulations. One common option to achieve the sustained release of the core content is diffusion through the permeable shell (AppaRao et al., 2010, SA et al., 2010). The microencapsulated active ingredient diffuses gradually through a permeable or semi-permeable shell over an extended period of time to achieve a long-lasting effect.

For the microencapsulation of fragrance oil, both the diffusion-controlled release and the pressure-activated release mechanisms are used. The pressure-activated release of fragrance oil has an advantage over the diffusion-controlled release. A longer sustained scent can be achieved from the pressure-activated release of fragrance oil because the fragrance oil only releases from microcapsules under friction stress during applications, rather than the fragrance oil releases since they are manufactured in the diffusion-controlled release mechanism. The release behaviours can be controlled through various parameters such as the morphology of the microcapsules, the shell thickness, the nature of the shell, mechanical strength, *etc.*

2.2 Metal coating on microcapsules using electroless plating (ELP)

In microencapsulation, producing an impermeable shell for the encapsulation of volatile and small molecules such as toluene and fragrance oil is still a challenge. Toluene and fragrance oil can penetrate through polymeric membranes, reducing the shelf life of the microcapsules (Patchan et al., 2012, Brannonpeppas, 1993). The permeability of toluene/fragrance oil can be improved by coating a thin metal membrane on the surface of the microcapsules. The metal membrane provides vastly improved barrier properties to the rapid diffusion of gas molecules and small organic molecules (Patchan et al., 2012, Wang et al., 2005, Prins and Hermans, 1959). An electroless plating method for coating an additional metal layer on the polymer microcapsules to reduce the permeability of the polymer shell and sustain the active ingredients for longer storage periods has been reported (Lance M. Baird, 2012, L, 1970).

2.2.1 Electroless metal plating

The term 'electroless metal plating' was first introduced by Brenner and Riddell (1946a). It is essentially a metal deposition process brought about through a chemical reaction between metal ions and reducing agents without external electrical current. It is also termed autocatalytic plating because the reduced metals can act as catalysts during the reduction process. Electroless metal plating has the advantages of being a simple process and providing a uniform thickness of coating deposited. It has been widely used in surface modification of non-conductive, semi-conductive, metal materials and microcapsules (Schlesinger and Paunovic, 2011, Ghosh, 2008, Qiu and Chu, 2008, Vakelis, 2006, Agarwala and Agarwala, 2003, Dennis and Such, 1993). ELP has been applied to deposit

various metals, such as the metals from the iron, nickel and copper family. Gold

and platinum electroless plating have also been reported, with good coverage and

high corrosion resistance to acid (Ge et al., 2009, Huang and Dittmeyer, 2006,

Díaz et al., 2006, Hejze et al., 2005). In this study, the silver coating on the

PEMA capsules will be conducted, due to the lower cost compared to gold and

platinum.

2.2.2 Mechanism of electroless metal plating

ELP is an electrochemical process, which involves electron donor-acceptor

reactions. The redox reactions take place with the transfer of electrons between

oxidising and reducing agents. In the ELP process, metal ions in an aqueous

solution react with reducing agents to produce a metallic coating. Reducing

agents have oxidised anodically on the catalytic surface, providing electrons,

while metal ions, accepting electrons, are reduced to form metal coatings

(Vakelis, 2006, Bindra, 1990). For example, the reactions between SnCl2 and

AgNO3 can be described below (Liu et al., 2005, Kobayashi et al., 2001). Sn^{2+}

ions were firstly deposited on modifying the surface of the silica spheres, and

then a redox reaction was carried out. Sn^{2+} ions were oxidised to Sn^{4+}, providing

electrons. At the same time, Ag^{+} ions accepted the electrons and were reduced

into metallic Ag on the silica surface.

Anodic oxidation $\qquad$ $Sn^{2+} \rightarrow Sn^{4+} + 2e$ $\qquad$ Equation 2.2-1

Cathodic reduction $\qquad$ $2Ag^{+} + 2e \rightarrow Ag$ $\qquad$ Equation 2.2-2
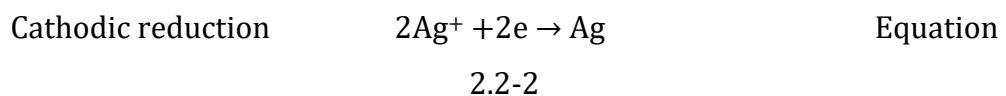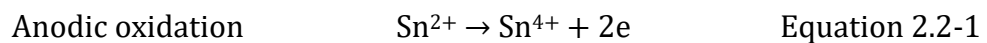
2.2.3 Modification of surface for electroless metal plating

The surface of the substance has been modified for the enhancement of metal deposition during the ELP process. In some cases, surfaces are simply roughened to enhance the retaining of ions. For example, polystyrene (PS) microspheres were chemically roughened with sulphuric acid to increase the surface contact area, therefore, enhancing the adsorption of Sn^{2+} on their surfaces to reduce Ag^+ during the ELP process (Ma and Zhang, 2012); Wang et al. at 2011 revealed that an oxidised silica surface is rougher than pure silica and provides better interlocking with ions particles.

The retaining of ions on the surface can be achieved by chemical bonds. For example, the polyester surface was modified through silanisation. Polyester was treated with (3-aminopropyl)trimethoxysilane (APTMS) to form $-NH_2$ groups on its surface, which are able to absorb Au NPs (catalyst) for silver ELP (Chen et al., 2008b). Poly(ethylene terephthalate) (PET) fabrics were modified with 3-mercaptopropyltriethoxysilane (MPPMS). The catalyst Cu NPs could be absorbed on the surface of PET fabrics through Cu-Si bonds to reduce Ag^+ during the ELP process (Wang et al., 2011).

The surface charge facilitates the electrostatic interaction between the surface and the ions. For example, a-Si wafer substrate has been coated with a positively-charged poly(allylamine hydrochloride)(PAH) layer to promote the interaction with negatively charged Au NPs and thereafter form Au coatings (Basarir, 2012). Also, a polystyrene film has been immersed in stearyl trimethyl ammonium

chloride (SC) solution to form a cationic surface before interaction with anionic Poly(vinylpyrrolidinone) (PVP) protected Pt colloids, which form the Pt seeds for Au coating(Horiuchi and Nakao, 2010).

In this work, a metallic silver coating was deposited on the surface of PEMA capsules, which had been previously modified with CTAB solution to improve the absorption of Au NPs. Au NPs were used as a catalyst in the oxidation and reduction process. Deposition of Au nanoparticles on PEMA microcapsules is essential for the deposition of the silver coating on it.

2.2.4   Plating solutions for electroless metal deposition

The selection of metal salts and reducing agents is very important for electroless metal deposition (Agarwala and Agarwala, 2003, Dennis and Such, 1993). A range of metal salts has been used in electroless metal plating, such as chloroauric acid ($HAuCl_4$) (Basarir, 2012, Horiuchi and Nakao, 2010), sodium gold sulfite ($Na_3[Au(SO_3)_2]$) (Blake et al., 2010) and potassium gold dicyanide ($KAu(CN)$)(Ko et al., 2010) for Au ELP; silver nitrate ($AgNO_3$) for silver plating solutions (Ma and Zhang, 2012, Wang et al., 2011, Chen et al., 2008b, Ye et al., 2008); copper sulphates/acetates/nitrates for Cu ELP (Rao, 2005, Agarwala and Agarwala, 2003); nickel sulphate (Guo et al., 2013, Patchan et al., 2012, Wu et al., 2009b) or nickel chloride (Lin et al., 2010) for Ni ELP. The loading and concentration of metal salts present an influence on the thickness of the shell (Cao and Zhang, 2013, Schaefers et al., 2006). The selection of reducing agents is dependent on which metal salts are used for the ELP. The reducing agents, formaldehyde (HCHO) in Cu ELP (Zhu et al., 2011, Fujiwara et al., 2010, Liu et al., 2005); sodium borohydride ($NaBH_4$) in Ni ELP (Agarwala and Agarwala, 2003, Dennis and Such, 1993); hydrogen peroxide (H_2O_2) and hydrazine (N_2H_4)

in Au ELP (Horiuchi and Nakao, 2010, Ko et al., 2010), have been reported.

Glucose has been used as a reducing agent in Ag ELP together with

poly(vinylpyrrolidinone) (PVP) as a stabiliser. PVP is a popular polymer

stabiliser to decrease the agglomeration during the ELP process because of its

steric structure and the surface bonding to particles (Song et al., 2006, Pastoriza-

Santos and Liz-Marzan, 2002, Li et al., 2000). In some cases, the pH of the

plating bath is adjusted to improve the ELP. Various solutions have been used for

different applications, such as citric acid (Ko et al., 2010), sodium hydroxide

(Zhu et al., 2011), and aqueous ammonia (Patchan et al., 2012). In this project,

the metal salt silver nitrate will be reduced to form a silver membrane on PEMA

microcapsule by formaldehyde in an alkaline condition. The redox reaction is

given in equation 2.2-3.

$$2Ag^+ + HCHO + 3OH^- \rightarrow 2Ag + HCOO^- + 2H_2O \qquad \text{Equation 2.2-3}$$

2.2.5 Catalysts in electroless metal plating

A catalyst is a substance that alters and usually increases the rate of reaction

without itself being consumed in the process. A catalyst is termed homogenous

when it is of the same phase as the reactant, and no phase boundary exists; it is

referred to as heterogeneous when it is separated from the reactants through a

phase boundary (Yan et al., 2009) (Astruc et al., 2005). Catalysts accelerate a

reaction by providing a lower activation energy pathway between the reactants

and products. For particle catalysts, the size of the particles plays an important

role in catalytic activity. The smaller the particle, the larger it is surface area, and

hence, the more the catalyst is exposed to the reactants and therefore the greater

its catalytic activity. Surface defects of solid-phase catalysts also have an

influence on the catalytic activity. Certain sites at a surface, *e.g.* steps, edges, ledges, corners and hollows, have increased surface energy and can provide lower activation energy pathways. Small particles generally contain more sites with defects and therefore provide better chemisorption for metals ions and better catalytic activity. Usually, for solid phase catalysts, high surface area (*i.e.* highly porous or small size) is favoured as it provides a larger number of active sites and therefore enhances the catalytic activity (Bowker, 1998, Thomas and Thomas, 1997, Bond, 1974). Other factors that are known to have an effect on catalytic activity, include reaction conditions (pressure, temperature, time, *etc.*), concentration of any stabilising polymers, extent of polymerisation, pH sensitivity, *etc.* (Moshfegh, 2009a, Astruc et al., 2005)

The properties of NPs catalysts are a small particle size results in a large surface area and increasing surface-to-volume (A/V) ratios. Hence, catalysts particles in nano-size are highly reactive when used as catalysts. Small particle sizes obviously lead to more active sites on the surface, *e.g.* edges and kinks, which show higher surface free energy and therefore higher reactivity; small particles also facilitate absorption of reactants at the surface (Moshfegh, 2009a).

However, NP catalysts can be unstable in the catalytic process due to their high energy surface atoms, which can drive aggregation, especially when highly concentrated NP dispersions were used. Finely dispersed NP dispersions can help to overcome these problems (Moshfegh, 2009a, Narayanan and El-Sayed, 2005).

NPs can be synthesised via many methods, such as hydrothermal, sol-gel, precipitation, laser ablation, *etc.* (Astruc, 2008, Lukehart and Scott, 2007, Gogotsi, 2006). One typical method for synthesising soluble NPs catalyst

involves reducing a metal precursor by reducing agent, such as NaBH$_4$ (Mei et al., 2007, Dai and Bruening, 2002, Sau et al., 2001).

2.2.5.1 The various pairing of NPs catalyst and metal coating

Various metal NP catalysts have been used to produce different metal depositions in ELP, and a summary of NP catalysts used. It has been found that NPs catalysts activate metal depositions and improve the uniformity of the coatings in electroless plating. Without NPs catalysts, the gold coating cannot be formed on the surface of the substrate, or uneven coating has been generated (Ko et al., 2010, Liu et al., 2005); a uniform surface coverage has been obtained by using NPs catalysts.

NP catalysts facilitate the condition of ELP by creating catalytic sites on the target surface. Many materials, such as polymers and ceramics, are not able to absorb the metal ions for metal deposition. NPs catalysts, such as Au, Sn and Pd, have been commonly used to induce sites for chemisorption and thereby create active nuclei sites on the surface. The active nuclei catalyses the anodic oxidation of reductants and induce negative charge for the metal to be deposited. For example, Pt NPs (Ma and Zhang, 2012) and Au NPs (Chen et al., 2008b) have been used as catalysts to promote Ag coatings. The loading of NP catalysts have an impact on the coverage and thickness of the metal deposited, as well as the speed of coating (Guo et al., 2013, Wang et al., 2011, Wu et al., 2009b, Liu et al., 2005).

2.2.5.2 Au NPs as catalyst in electroless silver plating

The application of Au NPs as catalyst for electroless silver plating is proposed (Inberg et al., 2012). Au NPs Catalysts are employed in electroless silver plating

to increase the rate of reaction between reducing agents and metal salts, as well as function the nuclear site of the metallic coating. Au NPs show a special optical property like surface plasmon resonance (SPR) absorption, which is affected by particle size and particle shape (Kobayashi and Ishii, 2013).

Au NPs also form catalytic nuclei on the surfaces of many materials, such as polymers and ceramics (Zhu et al., 2011). In many cases, without the NP catalysts, the target surfaces exhibited no metal deposition at all (Horiuchi and Nakao, 2010), resulted in metals only in bulk (Liu et al., 2005), or produced a coating on an unwanted location (*e.g.* glass beaker) other than the target surfaces (Patchan et al., 2012).

2.3   Parameters that have an influence upon size, morphology and shell thickness of microcapsules

Many parameters that may be varied during the preparation procedure can influence the physicochemical properties of the microcapsules. These parameters include stirring speed, the polymer molecular weight, solvent type, catalyst concentration, and the rate of solvent evaporation, *etc.* The influence that these parameters have on the size, morphology and shell thickness of the microcapsule is significant and is discussed in this report.

2.3.1   Solvent evaporation time

In the solvent evaporation method, the solvent of the dispersed phase must evaporate from the surface of the dispersion to produce the sufficiently solidified shells of the microcapsules. The rate of evaporation of volatile solvent can be controlled by varying the temperature: higher temperatures facilitate the evaporation rate of the solvent from the continuous phase. However at higher

temperatures (38-42 ºC), the microcapsules that are synthesised show wider size distributions and decreased particle density than those produced at lower temperatures (4-33 ºC) (Yang et al., 2000a, Yang et al., 2000b). By reducing the evaporation rate, microcapsules with larger core content and smaller size distribution can be obtained (Atkin et al., 2004). The boiling point of the solvent and the glass transition temperature (T_g) of the polymer also affect the evaporation rate. Basically, solvents with lower boiling points, *e.g.* ethanol or dichloromethane (DCM), are commonly used in order to favour the evaporation at room temperature. Atkin et al. (2004) have studied the microencapsulation of various polymers with different T_g values. They found that characterisation of a synthesized microcapsule was difficult when a polymer with a low T_g value was employed, while polymers with high T_g values restricted the precipitation of polymer leading to coalescence during the evaporation process. Polymers with an intermediate T_g value (~55 ºC) are more mobile in a solvent environment.

In the present study, a slow evaporation rate is desirable to achieve larger sizes with more content and better density of the shell of the microcapsule. Therefore, enough solvent evaporation time must be allowed for the solidification of the shell to occur.

2.3.2 Initial core-shell ratio

The initial weight ratio of core-shell materials is vital in determining the size, morphology and shell thickness of the microcapsules.

When other processing parameters are kept constant, the increase of initial weight ratio of core-shell results in the increase of the size of w/o emulsion droplets, which leads to an increase in the diameters of the synthesised microcapsules. The

increase in the shell materials results in a greater shell thickness, and the raised volume of core material reduces the shell thickness while increasing the oil droplet size (Yuan et al., 2006).

In another study, the mean diameter of polystyrene (PS) core-polycaprolactone (PCL) shell microcapsules decreased as the ratio of shell material (determined by the concentration of a PCL solution) was raised, while the concentration of core material (contained in a PS solution) was fixed and other process conditions remained the same. A low concentration of shell materials lead to irregular shapes and wide size distributions of the microcapsules, while high concentrations generated aggregation on the surface. The mean diameter of the microcapsules increased as the concentration of the core material was raised (Hwang et al., 2008).

When the shell material (polymer weight) was kept constant, an increase of the volume of solvent resulted in a reduction in the mean diameter of poly(DL-lactide-*co*-glycolide) (PLGA) shell microcapsules. This may be caused by the increase of the viscosity of the internal phase of the emulsion with decreased volume while the polymer weight was kept constant Sansdrap and Moes (1993).

However, excess shell or core materials may cause poor dispersion and aggregation of the polymer on the microcapsule surface. The core-shell ratio which gives highest yield of microcapsule is 1.00 - 1.25 (Yuan et al., 2006).

2.3.3 Catalyst loading

As mentioned previously, noble metal nanoparticles have been widely used as catalysts in electroless metal plating. They can initiate secondary metal coating

and increase the rate of reaction between reducing agents and metal salts, as well as functionalising the nuclear site of the metallic coating.

In a study of nickel nanoparticles synthesis by electroless plating carried out by Wu et al. (2009a), the loading of catalyst Ag was found to have an influence on nickel formation. With the Ag loading increased from 0.02 to 0.05 wt%, the nickel particle size decreased from ~100 to ~40 nm and the loading of the particles increased, which indicated that more nuclei were formed for subsequent nickel plating. The images of adsorption of nickel particles with different Ag loading are shown in Figure 2.3-1 Ni/TiO$_2$ samples with different Ag loadings (Wu et al., 2009a). It was also reported that the surface number, concentration and size of Ag sites increase with the growth of Ag loading.
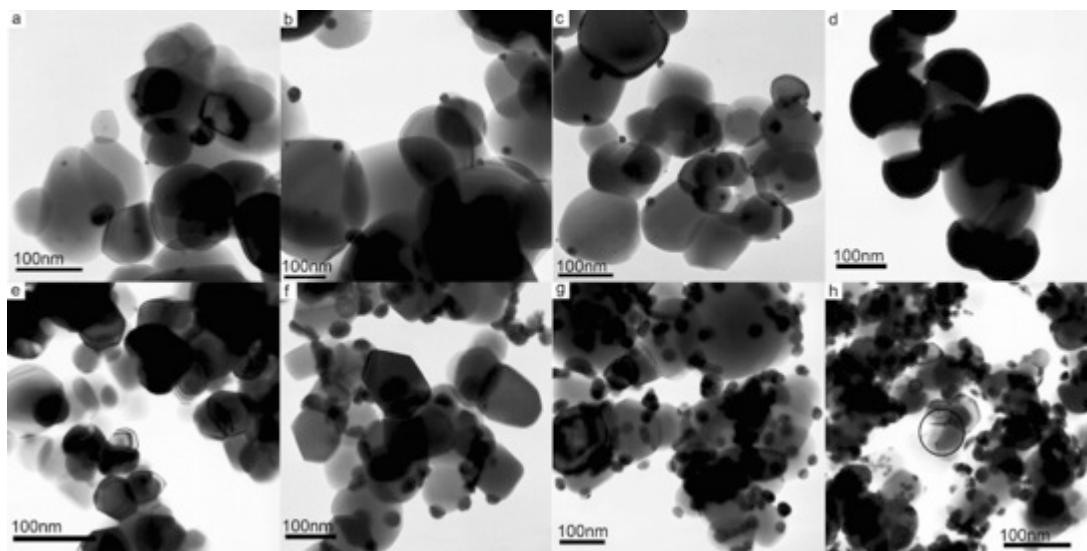
Figure 2.3-1 Ni/TiO$_2$ samples with different Ag loadings (Wu et al., 2009a)

The loading of catalyst has also been studied by Ge et al. (2006) in their work involving the hydrogenation of sulfolene to form sulfolane over different

supported amorphous Ni-B alloy catalysts. The deposition of amorphous Ni-B particles on MgO was carried out by a silver catalysed electroless plating technique. It was found, with increasing loading of silver on MgO, the loading of nickel increases as shown in following Figure 2.3-2 Plots loading of nickel *vs* loading of silver (Ge et al., 2006).
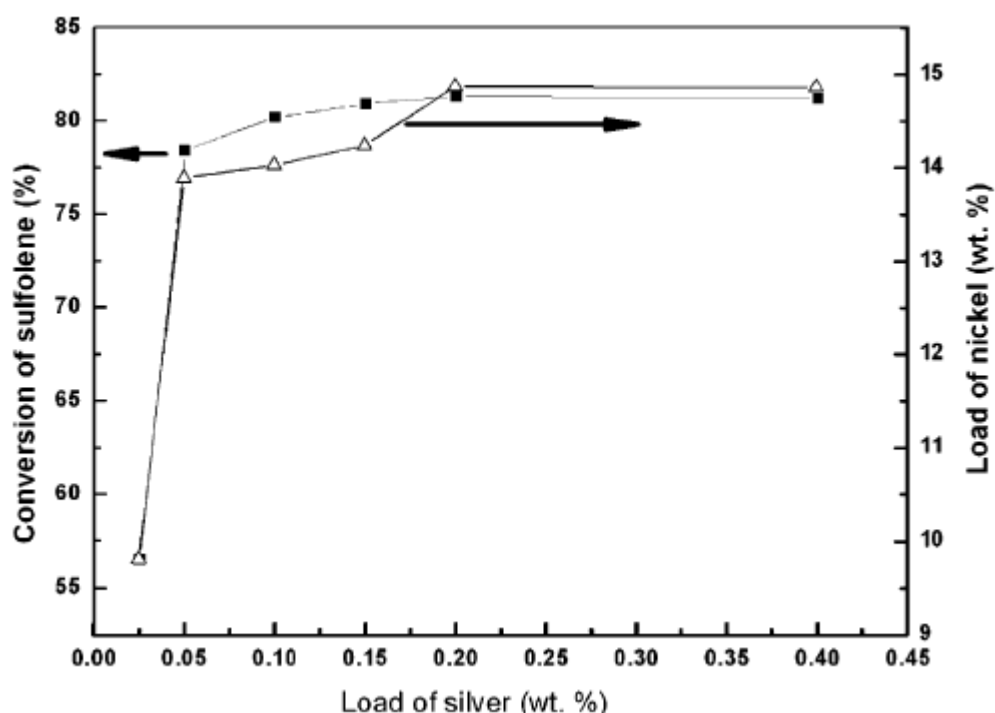
Figure 2.3-2 Plots loading of nickel *vs* loading of silver (Ge et al., 2006)

The increase of catalyst loading has increased not only the absorption of secondary metal coating but also the surface area of the metal. Cu has been used as the catalyst in the electroless deposition of Pd on graphite electrodes. With an increasing initial Cu loading, the increase of Pd electroactive surface area has also been observed (Ghodbane et al., 2008).

Meanwhile, the observation that the loading of the catalyst has an influence on the secondary metal shell thickness has been reported in the work of Liu et al. (2011). Ag was used as a catalyst to facilitate the subsequent growth of silver on a SiO_2 surface. The thickness of the silver shell decreased when the Ag/SiO_2 ratio was decreased. At low ratios of Ag/SiO_2, the silver shell was not completely formed, as shown in Figure 2.4-3 Typical force-displacement profile.
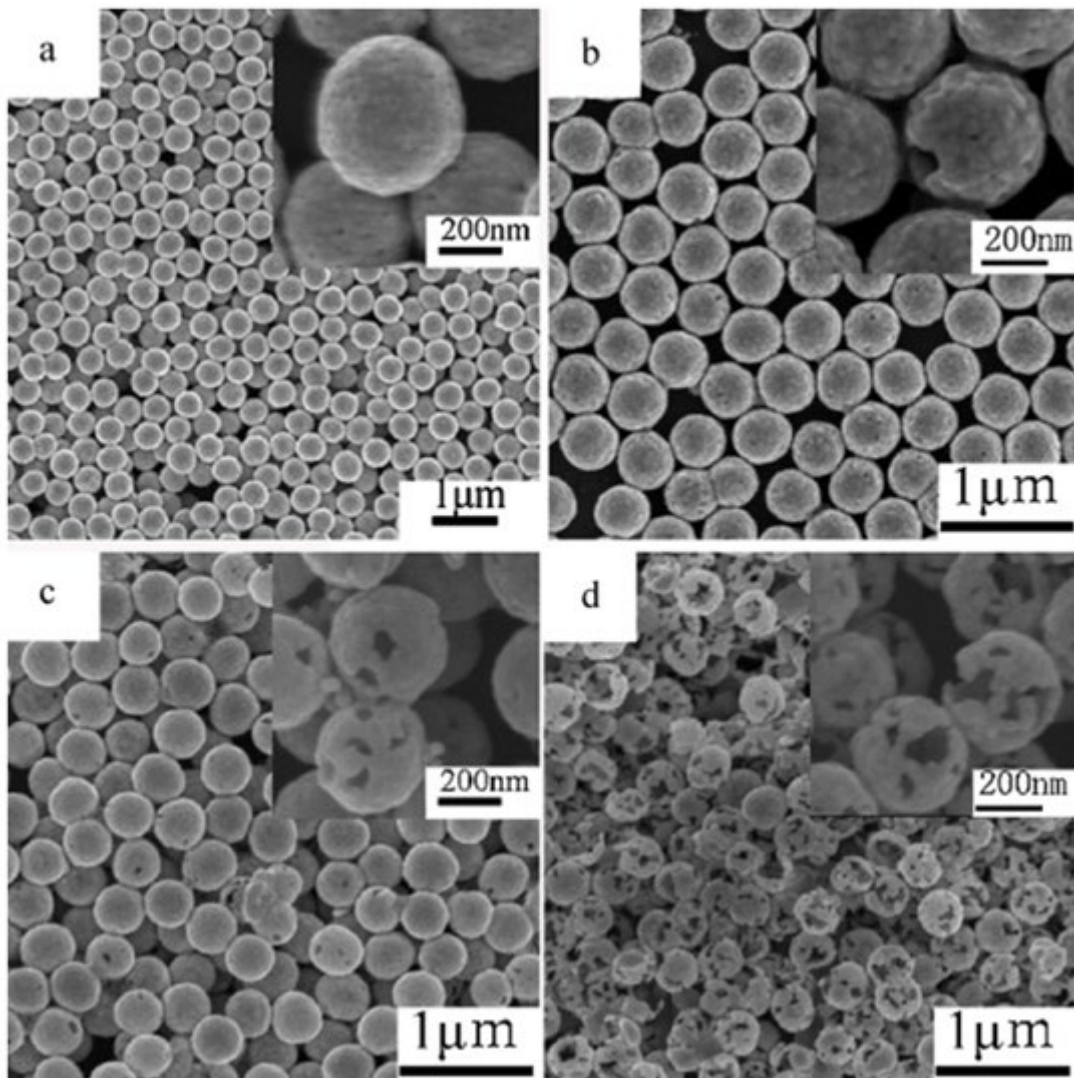
Figure 2.3-3 Silver hollow particles with different shell thickness and Ag/SiO_2 ratio (Liu et al., 2011)

2.3.4   Metal salt loading

The metal salt loading has a straightforward influence on the final metal shell

morphology and thickness. In a study of the electroless deposition of Pd on Cu-

modified graphite electrodes carried by Ghodbane et al. (2008), the metal salt

loading was varied by changing the concentration of $PdCl_2$, which lead to

significant morphological and structural changes to the graphite surface. At low

concentrations of $PdCl_2$, the presence of the uncovered surface was observed. By

increasing the Pd concentration, the uncovered surface area decreased and the

thickness of the Pd layer increased. Sun and Xia (2004) also demonstrated in their

work that a high concentration of metal salts leads to less evidence of uncovered

surfaces.

Chen et al. (2008a) also demonstrated that the thickness of the metal shells could

be controlled by adjusting the ratios of metal salts to the surface, as shown in

Figure 2.3-4 Silver shells on PS spheres with different mass ration of $AgNO_3$/PS
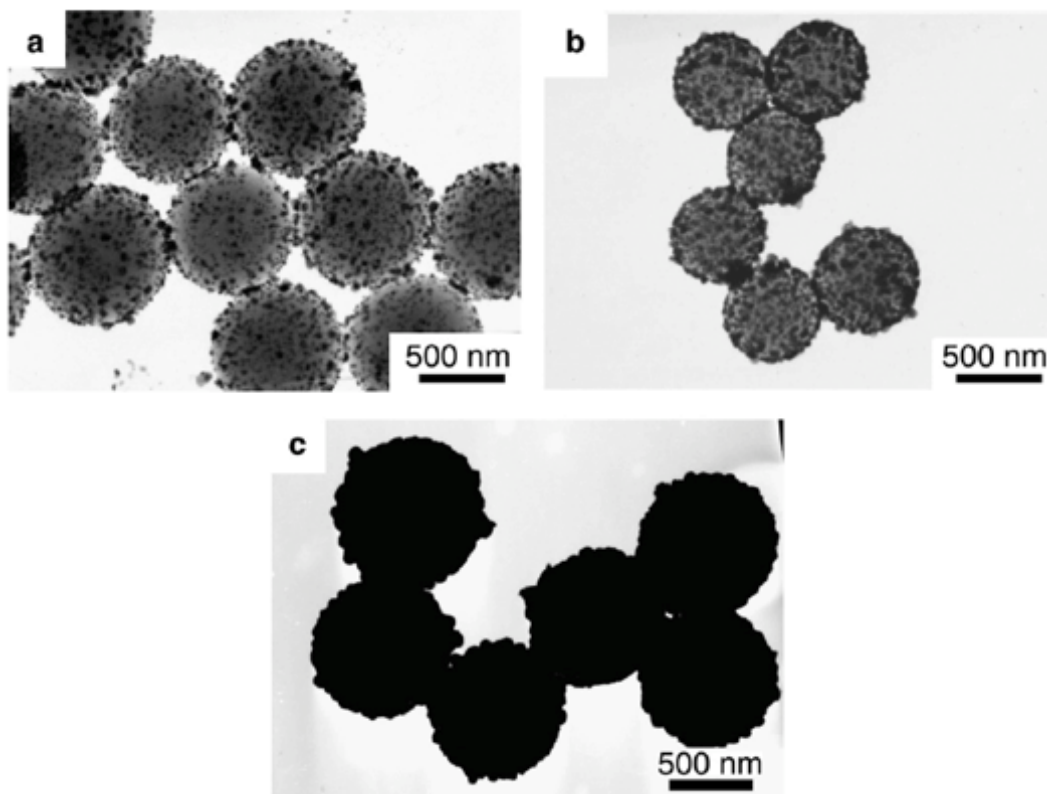
of (a) 1:2; (b) 2:1; (c) 10:1..

Figure 2.3-4 Silver shells on PS spheres with different mass ration of AgNO₃/PS of (a) 1:2; (b) 2:1; (c) 10:1.

In this study, the silver shells became thicker and more compact when more silver atoms were deposited on the PS nanoshells by increasing the ratio of $AgNO_3$/ PS.

However, at high concentrations of the metal salt, aggregation may occur, leading to an increase in the number of metal atoms and a decrease in the distance between neighbouring metal atoms. This, in turn, facilitates the overlapping and agglomeration observed.

2.3.5   Reducing agent loading

When subjected to the electroless metal plating process, the loading and concentration of the reducing agent play an essential role in the system; a sufficient amount of reducing agent is required for the reducing activity to be

carried out. Dimethylamine borane (DMAB) was employed to reduce the nickel on the surface of poly(methyl methacrylate) (PMMA) beads by Lin et al. (2013). The DMAB was used to supply electrons so that Ni ions in the $NiCl_2$ solution were converted to their zerovalent metal state. A discontinuous layer of the Ni coating was observed at low DMAB concentrations (*i.e.* ≤ 0.010 mol dm^{-3}) because of the lack of a continuous supply of electrons from the reducing agent. When the DMAB concentration was increased, a continuous Ni coating was formed on the PMMA bead surface. This also resulted in the increase in the thickness and density of deposited Ni coating. This was confirmed by both Scanning Electron Microscopy (SEM) and X-ray Diffraction (XRD) characterisation techniques.

In addition to the improvement of the thickness and smoothness of the coated metal surface, an increase in the reducing agent concentration also accelerated the metal coating speed. Wang et al. (2014) showed that the plating speed of copper on Ti_3AlC_2 particles grows with the increase of reducing agent formaldehyde (HCHO). However, when the HCHO content reached a certain amount, the rate of increase slowed or stopped entirely. Similar results were reported by Zhang et al. (2004) for the electroless coating of Co on nano-scale Al_2O_3 surfaces.

2.3.6   Plating time

The plating time has also been found to have an impact on metal coating thickness in electroless plating. Tierno and Goedel (2006) conducted studies on the influence of various plating times on the metal coating. It was reported that the thickness of the nickel layer increased by prolongation of the immersion time of the PMMA particles in the electroless bath. As the plating time increased, the metallic layer first started to form a completed layer and become smooth before

achieving a greater thickness. The results have been revealed by SEM, Transmission Electron Microscopy (TEM) and Thermogravimetric Analysis (TGA) data.

Similar results were found by Zhang et al. (2007) in the synthesis of silica-core-Ag-Cu alloy shell particles. A uniform Ag shell was formed on the surface of the silica particles after the seeding process. As the plating times increased, so did the coverage and size of the Ag NPs, as well as the mean thickness of the silver shells.

2.4 Characterisation of mechanical strength

Mechanical properties include various aspects, such as Young's modulus, specific modulus, tensile strength, compressive strength, shear strength, yield strength, stress-strain behaviour, etc. By characterising the microcapsule's mechanical properties, one can prevent the damage to capsules in processing equipment, maintain their long-term mechanical stability and realise triggered release of active ingredients from capsules by mechanical forces. In principle, the mechanical strength can be determined by measuring their deformation under a mechanical force, i.e. stress-strain behaviour.

2.4.1 Characterisation techniques of mechanical strength

Various techniques have been developed to characterise the mechanical properties of microcapsules, and they are mainly divided into two categories: characterisation of microcapsule population and of the single microcapsule.

2.4.1.1 Shear force breakage

One method for characterising microcapsule population is the measurement of breakage of, *e.g.* nylon membrane microcapsules in a ''shear'' device, for example, a turbine reactor or a bubble column. The nylon capsules were broken by applied shear force, and the concentration of encapsulated core, *i.e.* dextran, has been measured before and after shear breakage. The volumetric fraction of unbroken capsules and the breakage kinetics was determined. However, in this method, the mechanical breakage depends not only on mechanical strength but also on the hydrodynamics of the processing equipment.(Lu et al., 1992, Poncelet and Neufeld, 1989).

2.4.1.2   Osmotic pressure test

Another approach to characterising the microcapsule population is to make use of osmotic pressure. Van Raamsdonk and Chang (2001) have studied the mechanical strength of alginate microcapsules by exposing them to a graded series of hypotonic solutions and quantifying the percentage of broken microcapsules. This method is simple and rapid. However, it is limited to microcapsules with semi-permeable shells and relatively low mechanical strength.

2.4.1.3   Optical trapping/laser tweezers

This method is a very sensitive method and is mainly used to study biological samples (such as individual viruses and bacteria). It uses a highly focused laser beam to trap and manipulate particles and produces a light pressure/gradient force (range from tens of fN to hundreds of pN). One of the advantages of the optical trapping method is that least damage to the sample due to the limited physical contact. However, it is difficult to measure the mechanical behaviour of samples

to large deformations due to the small forces exerted (Neubauer et al., 2014, Zhang et al., 2009, Lim et al., 2006).

2.4.1.4   Micropipette aspiration

This method has originally been developed by Mitchison and Swann (1954) in their study of mechanical properties, i.e. elastic properties of cell surface and has thereafter been widely used in investigating the mechanical behaviour of living cells (Fiddes et al., 2009, Lim et al., 2006, Hochmuth, 2000). In this method, a single cell is partially aspirated into the tip of a pipette. The suction pressure inside and outside of the pipette was measured, and the information of mechanical properties can be obtained through the bulging of the cell membrane. This method is easy and quick to use, but a major disadvantage is that friction occurs between the cell surface and the pipette. This may interfere with the mechanical behaviour of the cell during the aspiration. The forces exerted on the microcapsule are relatively small, *i.e.* between pN to nN, which is suitable for cells that are easily deformed.

2.4.1.5   Atomic Force Microscopy (AFM)

The AFM is a high-resolution type of scanning probe microscopy. It obtains the images and information by measuring the movement of the cantilever-mounted tip scanning across the sample surface. When the tip is brought to the sample surface, forces between the tip and the sample lead to deflect the cantilever. The deflection is detected by a laser focus on the back of the cantilever, which is reflected into a photodetector and then converted into a 3D image (Zhang et al., 2009, Lim et al., 2006). Figure 2.4-1 shows a schematic of a typical AFM instrument.
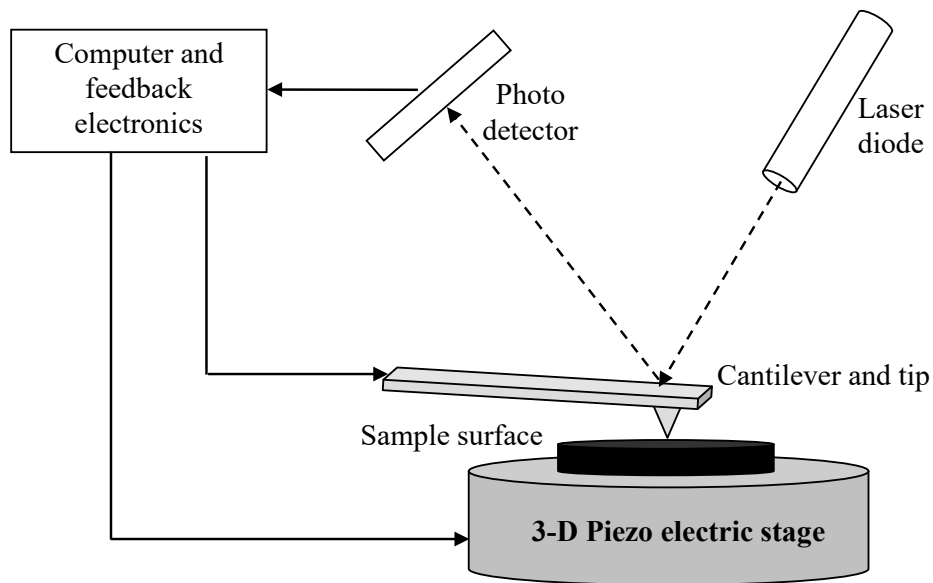
Figure 2.4-1 Schematic of AFM setup (Zhang et al., 2009)

Ducker et al. (1991) developed a colloidal probe for AFM to measure the force between an individual colloidal particle, *i.e.* silica sphere, and a planar surface. Lulevich et al. (2003) also used AFM to study the deformation of "filled" (with a neutral polymer) polyelectrolyte microcapsules under applied load. In the study, a glass sphere (diameter of ˜40μm) is attached to the tip-less cantilever to achieve well-defined sphere-sphere deformation geometry. The force range in AFM is in the range of small value (pN to μN) and therefore it is suitable for microcapsules with small deformation regime on the order of the shell thickness. However it does not have the ability to rupture the wall since it can only measure the small forces. The size of microcapsule should also be smaller than the colloidal probe to ensure the deformation of the whole capsule taken place.

2.4.1.6 Micromanipulation based on diametrical compression

Diametrical compression, i.e. the compression of a single particle between two rigid plates, has been developed and employed to measure the mechanical properties of powders directly. This technique relates the breakage of an individual particle to its mechanical properties through sophisticated mathematical models (Sun and Zhang, 2002, Zhang et al., 1999). Samimi et al. (2005) carried out studies on the deformation and failure behaviour of particulate solids using both single and bulk compression analysis. However, they pointed out that the use of bulk compression method to infer single-particle properties should be made with great caution because the initial packing condition, shell friction, as well as the sliding and rearrangement of the particles all have an impact on the mechanical properties of the single particles.

A micromanipulation technique was developed to investigate the mechanical strength of single microcapsules. This technique is based on diametrical compression and was used to measure the bursting force and deformation at the bursting of single microcapsules and to determine the elastic, viscoelastic or plastic behaviours of single microcapsules. The intrinsic mechanical property parameters of the microcapsules, such as Young's modulus, Poisson ratio, relaxation time, yield stress, etc. may be determined by mathematical modelling (Zhang et al., 2009, Sun and Zhang, 2002, Zhang et al., 1999, Liu et al., 1996).
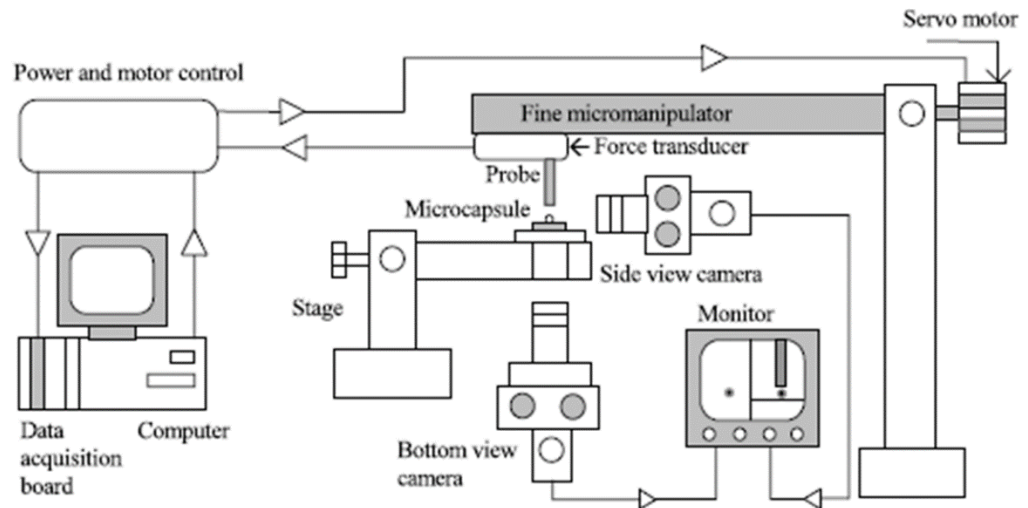
Figure 2.4-2 Schematic diagram of micromanipulation rig (Sun and Zhang, 2002)

The schematic diagram of the micromanipulation rig was shown in The rig consists of a fine glass probe, which is connected to a force transducer. The probe is positioned perpendicular to the sample slide and programmed to travel towards the microcapsule at a given speed. When a microcapsule is compressed by the probe, the force being imposed is measured simultaneously by sampling the voltage signal from the force transducer. When the probe eventually touches the slide, they are separated to return the imposed force to zero. From the curve of force versus displacement of the probe, the relationship between the force and the microcapsule deformation to bursting can be obtained. A typical force-displacement profile obtained using the micromanipulation device is shown in Figure 2.1-1. The probe meets the particle at point A. The measured applied force increases until the particle breaks at point B. The probe meets no further resistance until C, where it begins to compress particle debris. At D, the probe experiences resistance from the substrate. The displacement from point A to D

serves as an estimate of particle size (O'Sullivan et al., 2009, Sun and Zhang, 2002).
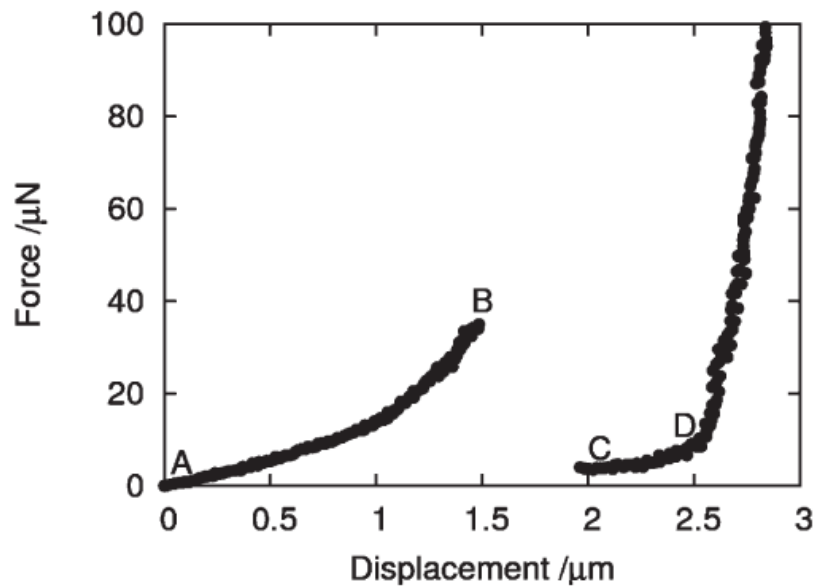
Figure 2.4-3 Typical force-displacement profile

This technique has been used to study the relationship between the mechanical strength of microcapsules with silicone oil cores and solid silica-like shells (a mixture of tetraethoxysilane and diethoxydimethylsilane) and its shell thickness by O'Sullivan et al. (2009). A reasonably linear correlation between shell thickness and the force required to break the shell for particles is discovered, although the thinnest shells give higher breaking force values, which might be caused by less amount of diethoxydimethylsilane in the shell, and the major component is tetraethoxysilane, which has a more silica-like structure.

Sun and Zhang (2002) have also used this technique to study the mechanical strength of microcapsules made of three different wall materials, including

melamine–formaldehyde resin, urea-formaldehyde resin and gelatin-gum arabic coacervate. In addition to the force-displacement profile, the relationship between bursting force and microcapsule diameter was also investigated.

2.4.2 Stress-strain behaviour

Stress-strain behaviour describes the deformation characteristics of microcapsules upon compression. The force is expressed as stress when it is expressed as the force exerted per unit area, and the deformation caused by the stress can be expressed as strain through the ratio of the extension to the original linear dimension. The deformation characteristic of microcapsules upon compression may be elastic, viscoelastic or plastic and may involve fracture or a combination of these deformation mechanisms. Therefore the mechanical strength of a material can be described by the relationship between stress and strain, *i.e.* a stress-strain curve, and a typical example is shown schematically in Figure 2.4-4.
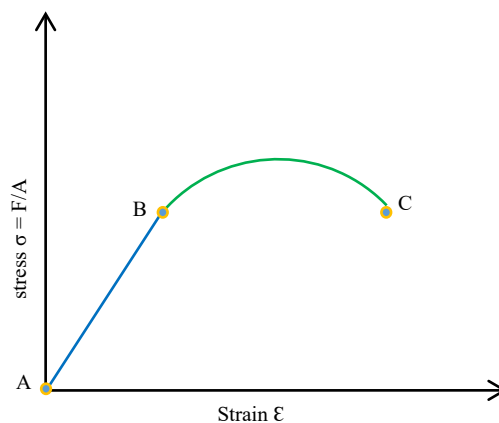
Figure 2.4-4 Stress-strain relation

In Figure 2.4-4, the linear portion between A and B represents the material undergoing elastic deformation, wherein the applied stress is proportional to the strain. At this stage, the material is able to return to its previous shape after stress

is released and no permanent deformation occurs. Plastic deformation starts after point B, which is an irreversible and permanent strain after the removal of the loading stress. A fracture occurs after the material has reached the end of the elastic and plastic deformation ranges (point C), which indicates the strength of the material.

The measured stress at the fracture point (C) is termed as the fracture/rupture stress. It is the maximum stress the microcapsule can withstand before its fracture under pressure. It depends on the force applied, dimension, and shell thickness of the microcapsules and can be calculated.

The elastic deformation of spherical contacts was investigated by Yap et al. (2008). In that particular study, the single particles of the copolymers were compressed to various nominal strains. Experiment data show that, at a nominal strain of 4.3%, the particle exhibited elastic deformation; at a strain of 6.0%, the particle presented plastic deformation. The elastoplastic deformation behaviour of the particles was determined through the rupture strength, which was calculated using Equation 2.4-1.

$$\sigma_r = \frac{F_r}{\pi D^2} \qquad\qquad \text{Equation 2.4-1}$$

where

σ_r = nominal rupture stress

F_r = rupture force

D = diameter of the particle

The mechanical strength was studied through the relationship between the ratio of the mean diameter to the wall thickness and rupture stress by Taguchi and Tanaka

(2001). It was found in the study that the mechanical strength of polymer shell microcapsules decreased as the ratio of the mean diameters to the wall thickness increased. The nominal rupture stress can be calculated in Equation 2.4-2.

$$\sigma = \frac{P}{4(\frac{dp_a}{T})} \qquad \text{Equation 2.4-2}$$

where

σ = nominal rupture stress
P = loaded pressure
dp_a = mean diameters of the microcapsules
T = shell thickness

Pan et al. (2013) studied the mechanical properties of consumer-friendly PMMA microcapsules. They have found that the force-displacement profiles obtained from compression of single PMMA microcapsules are dependent on polymer shell thickness. Thus, thin shell microcapsules showed a clear bursting point, whereas, for thicker shells, no bursting was observed. However, the intrinsic mechanical properties of PMMA shells, such as the elastic modulus and the rupture stress, were found to be independent of shell thickness. The compression force here also refers to the nominal rupture stress, which can be determined using Equation 2.4-1. The rupture force, *i.e.* the force at the bursting point, was found to be dependent on the capsule size.

Chpater 3 Experiment materials and research methodologies

3.1 Materials and synthesis methods

All the chemicals were used as received. All the water used in the experiments was purified Millipore Milli-Q water, which resistivity is 18.2 MΩ•cm at 25 °C. All the experiments were carried out under ambient temperature.

3.1.1 Preparation of polymer shell microcapsules

3.1.1.1 Materials

- MilliQ water

- Hexadecyltrimethyl-ammonium bromide (C_{16}TAB), purchased from Sigma-Aldrich, CAS 57-09-0

- Dichloromethane (DCM), purchased from Acros, CAS 75-09-2

- Poly(ethyl methacrylate) (PEMA), purchased from Sigma-Aldrich, CAS 9003-42-3, average molecular weight ~515,000

- Polymethylmethacrylate (PMMA), purchased from Sigma-Aldrich, CAS 9011-14-7, average molecular weight ~120,000

- Toluene purchased from Fisher Scientific, CAS 108-88-3

- Hexadecane, purchased from Fisher Scientific, CAS 544-76-3

- Hexyl salicylate, supplied by industrial sponsor Procter & Gamble, CAS 6259-76-3, a type of fragrance oil, molecular weight 222.28

- Cyclamen aldehyde, supplied by industrial sponsor Procter & Gamble, CAS 103-95-7, a type of fragrance oil, molecular weight 190.28

- Dihydro-mercenol, supplied by industrial sponsor Procter & Gamble, CAS 18479-58-8, a type of fragrance oil, molecular weight 156.27

- Gold (III) chloride hydrate (HAuCl4·H2O), supplied by Sigma-Aldrich, CAS 27988-77-8

- Silver nitrate (AgNO3), supplied by Fisher Scientific, CAS 7761-88-8

- Hydrochloric acid (HCl), 37% in H_2O, supplied by Sigma-Aldrich, CAS 7647-01-0

- Sodium borohydride (NaBH4), supplied by Sigma-Aldrich, CAS 46940-66-2)

- Sodium hydroxide, supplied by Sigma-Aldrich, CAS 1310-73-2

- Formaldehyde solution (HCHO), 37% in H_2O, supplied by Sigma-Aldrich, CAS 50-00-0

- Ammonia solution, 25% in H2O, supplied by Merck KGaA, CAS 105432

3.1.1.2 Experiment method

Three sets of polymer shell microcapsules were prepared in this section, namely PEMA shell toluene core microcapsules, PMMA shell hexadecane core microcapsules, and PMMA shell fragrance oil core microcapsules. All the polymer shell microcapsules were prepared using the same solvent evaporation and extraction method, illustrated in Figure 3.1-1. This method was based on Loxley and Vincent (1998)'s method of preparing PMMA microcapsules with liquid cores.
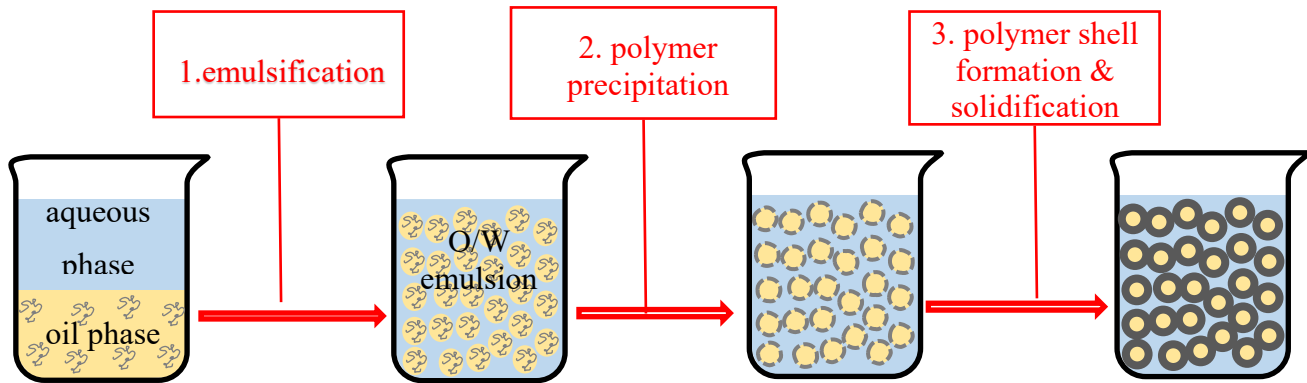
Figure 3.1-1 Schematic of the polymer shell oil core microcapsules preparation process

Firstly, the aqueous phase was prepared by dissolving 1.4g (28%wt) C_{16}TAB in 500ml water. The oil phase was prepared by dissolving 11.3g (5%wt) PEMA in a mixture of 183g (81%wt) DCM and 31.6g (14%wt) toluene.

Secondly, 7 mL polymer solution (the oil phase) was added into an equivalent volume of CTAB solution (the aqueous phases) in a 40 mL glass vial. The oil/water mixture was then emulsified using an IKA T25 digital Ultra-Turrax homogeniser at 15,000 rpm for 2 minutes. The formed O/W emulsion was transferred to a 250 mL beaker and stirred magnetically at 400 rpm on an IKA-Werke stirrer while a further 86 mL aqueous CTAB solution was added to the emulsion gently. The addition of the aqueous CTAB solution accelerates the extraction and evaporation of DCM out of the oil phase. The diluted O/W emulsion was left stirred at 400 rpm for 24 hours at ambient temperature, allowing the polymer precipitation at the o/w interface and formation of the polymer shell microcapsules.

The resulting polymer capsules were "washed" to remove the excessive CTAB from the system. The washing step was performed by separating the capsules from the aqueous CTAB solution via centrifugation (Heraeus Megafuge R16) at 7000 rpm for 2 minutes. After centrifugation, the supernatant was carefully removed, and the polymer capsules were redispersed in 40 mL of Milli Q water. The washing step was repeated two times before the cleaned polymer capsules were redispersed in 25 mL of water.

3.1.2 Au NPs Synthesis

3.1.2.1 Materials

The following chemicals were purchased from Sigma-Aldrich and were used as received.

- Gold (III) chloride hydrate ($HAuCl_4 \cdot H_2O$), CAS 27988-77-8, molecular weight 339.79

- Hydrochloric acid (HCl, 37% in H2O), CAS 7647-01-0

- Sodium hydroxide, CAS 1310-73-2

- Sodium borohydride ($NaBH_4$), CAS 16940-66-2

3.1.2.2 Synthesis method

The synthesis of Au NPs was based on the method used by Martin et al. (2010). Firstly, an aqueous stock solution of 50mM gold chloride anions ($AuCl_4^-$) was prepared by adding 169.895mg of $HAuCl_4 \cdot H_2O$ in 10mL of the same molar amount of HCL, and an aqueous stock solution of 50mM borohydride anions (BH_4^-) was prepared by dissolving 94.597mg of $NaBH_4$ granules in 50mL of the same molar amount of NaOH.

1mL of $AuCl_4^-/H^+$ solution and 3mL of BH_4^-/OH^- solution was added into 100mL water while stirring on an IKA RH basic KT/C hot plate at ambient temperature at a stirring speed of 400rpm to achieve uniform mixing.

The solution changed colour from light yellow to orange immediately, and then to red, while the mixture was stirred for 10 min to release hydrogen gas molecules. The concentration of formed Au NPs suspension was 0.5mM.

3.1.3 Au NPs adsorption to polymer microcapsule surface

0.5mL of polymer shell capsule suspension prepared in Chapter 3.1.1.2 was added dropwise into 6mL Au NPs suspension while stirring on an IKA RH basic KT/C hot plate at ambient temperature at a stirring speed of 800rpm for 10 minutes to allow the adsorption of Au NPs onto the polymer capsule surface.

The resulting Au NPs- attached polymer microcapsules were collected and washed to remove the excessive Au NPs. The wash step was carried out via centrifugation (Heraeus Megafuge R16) at 7000 rpm for 2 minutes. After centrifugation, the supernatant was carefully removed, and the Au NPs adsorbed polymer capsules were redispersed in 40 mL of Milli Q water. The washing step was repeated three times before the cleaned Au-loaded polymer capsules were redispersed in 2mL of water.

3.1.4 Electroless silver plating on polymer shell capsules

3.1.4.1 Materials

- Silver nitrate ($AgNO_3$), purchased from Fisher Scientific, CAS 7761-88-8
- Formaldehyde solution (HCHO), 37% in H2O, CAS 50-00-0

- Ammonia solution, 25% in H_2O, purchased from Merck KGaA, CAS 105432

3.1.4.2 Synthesis method

2mL of the Au NPs adsorbed polymer capsule suspension was added dropwise into an aqueous $AgNO_3$ solution under gentle agitation. The total amount of mixture was controlled to be 20mL so that the concentration of Ag ions is 0.25mM. Then 50μL HCHO was added into the mixture to reduce the Ag ions. The pH value is controlled at ~10 by adding an ammonia solution. The colour of the mixture changed to dark brown in 10 minutes which indicated the formation of silver coating.

The resulting silver shell microcapsules were washed via centrifugation two times before being redispersed in MilliQ water.

3.2 Equipment, techniques, and methodologies used for the microcapsules characterisation

3.2.1 Size and size distribution of the microcapsules

Laser diffraction

In this study, a Malvern Mastersizer Hydro 2000SM has been used to determine the size and size distribution of polymer and silver shell microcapsules. Mastersizer uses the technique of laser diffraction, which is a simple and non-invasive technique to determine the size and size distribution of the microcapsules. The principle of laser diffraction is that the laser beam passes through the sample suspension and is scattered by colloidal particles. The angle and the intensity of light scattering from the particles were measured, and the

particle size was obtained from the light scattering information (Hulst and van de Hulst, 1957, Bohren and Huffman, 2007).

Optical and electron microscopy

In addition to the Mastersizer, an Olympus BX51 optical microscope (with LMPlanFLN 50x lens) and an LEO 1530 Gemini Field Emission Gun Scanning Electron Microscopy (FEGSEM) were used to confirm the size of the polymer and silver shell capsules during the capsules morphology studies.

3.2.2 Morphology of the microcapsules

3.2.2.1 Morphology prediction

Interfacial tension measurement

The morphology of the polymer microcapsules was predicted via the interfacial tension between oil, water, and polymer phases. The interfacial tension was measured using the pendant drop method via a KSV CAM200 tensiometer (Biolin Scientific, Finland). The measurements were conducted at room temperature using droplets close to the critical detachment volume and a horizontal needle tip with an inner diameter of 0.51 mm. The interfacial tension was calculated from the image of the drop via the pendant drop shape analyser.

Contact angle measurement

When determining the interfacial tension between oil and polymer phases, one approach used the final components of polymer capsules as the polymer phase. The oil surface tension and the contact angle of the oil droplets on spin-coated PMMA film were measured using the sessile drop method via the same KSV CAM200 tensiometer. The mean contact angle value was obtained based on the

average of five drops at different positions on the film. Interfacial tension was calculated from these the surface tension and the contact angle using equation 3.2-1.

$$\gamma_{OP} = \gamma_P + \gamma_O cos\theta \qquad\qquad \text{Equation 3.2-1}$$

Where

γ_{OP} = the polymer-oil interfacial tension

γ_P = the polymer surface tension

γ_O = the oil surface tension

θ = contact angle of oil on PMMA coated film

3.2.2.2 Morphology confirmation

Optical microscopy

The resulting polymer and silver shell microcapsules were observed under an Olympus BX51 optical microscope (with LMPlanFLN 50x lens) to confirm the core-shell structure initially. Optical microscopy has the advantage of low cost, simple sample preparation and straightforward observation of the samples. However, its resolution is limited to around 0.25 μm. More morphology details were studied under an electron microscope.

Scanning Electron Microscopy (SEM)

Electron microscopy is widely used in characterising the morphology and structure of the materials by detecting the interaction between electrons and sample particles. Small wavelength electrons were used to achieve greater resolution (up to 3.5 - 6nm). The information on sample surface (1-30 nm) and sub-top (10-100 nm) topography can be obtained via secondary electrons (SE) and backscattered electrons (BSE), respectively. BSE mode provides better depth

resolution but poorer lateral resolution than SE mode. An LEO 1530 Gemini Field Emission Gun Scanning Electron Microscopy (FEGSEM) was used to confirm the morphology of the polymer and silver capsules.

Energy Dispersive X-ray (EDX)

EDX mapping uses the X-rays emitted by low-energy electrons produced up to 1 μm below the surface. The energy and wavelengths of x-rays emitted by individual atoms are different. Therefore, the x-rays can be used for elemental analysis (Brydson and Hammond, 2005, Goodhew et al., 2000, Brydson). An Oxford Instruments INCA 350 Energy Dispersive X-ray Spectroscopy (EDS) with 80mm X-Max SDD detector, which is installed in FEGSEM was employed to analyse the chemical composition of Ag coated microcapsules.

3.2.3 Au NPs size and size distribution

The size and size distribution of the synthesised Au NPs was analysed using both Ultraviolet-visible spectroscopy (UV-Vis) and TEM micrographs combined with ImageJ software.

Ultraviolet-visible spectroscopy (UV-vis)

UV-vis uses light in visible and adjacent ranges to characterise the samples. The intensity of the light was measured before and after passing through a sample. The difference between the intensity was expressed as absorbance. It was found that the Au NPs showed the typical plasmon peak around ~510 nm, which was similar to the previous study (Zimbone et al., 2011, Zuber et al., 2016, Mohd Sultan and Johan, 2014).

An Agilent 8453E UV-vis spectroscopy was used to analyse the synthesised Au NPs in water, stabilised by physisorbed boron-based anions. The result is shown in Figure 3.2-1. It shows that the resulting Au NPs in water are monodispersed with the plasmon peak around ~510 nm.
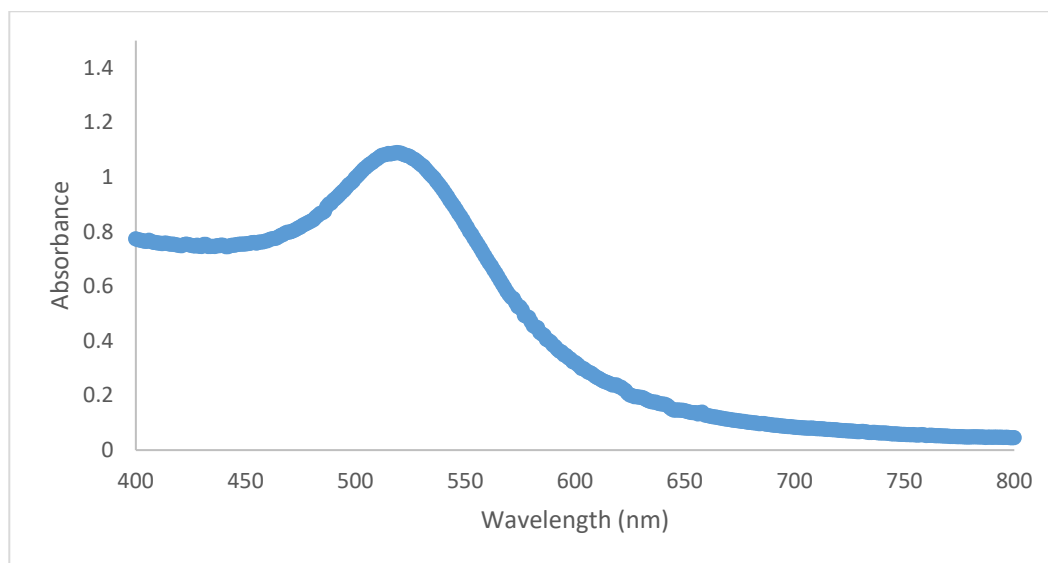
Figure 3.2-1 UV-Vis result of Au NPs with a concentration of 0.5 mmol/dm^3, showing a typical plasmon peak around ~510 nm, indicates the resulting Au NPs are monodispersed

Transmission Electron Microscopy (TEM)

An FEI Tecnai TF20 Field Emission Gun Transmission Electron Microscopy (FEGTEM) fitted with HAADF detector, and Gatan Orius SC600A CCD camera was used to characterise the morphology and the size and size distribution of Au NPs. Au NPs adsorbed polymer capsules were also studied using FEGTEM.

Similar to SEM, TEM also employs the electron beam to interact with the specimen but with a high accelerating voltage (typically 100-400 kV). The higher

accelerating voltage results in a short wavelength and high resolution (which reaches 0.1 nm). The higher voltage also increases the depth of penetration of the electrons into the specimen. In this way, TEM is used to investigate the internal structure of thin specimens.

The synthesised Au NPs were loaded on the TEM grids and air-dried. Typical micrographs of Au NPs taken via TEM are shown in Figure 3.2-2.
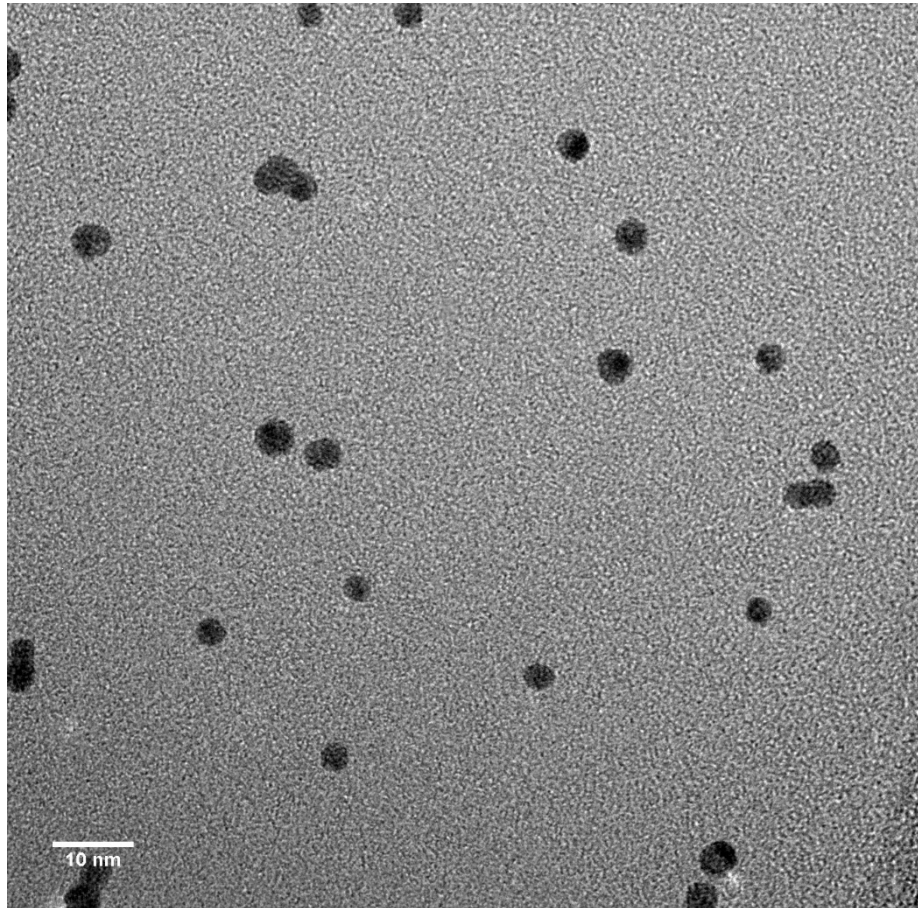
Figure 3.2-2 TEM micrograph of synthesised Au NPs with 0.5 mmol/dm^3 concentration

The average size of the Au NPs was measured based on 50 Au NPs and five

measurements on each Au NPs using ImageJ software. The average size of the

Au NPs and the size distribution are shown in Figure 3.2-3. It was found that the

resulting Au NPs were monodispersed, and the average size of Au NPs is 3.4

±0.4 nm.
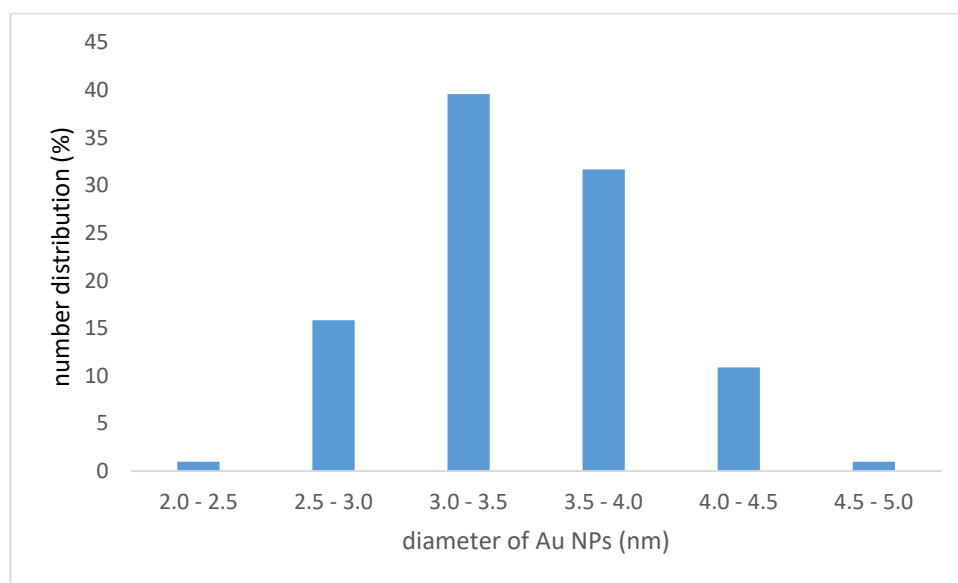
Figure 3.2-3 Size and size distribution of Au NPs with a gold concentration of 0.5 mmol/dm³ obtained through analysis of TEM micrographs via ImageJ. The Au NPs with a diameter of 3.0-3.5 shows the largest number count, i.e. 40%

3.2.4 Au NPs adsorption density on polymer capsules surface

Zeta potential (ZP) measurement

A Malvern Nano-ZS Zetasizer was used in characterising the synthesised Au

NPs, and in the study of the influence of surfactant on the Au NPs adsorption to

the polymer capsule surface. The Zetasizer measure the zeta potential of the Au

NPs suspension by determining the electrophoretic mobility of the particles. In colloidal dispersion, the zeta potential refers to the potential at the interface of the particles' electrostatic double layers (stern layer and diffuse layer). When the particles show large negative or positive zeta potential, particles tents to repel each other and form a stable system. When the zeta potential is low, the particles might attract each other and cause agglomeration.

A set of samples of Au NPs mixed with surfactant at different ratios was prepared, and the zeta potential was measured to study the stability of the suspension.

Ultraviolet-visible (UV-Vis) spectroscopy

The Agilent 8453E UV-vis spectroscopy was used to analyse the Au NPs adsorption density.

A set of Au NPs samples of known concentration from 1-100 mg/dm^3 were prepared, and the UV-vis results are plotted in Figure 3.2-4. This curve was used as the calibration curve to determine the Au NPs concentration in the supernatant of Au NPs adsorbed polymer capsules.
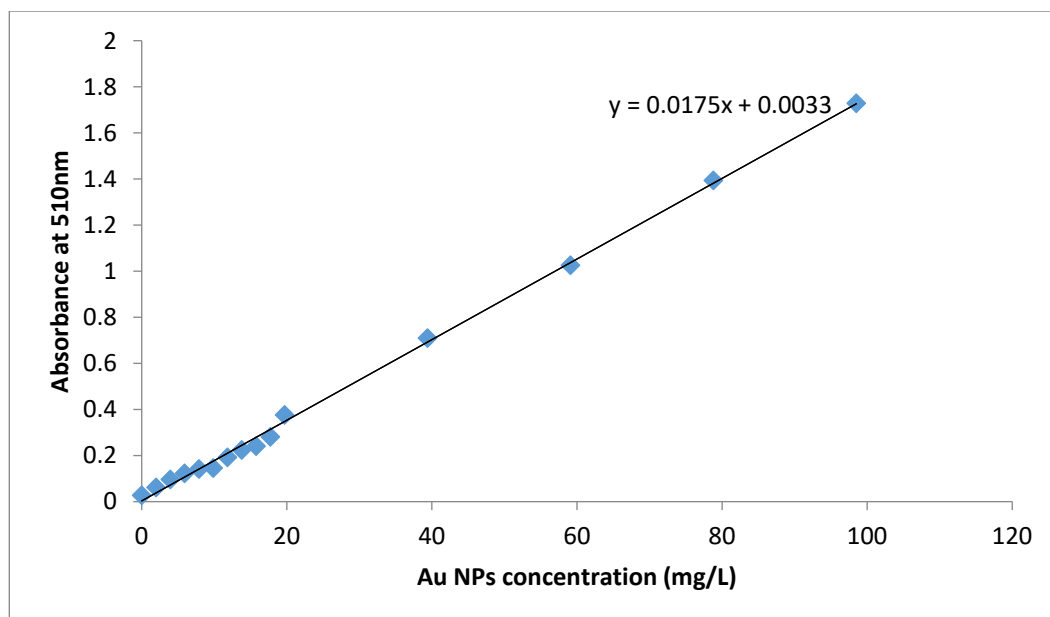
Figure 3.2-4 Calibration curve of Au NPs

Thermal gravimetric analysis (TGA)

TGA is a type of thermal analysis in which the mass of the sample is measured over time when the temperature increases. It gives information on the microcapsule mass change when the polymer is under thermal decomposition.

A Perkin-Elmer, Pyris 1 thermogravimetric analyzer was used to detect the Au NPs adsorption density on the polymer capsules surface by comparing the weight of Au NPs adsorbed polymer capsules at 100 and 800 °C.

Polymer capsules were mixed with Au NPs aqueous suspension of different concentrations for Au NPs adsorption. The capsules were rinsed after the Au NPs adsorption and air-dried before TGA analysis. The analysis was run from room temperature to 900 °c, with a temperature ramp rate of 1°c per minute. At 100°c, 200°c and 400°c, the temperature was held for 60 minutes before the next increment to allow the complete decomposition of water and the polymer.

TEM

The FEI Tecnai TF20 Field Emission Gun Transmission Electron Microscopy

(FEGTEM) was also used to observe the Au NPs adsorption density on the

polymer capsule surface.

3.2.5 Shell thickness of the microcapsules

Focused Ion Beam Scanning Electron Microscopy (FIBSEM) for polymer shell

An FIE Nova200 Duelbeam FIBSEM was used to cut through the sputter-coated

polymer capsules. The shell thickness could be measured at the cross-section. An

example SEM micrograph is shown in Figure 3.2-5.
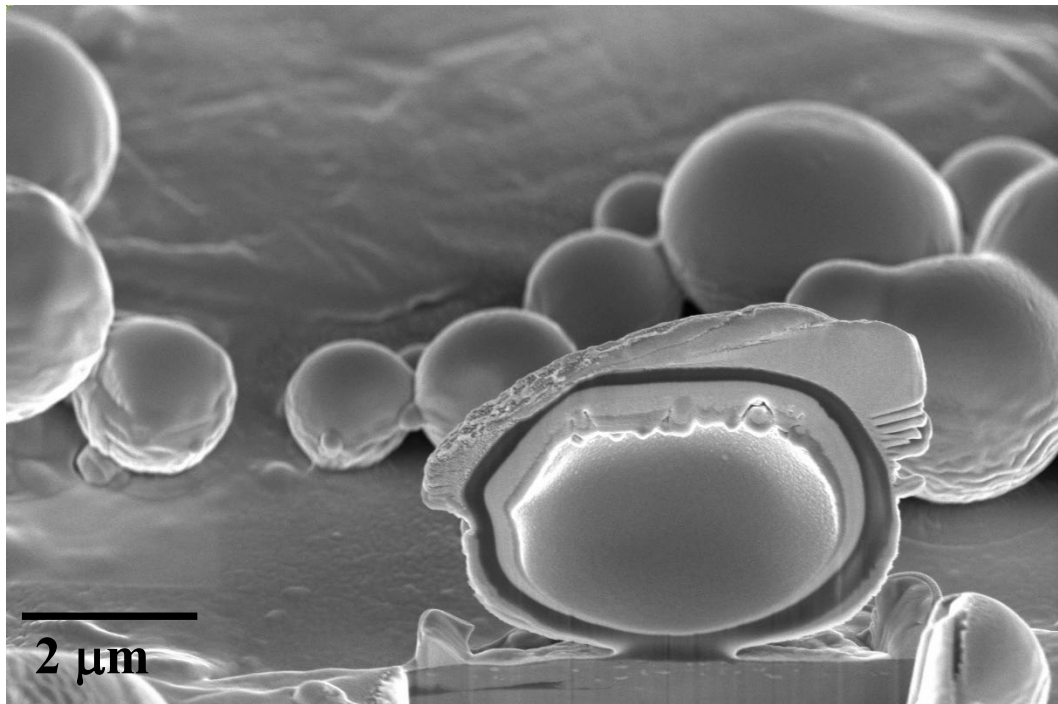
Figure 3.2-5 Cross section of PMMA-HS microcapsules with a core-shell ratio
of 1.0 via FIBSEM

In Figure 3.2-5, the cross-section of a PMMA shell HS core microcapsules was obtained via FIBSEM. The shell thickness (the dark area) was measured using Image J software. However, it was challenging to get a decent cross-section without a tilt angle, and it was time-consuming to conduct quantity FIBSEM analysis. Therefore, the theoretical calculation results of the polymer shell thickness were used in the later discussion, while the results obtained from FIBSEMM analysis were used for confirmation. The obtained measurement distribution was plotted in Figure 3.2-6.
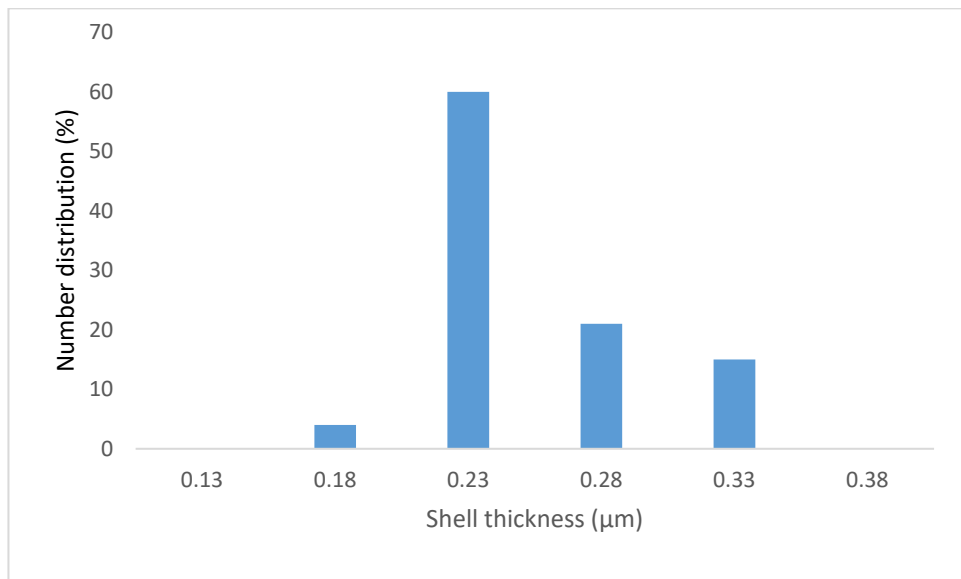
Figure 3.2-6 Shell thickness distribution of PMMA-HS microcapsules with the core-shell ratio of 1.0 obtained through analysis of SEM micrographs via ImageJ. The polymer microcapsules with a shell thickness of 0.23μm show the largest number count, i.e. 60%

However, it was challenging to get a decent cross-section without a tilt angle, and it was time-consuming to conduct quantity FIBSEM analysis. Therefore, the theoretical calculation results of the polymer shell thickness were used in the later

discussion, while the results obtained from FIBSEMM analysis were used for confirmation.

TEM with a microtome technique for silver shell

The microtome technique was used to get the cross-section of synthesis silver shell microcapsules. The clean and air-dried silver capsules were mixed in Struers Epofix and the epoxy resin. After the resin was completely dry and solidified, an Agar Scientific microtome blade Y515ZA was used to cut the samples into slices and then the slices were transferred to TEM grids for later analysis.

3.2.6 Retention and release of the oil core

Gas Chromatography (GC)

Gas chromatography (GC) is an analytical technique that separates and identifies volatile components. It can be used for either quality or quantity analysis. The retention and release of the oil core content of both polymer and silver shell capsules were analysed using GC.

For the analysis, a Perkin Elmer Clarus 580GC with Elite-1 capillary column (length 30m, internal diameter 0.25mm) was used. The temperature ramp rate was 20°C/minute from 50 to 300°C, and the flow rate was 2mL/min.

A set of oil core samples (toluene and hexylsalicylate in this study) with known concentrations was prepared as the standards for quantitive analysis. The GC results (the peak area) were plotted in Figure 3.2-7 and Figure 3.2-8 as the standard curves.
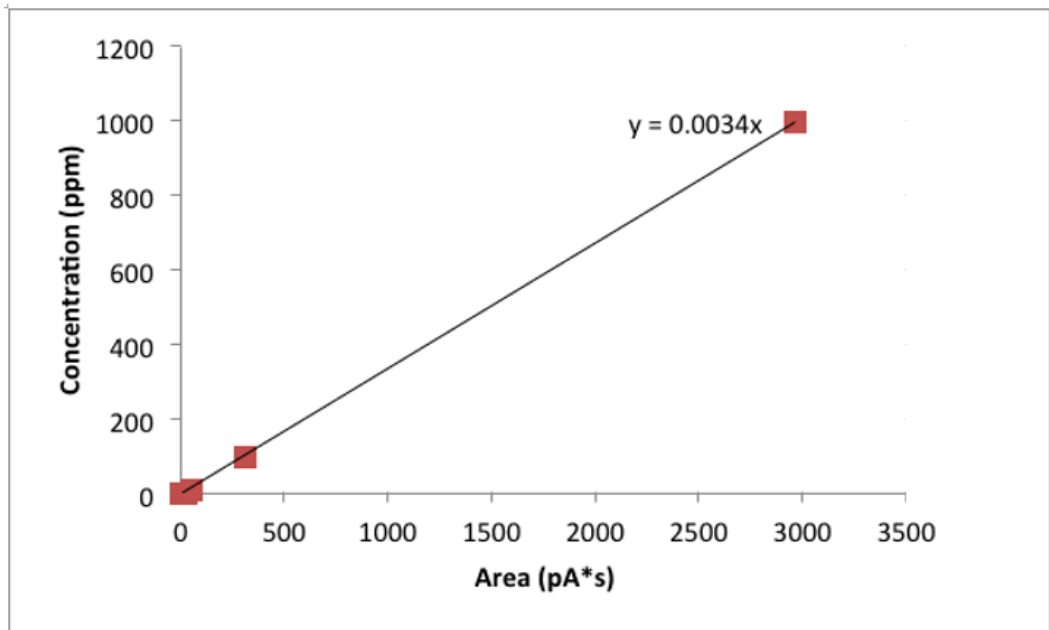
Figure 3.2-7 Standard curve of toluene
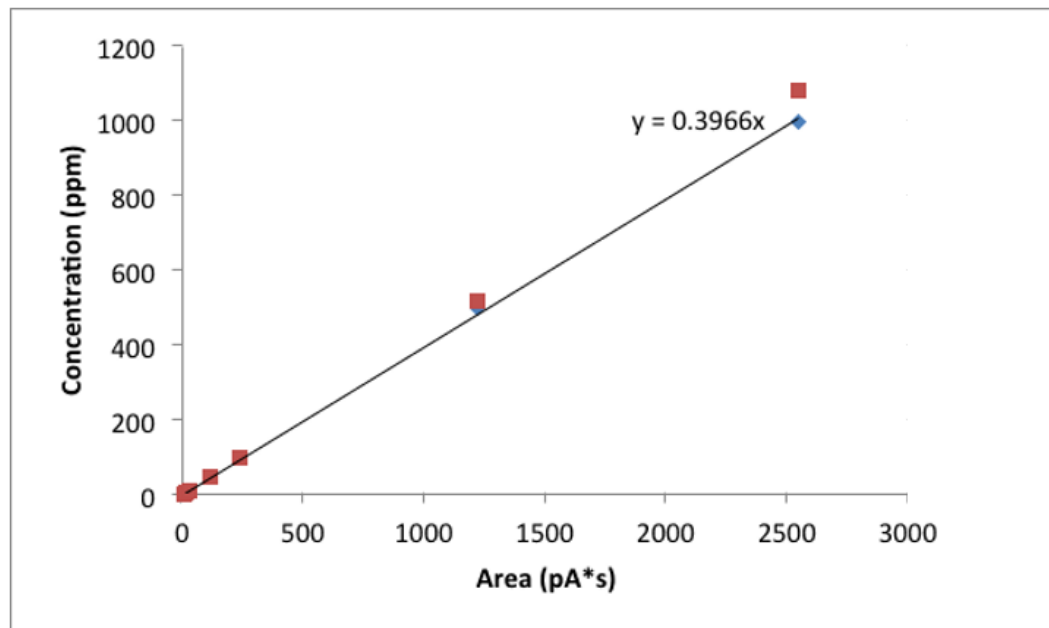
Figure 3.2-8 Standard curve of hexylsalicylate

After the wash cycles, the cleaned microcapsules were redispersed in 2mL of

MilliQ water. Bulk samples were prepared by adding 8mL of absolute ethanol to

the 2mL of microcapsule suspension. 1mL of the capsule ethanol mixture was taken from the bulk samples at known time intervals over a period of two weeks and centrifuged at 7000rpm for 2 minutes. The capsules were separated from the liquid, and the supernatant was used for GC analysis.

After two weeks, the silver capsules in bulk samples were placed on a glass slide and crushed using another glass slide. The crushed silver capsules were immediately rinsed back into the conical microtube for centrifugation. The supernatant of the crushed silver capsules in the ethanol-water mixture was used for GC analysis.

3.2.7 Mechanical strength

The deformation behaviour and mechanical strength (breaking stress) of individual microcapsules were investigated using a micromanipulation technique in the chemical engineering laboratory at the University of Birmingham. The technique is based on diametrical compression, where a single particle is crushed between two parallel surfaces and the force required to cause rupture is measured.

In this study, the polymer and silver microcapsules' mechanical strength and deformation behaviour were investigated through the force-displacement profile and breaking stress. An Aurora Scientific 402A force transducer is employed to measure the force, and the probe travels at a constant speed of $2\mu m/s$ for all the experiments performed. The compressive displacements were corrected for the total compliance of the transducer and the probe.

3.3 Calculations

3.3.1 The surface area of polymer capsules

The total surface area of the polymer capsules was calculated from the size and size distribution data collected from MasterSizer measurement. Figure 3.3-1 shows a size distribution based on volume contribution at bin limit result obtained from Mastersizer.
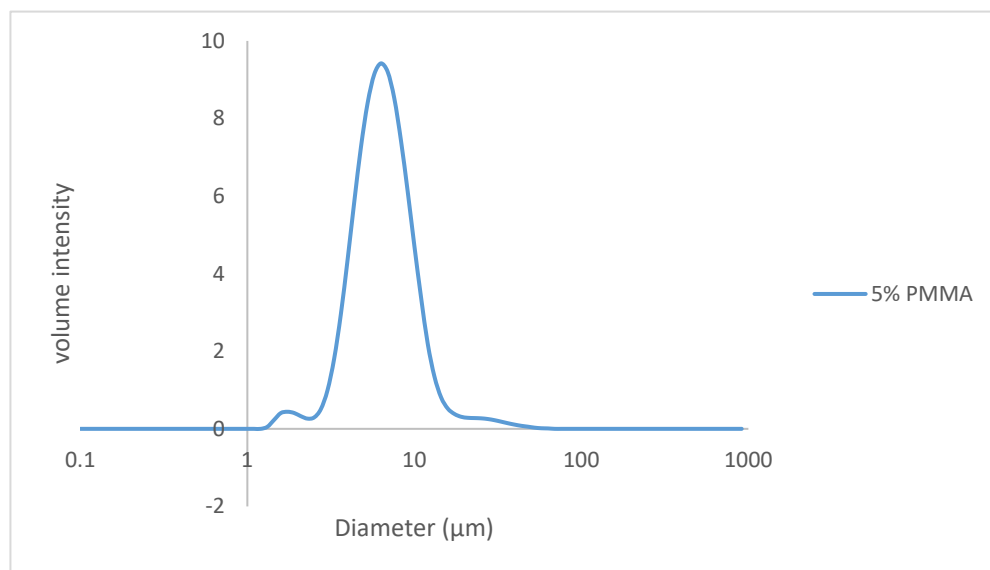
Figure 3.3-1 A sample measurement of size and size distribution of PMMA capsules with 5% PMMA. The diameter of the capsules at bin limit (D_{lim}) is based on volume contribution at bin limit ($V_{\%}$)

At a certain diameter range (bin limit), the number of capsules of bin limit (N_{lim}) could be worked out by dividing the actual volume contribution at bin limit (V_{lim}) by the volume of the individual capsule at bin limit (V_{cap}).

$$N_{lim} = \frac{V_{lim}}{V_{cap}}$$

With the known total volume of polymer and oil in disperse phase (V_T) and

measured percentage of the volume contribution at bin limit ($V_\%$), V_{lim} can be calculated as follows.

$$V_{lim} = V_\% \times V_T$$

While V_{cap} could be worked out via the diameter of the capsules at bin limit (D_{lim}), assuming all the capsules were spheric in shape.

$$V_{cap} = \frac{4}{3}\pi \left(\frac{D_{lim}}{2}\right)^3$$

Therefore the number of capsules of bin limit could be worked out

$$N_{lim} = \frac{V_{lim}}{V_{cap}} = \frac{V_\% \times V_T}{\frac{4}{3}\pi \left(\frac{D_{lim}}{2}\right)^3}$$

The surface area of an individual capsule at bin limit (S_{cap}) can also be worked based on D_{lim}.

$$S_{cap} = \pi D_{lim}{}^2$$

The surface area of all the capsules at bin limit (S_{lim}) could be obtained via S_{cap} times N_{lim}, and the total surface area of all the capsules can be obtained using equation 3.3-1.

$$S_{lim} = S_{cap} \times N_{lim}$$

$$= \pi D_{lim}{}^2 \times \frac{V_{lim}}{V_{cap}}$$

$$= \pi D_{lim}{}^2 \times \frac{V_\% \times V_T}{\frac{4}{3}\pi \left(\frac{D_{lim}}{2}\right)^3}$$

$$= \frac{6 V_\% V_T}{D_{lim}}$$

$$S_{total} = \sum_{D_{lim}=0}^{\infty} \frac{6V_\%V_T}{D_{lim}} \qquad\qquad \text{Equation 3.3-1}$$

where

S_{lim} = surface area of all the capsules at bin limit

S_{cap} = surface area of individual capsule at bin limit

N_{lim} = numbers of the capsules at bin limit

D_{lim} = capsule diameter at bin limit

V_{lim} = actual volume contribution at bin limit

V_{cap} = volume of individual capsule at bin limit

$V_\%$ = percentage of the volume contribution at bin limit

V_T = total volume of polymer and oil in disperse phase

S_{total} = total surface area of the capsules

3.3.2 Shell thickness of polymer capsules

The shell thickness of polymer capsules was obtained using theoretical

calculation. The ImageJ measurement based on FIBSEM cross-section

micrographs was used to confirm this calculation results. The schematic of a

polymer shell oil core microcapsule is shown in Figure 3.3-2. The polymer shell

thickness is calculated by deducting the oil core radius from the polymer

microcapsule radius $(r' - r'')$.

The polymer capsule radius (r') is obtained through the halving diameter of the

capsules, which was measured using Mastersizer, as mentioned in 3.3.1.
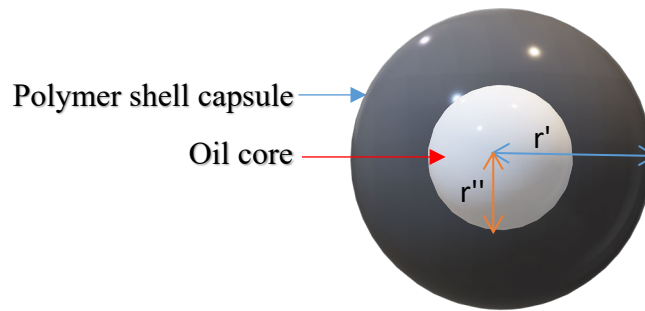
Figure 3.3-2 Schematic of a polymer shell oil core microcapsule

The oil core radius (r'') of the capsules at a certain diameter (bin limit), can be calculated from the volume of individual oil core at bin limit (V_{core}) using

$$r'' = \sqrt[3]{\frac{3V_{core}}{4\pi}}$$

Equation 3.3-2

The volume of individual oil core at bin limit (V_{core}) can be calculated using equation 3.3-3 and equation 3.3-1.

$$V_{core} = \frac{V_{lim}}{N_{lim}} = \frac{V_{total} \times oil\% \times V_\%}{N_{lim}}$$

Equation 3.3-3

where

Vcore = volume of individual oil core at bin limit

Vlim = actual volume contribution of oil at bin limit

Nlim = number of capsules at the bin limit

Vtotal = total volume of polymer and oil droplets in the final capsule

Oil% = oil percentage in polymer oil droplets in final capsule (assuming total removal of DCM)

V% = percentage of the capsule volume contribution at bin limit

The numbers of the capsules at the bin limit were calculated using the method described in 3.3.1.

3.3.3 Au NPs adsorption density on the polymer capsule surface

Au NPs adsorption density was expressed using the input ratio of Au NPs to polymer capsule surface. It was calculated using the Au NPs volume and concentration used in Au NPs adsorption and the total surface area of the polymer capsules, using Equation 3.3-2.

$$\beta = \frac{m_{Au}}{S_{total}} = \frac{C_{Au} \times V_{dis} \times M_{Au}}{S_{total}} \qquad \text{Equation 3.3-4}$$

where

β = input ratio of the Au NPs to polymer capsule surface area

m_{Au} = mass of the Au NPs used

C_{Au} = molar concentration of the Au NPs used

V_{dis} = volume of the Au NPs dispersion used

M_{Au} = molar mass of the Au NPs

S_{total} = total surface area of the capsules

3.3.4 Input ratio of CTAB to Au NPs

The input ratio of CTAB to Au NPs was calculated based on the mass of CTAB and the surface area of the Au NPs used in the experiment. The total volume of the Au NPs used in the experiment was calculated using Equation 3.3-3. Based on the total volume, the numbers of the Au NPs used were calculated using Equation 3.3-4, and the input ratio of CTAB to Au NPs was obtained using equation 3.3-5.

$$V_{Au} = \frac{m_{Au}}{\rho_{Au}} = \frac{V_{dis} \times C_{Au} \times M_{Au}}{\rho_{Au}} \qquad \text{Equation 3.3-5}$$

where

V_{Au} = volume of the Au NPs used

m_{Au} = mass of the Au NPs used

ρ_{Au} = density of the Au NPs

V_{dis} = volume of the Au NPs dispersion used

C_{Au} = molar concentration of the Au NPs

M_{Au} = molar mass of the Au NPs

$$N_{Au} = \frac{V_{Au}}{V_{NP}} = \frac{V_{Au}}{\frac{4}{3}\pi(\frac{D_{Au}}{2})^3}$$

Equation 3.3-6

where

N_{Au} = numbers of the Au NPs used

V_{Au} = volume of the Au NPs used

V_{NP} = volume of individual Au NP

D_{Au} = mean diameter of the Au NPs

$$R = \frac{m_{CTAB}}{S_{Au} \times N_{Au}} = \frac{C_{CTAB} \times V_{CTAB} \times M_{CTAB}}{\pi D_{Au}^2 \times N_{Au}}$$

Equation 3.3-7

where

R = input ratio of the CTAB to Au NPs surface area

m_{CTAB} = mass of the CTAB used

S_{Au} = surface area of individual Au NP

N_{Au} = numbers of the Au NPs used

C_{CTAB} = molar concentration of the CTAB used

V_{CTAB} = volume of the CTAB solution used

M_{CTAB} = molar mass of the CTAB

D_{Au} = mean diameter of the Au NPs

3.3.5 The surface density of silver microcapsules

The surface density of silver-shell microcapsules was expressed via the input ratio of Ag to capsule surface area. It was calculated using Equation 3.3-6.

$$R = \frac{m_{Ag}}{S_{total}} = \frac{C_{Ag} \times V_{dis} \times M_{Ag}}{S_{total}}$$
Equation 3.3-8

where

R = input ratio of the Ag to polymer capsule surface area

m_{Ag} = mass of the Ag used

C_{Ag} = molar concentration of the Ag salt used

V_{dis} = volume of the Ag salt dispersion used

M_{Ag} = molar mass of the Ag

S_{total} = total surface area of the capsules

3.3.6 Mechanical strength of single capsule

The mechanical strength of the microcapsule was expressed using the nominal rupture stress, and it was calculated using Equation 3.3-10. Rupture force (F_r) and the capsule diameter (D_{cap}) were measured using a micromanipulator.

$$\sigma_r = \frac{F_r}{S_{cap}} = \frac{F_r}{\pi D_{cap}^2}$$
Equation 3.3-9

where

σ_r = nominal rupture stress

F_r = rupture force

S_{cap} = surface area of the capsule

D_{cap} = diameter of the capsule

Chpater 4 Polymer shell microcapsules formation, core material selection and core/shell ratio selection

4.1 Introduction

This study aims to achieve long-term retention of the volatile, small molecular fragrance oil particles. This aim was attained by forming capsules with a polymer shell and fragrance oil core, followed by growing a thin layer of metal coating on the polymer surface. As a result of the small molecule weight of fragrance oil particles, it tends to penetrate the polymer membranes and fails to long-term retention. By growing a thin layer of metal coating on the polymer surface of the microcapsules, the rapid diffusion of small molecules was stopped by the barrier. Before growing the thin layer of metal coating, Au NPs were adsorbed to the polymer capsule surface as catalysts to facilitate the metal layer's growth. The whole process is described in Figure 4.1-1.
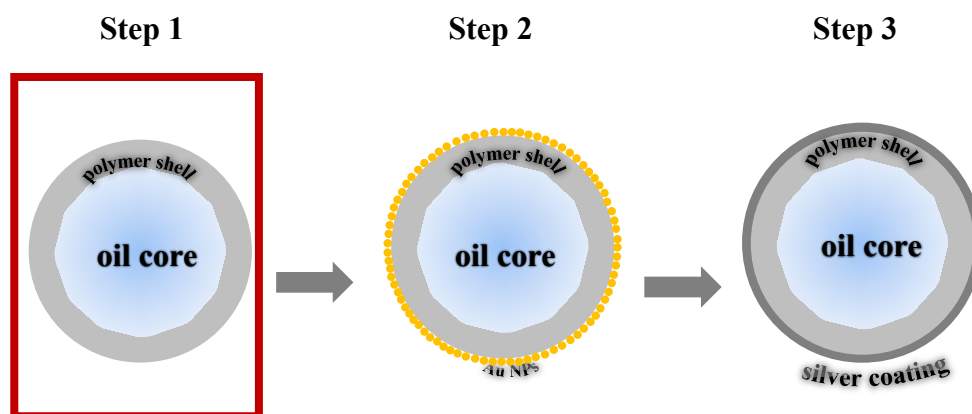
Figure 4.1-1 Silver shell microcapsules synthesis process: Step 1: Formation of polymer shell oil core microcapsule· Step 2: Au NPs adsorption to polymer microcapsule surface as the catalyst· Step 3: Silver coating on the polymer microcapsules' surface via electroless plating method

The work in this Chapter focused on preparing the core-shell structured capsules with a polymer shell and fragrance oil for the experiments in the following two chapters.

First, a model system of capsules with polymer shell oil core was prepared using solvent evaporation and extraction method. The prepared microcapsules were observed under an optical microscope and Scanning Electron Microscopy (SEM) and demonstrated a core-shell structure.

Then the elements which affect microcapsule morphology were investigated. It was reported that the morphology of microcapsule was affected by the interfacial tension and spreading coefficient between the oil, water and polymer phases (Tasker et al., 2016, Loxley and Vincent, 1998, Torza and Mason, 1970). By studying the interfacial tension between these three phases, the morphology of the microcapsules prepared using different polymers and fragrance oil combinations could be predicted.

Based on this morphology prediction, various fragrance oils were tested and selected as core to form desired core-shell structured capsules for the experiments in the following chapters. The effect of the core-shell ratio on the capsule diameter and polymer shell thickness was also studied in this Chapter.

4.2 Preparation of a model system of oil core-polymer shell microcapsules

The model system of oil core-polymer shell microcapsules used solvent evaporation and extraction method. This method was based on Loxley and Vincent (1998)'s study on PMMA shell and oil core microcapsules. In their

study, core/shell microcapsules were formed by controlled phase separation of PMMA within the droplets of an oil-in-water emulsion, providing hexadecane or decane was used as non-solvent and polymeric emulsifiers were employed.

In this study, PEMA was used as polymer shell material. PEMA has similar properties to PMMA but lower Tg. Tg of PEMA is 66 °C and PMMA is 105 °C. Lower Tg of PEMA enables the more straightforward preparation process of microcapsules. The heating step in Loxley and Vincent (1998)'s microcapsule preparation was therefore omitted in this study's capsule shell formation and solidification stage.

Toluene was chosen as the non-solvent in the model system in this study. Toluene is an aromatic hydrocarbon compound with a molecular weight of 92.14 g mol^{-1}. With its small molecular weight, toluene is volatile and not easy to be encapsulated and stored for long-term retention using conventional methods. Hence it became a good choice of core content in the model system as a substitute for the fragrance oil.

DCM is the good solvent for the polymer in the system. The polymer and oil were dissolved in DCM to form an oil phase. The solution of polymer, oil and DCM was diluted by an equivalent volume of aqueous solution of surfactant (CTAB), and emulsified under high-speed homogenisation. The resulting emulsion was diluted in 100ml of CTAB solution.

The low boiling solvent DCM was initially dissolved in the water. After it reached the saturation point of 1.38 g per 100 ml in water at 20 °C (Wexler et al., 2005, Wexler, 2014), the remaining DCM diffused to the air/water interface and

then evaporated. The addition of a large amount of water extracted DCM and speeded up its evaporation speed.

When the oil droplet composition reached the binodal boundary, the polymer phase separated and migrated to the oil/water interface. As the further removal of DCM in the polymer phase, the polymer PEMA dissolved in the DCM precipitated at the oil-water interface and formed a polymer film surrounding the oil droplet.

Core/shell microcapsules were formed when PEMA precipitated at the oil-water interface in the O/W emulsion while the good solvent DCM was evaporated and extracted. The oil phase of the emulsion contained PEMA, a good solvent for PEMA, i.e. DCM, and non-solvent toluene. The water phase contained MilliQ water and surfactant CTAB.

The O/W emulsion was formed by mixing an equivalent amount of oil and water phases and then homogenised the mixture using a high-speed stirrer.

In this experiment, a cationic surfactant $C_{16}TAB$ was used to help form and stabilise the oil droplets in the water. $C_{16}TAB$ contains quaternary ammonium cation as the hydrophilic head and the long hydrocarbon chain as the hydrophobic tail, as shown in Figure 4.2-1.
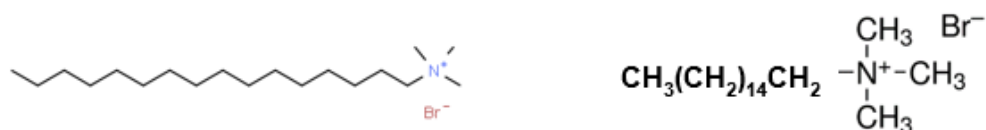
Figure 4.2-1 Structural formula and molecular structure of $C_{16}TAB$

During the mixing and homogenisation of the oil and water phases, $C_{16}TAB$ was adsorbed at the interface between two phases, with its hydrophilic head towards the aqueous phase and its hydrophobic tails towards the oil phase. It helped to form and stabilise the oil droplets in the water.

After O/W emulsion was formed, an additional amount of aqueous $C_{16}TAB$ solution was added to the emulsion. The whole diluted mixture was left stirred at a gentle speed at ambient temperature for 48 hours.

During this process, the good solvent DCM evaporated due to its low boiling point. As the decrease of DCM amount in the oil droplets, the polymer PEMA dissolved in the DCM precipitated at the oil-water interface and formed a polymer film surrounding the oil droplet. With the excessive amount of aqueous $C_{16}TAB$ solution added to the O/W emulsion, water extracted the DCM from the emulsion and accelerated polymer film formation.

After 48 hours, the polymer film was solidified, and toluene core PEMA shell microcapsules were obtained. The preparation process is schematised in Figure 4.2-2.
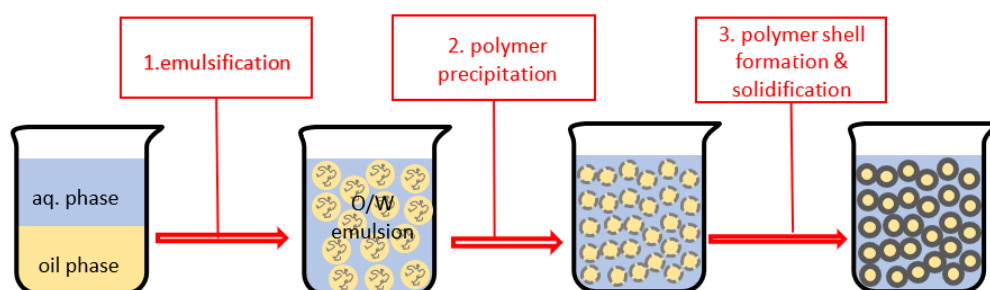
Figure 4.2-2 Synthesis of oil core-polymer shell microcapsules using solvent evaporation and extraction method. 1. equivalent amount of water and oil

phase was mixed and emulsified under high-speed homogenisation to form an emulsion of oil droplets in water. 2. The polymer dissolved in oil droplets precipitated at the oil water interface to form a polymer film surrounding the oil droplet, while the good solvent was extracted and evaporated from the emulsion. 3. Allow at least 48 hours of solvent evaporation time for polymer shell solidification in this case.

The resulting microcapsules were washed repeatedly to remove the excessive CTAB adsorbed at the surface. The microcapsules were dried in air and observed under SEM. From the images shown in Figure 4.2-3, the sphere-shaped microcapsules were observed in a), and a fractured PEMA capsule was observed in b), which indicated its hollow structure. Indentations were observed on the microcapsule surface in Figure 4.2-3 b). These appeared to be the collapse of the capsules under the high vacuum environment in the SEM. This phenomenon also indicated the hollow structure of the PEMA shell toluene core microcapsules.
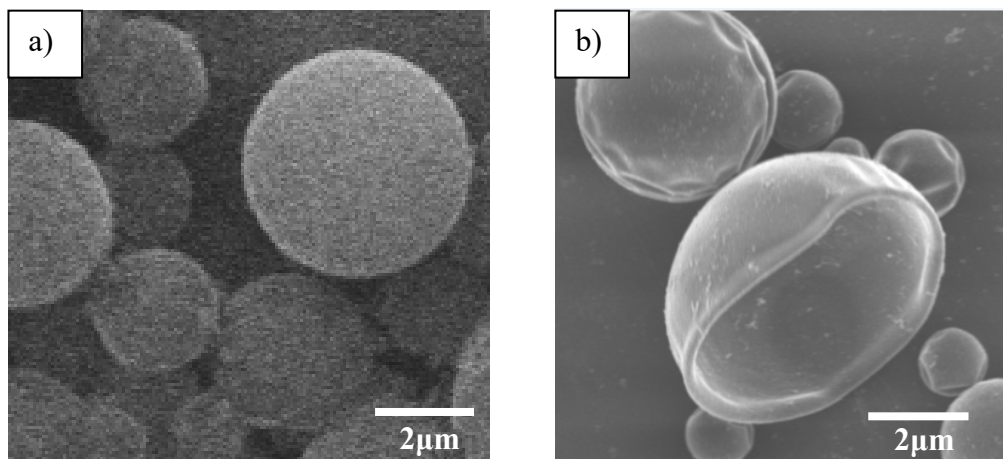
Figure 4.2-3 Micrographs of PEMA microcapsules under a scanning electron microscopy

The microcapsules observed in SEM micrographs in Figure 4.2-3 demonstrated spherical shape and hollow structure, i.e. core-shell structure. The morphology of the prepared microcapsules was affected by the interfacial tension and spreading coefficient between the oil, water and polymer phases. By studying the interfacial tension between these three phases, we could predict the morphology of the microcapsules prepared using different polymers and fragrance oil combinations.

4.3 Core material selection via microcapsule morphology prediction

As a small, volatile oil, toluene was proved to be a suitable model for typical fragrance oils in forming polymer shell oil core microcapsules and subsequent gold nanoparticles adsorption and secondary metal shell coating. However, its relatively high solubility in water, i.e. 526 mg/L at 25 deg C (Sanemasa et al., 1982), hindered its use for release testing. The fact that no toluene was detected from PEMA shell toluene core microcapsules through Gas Chromatography analysis indicates that toluene has been released during the process of solvent evaporation.

In this case, some commercially available fragrance oils were selected to substitute toluene, namely hexyl salicylate, cyclamen aldehyde, and dihydro-mercenol. Those fragrance oils are less volatile and have poorer water solubility than toluene, which are advantageous in the following core release test.

In the process of PEMA shell fragrance oil core microcapsules, PEMA was found not compatible with hexyl salicylate. The polymer used in the study was changed to PMMA.

4.3.1 Theory of morphology prediction

The resulting microcapsules have the possibility of various morphologies besides the desired core-shell structure. The possible morphologies are depicted in Figure 4.3-1. Alternative morphologies include acorn, where the polymer precipitates separately to the oil and a completed dissociation between the core and shell.

Core-shell   **Acorn**   **Dissociation**
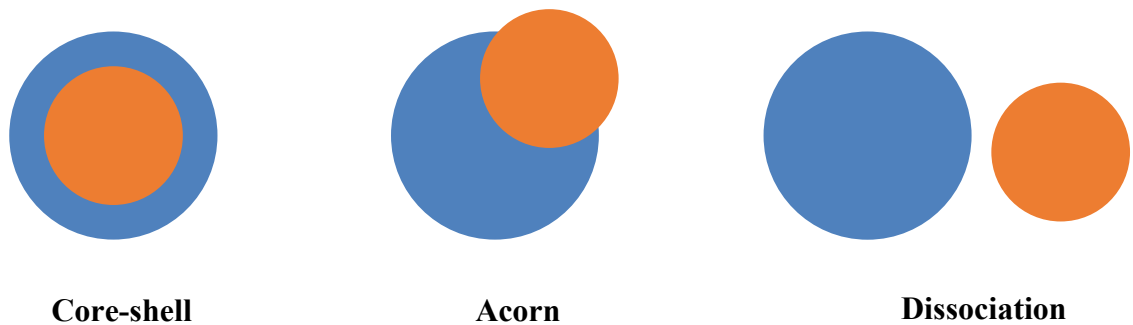
Figure 4.3-1 Schematics of different morphologies may occur in the formation of microcapsules

Torza and Mason (1970) studied the behaviour of systems where two immiscible liquid drops were suspended in a third immiscible liquid. The resulting equilibrium morphology could be predicted from the interfacial tension (γ) and spreading coefficient (s) between the three phases. The spreading coefficient is calculated from the interfacial tensions using Equation 4.3-1.

$$S_3 = \gamma_{12} - (\gamma_{23} + \gamma_{13})$$ Equation 4.3-1

Where γ_{12} is the interfacial tension between phase 1 and phase 2. As the convention phase 2 is usually the aqueous phase. Phase 1 is of the highest interfacial tension with water, i.e. polymer. Therefore in this study phase 1 is

defined as the polymer phase (short for $_p$), phase 2 is the aqueous phase (short for $_w$), and phase 3 is the oil core (short for $_o$). In terms of the negative spreading coefficient of the oil phase (S_o), a core-shell structure could be formed when the spreading coefficient of the polymer phase (S_p) is positive. The positive spreading coefficient of the aqueous phase (S_w) leads to a completed dissociation morphology. When all three coefficients are negative, an acorn shape is produced. These conditions are described in Table 4.3-1 as below.

Table 4.3-1 Conditions and predicted morphology

Conditions			Predicted morphology
$S_p < 0$;	$S_w < 0$;	$S_o > 0$	Core-shell
$S_p < 0$;	$S_w < 0$;	$S_o < 0$	Acorn
$S_p < 0$;	$S_w > 0$;	$S_o < 0$	Dissociation

4.3.2 Morphology prediction and confirmation

Various oil cores, including commercially available fragrance oils, have been used for the substitution of toluene. Before the preparation process, the interfacial tensions of oil, polymer and aqueous phases were measured using a pendant drop machine with KSV CAM200 system. When we decided on the interfacial tension between oil and polymer phases, two methods were considered. One approach is to use the final components of polymer capsules as the polymer phase. The surface tension of the oil droplets and the contact angle of the oil droplets on spin-coated PMMA film were measured using the sessile drop method. Interfacial tension was calculated from these two measurements. This method replicated the

final status of the resulting polymer microcapsules. Another way considered the fact that at point of polymer started to precipitate, DCM still presented in oil core. In this approach, the polymer phase was represented by dissolving PMMA in DCM, and the interfacial tension between phases was measured via the pendant drop method. The studies carried out by group members Tasker et al. (2016) show that using the final capsule components gives a more precise prediction of resulting morphologies out of the two approaches.

The interfacial tension and spreading coefficients between phases and the microcapsule morphology prediction based on these data are shown in Table 4.3-2.

Table 4.3-2 Interfacial tensions, spreading coefficients and morphology predictions of polymer capsules with different oil cores

Oils	γ_{ow} /mN.m^{-1}	γ_{pw} /mN.m^{-1}	γ_{op} /mN.m^{-1}	S_o	S_w	S_p	Predicted shape
Hexadecane	4.7 (±0.1)		14.2 (±0.1)	-27.7	-8.7	-0.7	acorn
Hexyl salicylate	3.3 (±0.3)	18.2 (±0.1)	16.0 (±3)	-30.6	-5.8	-0.8	acorn
Toluene	3.3 (±0.7)		14.3 (±0.4)	-29.2	-7.2	0.6	core-shell
Cyclamen aldehyde	1.8 (±0.2)		11.5 (±0.5)	-27.9	-8.5	4.9	core-shell

Dihydro-mercenol	2.7 (±0.1)		13.8 (±2)	-29.3	-7.1	1.7	core-shell

The prepared microcapsules with various oil cores were cleaned and dried. The capsules were observed using an SEM and used for later on oil core release study. The formed microcapsules are illustrated in Figure 4.3-2.
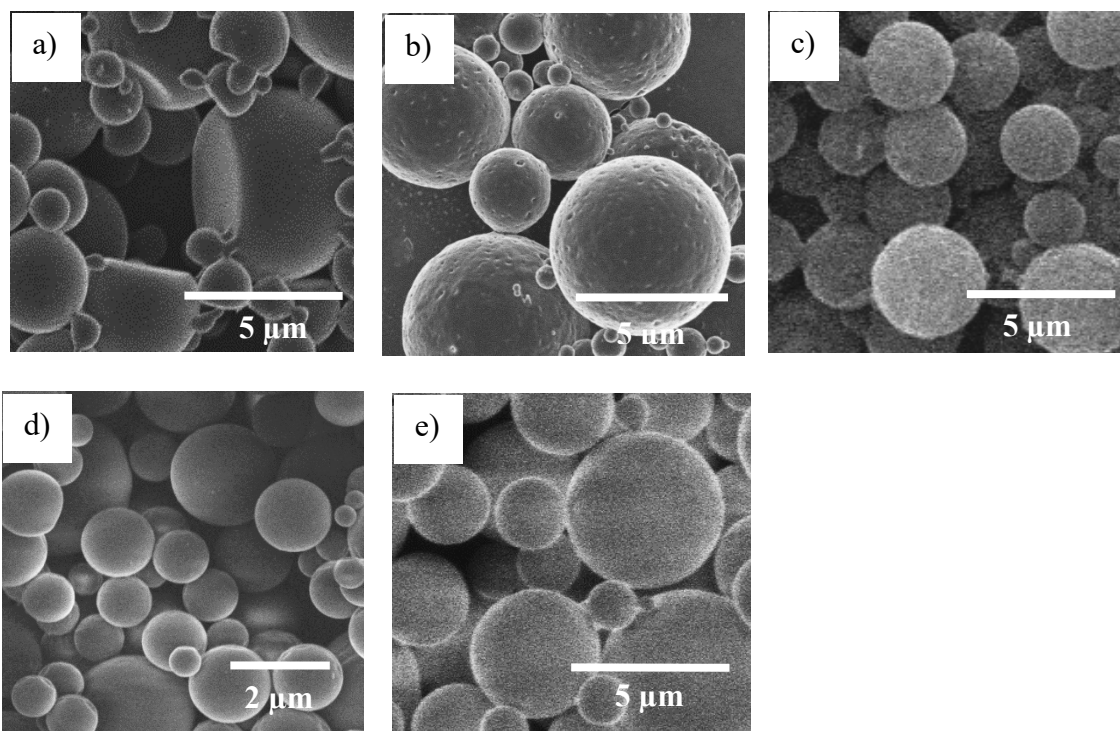
Figure 4.3-2 SEM micrographs of PMMA shell microcapsules stabilised by CTAB with various oil cores: a) hexadecane core; b) hexyl salicylate core; c) toluene core; d) cyclamen aldehyde core; and e) Dihydromercenol core. The predicted and confirmed morphologies of the microcapsules with various oil cores are listed in Table 4.3-1.

Table 4.3-3 Microcapsules prediction vs observation

Oils	Predicted shape	Observed shape
Hexadecane	acorn	acorn
Hexyl salicylate	acorn	core-shell
Toluene	core-shell	core-shell
Cyclamen aldehyde	core-shell	core-shell
Dihydro-mercenol	core-shell	core-shell

It was found that most morphology observations of resulting capsules followed the predictions except the one with hexyl salicylate (HS) core. The relatively

large error in interfacial tensions measurement between the oil and polymer phases might cause this exception. All the PMMA microcapsules formed a core-shell structure, except the ones with hexadecane core formed acorn shape. In the subsequent studies, commercially available fragrance oil hexyl salicylate was chosen as the oil core in all the encapsulation processes due to commercial consideration.

The prepared PMMA shell hexyl salicylate core microcapsules were observed under a Focused Ion Beam Scanning Electron Microscopy (FIB-SEM). With this technique, the capsules were cut through via the ion beam, and the capsules' cross-section was observed.
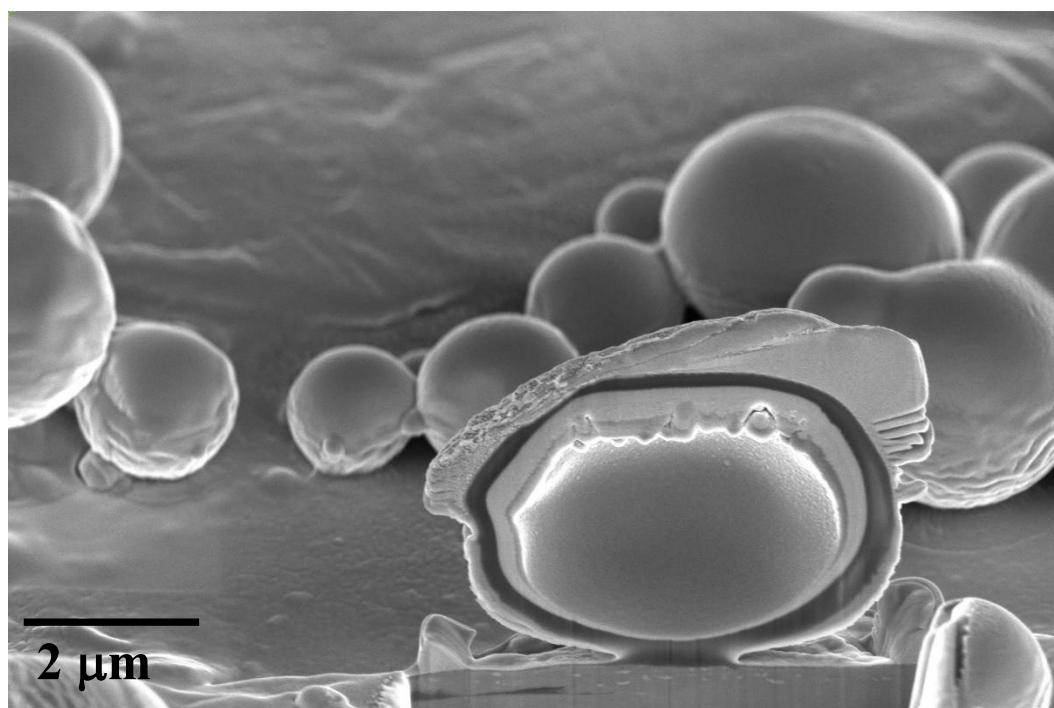
Figure 4.3-3 FIB-SEM micrograph of the cross-section of PMMA-HS microcapsules with a core/shell ratio of 1:1

The cross-section of a microcapsule is shown in Figure 4.3-3, where a core-shell structure of the microcapsule was observed. One thing worth mentioning is that the polymer shell thickness of the microcapsule was homogeneous in a capsule, it appeared thicker on the top part of the capsule in Figure 4.3-3 due to the tilted angle of the camera.

4.4 The influence of core/shell mass ratio on the encapsulated oil core retention and polymer shell thickness

Core/shell ratio is one of the factors which impact the microcapsule's core size and shell thickness. In preparation of PMMA shell hexyl salicylate core microcapsules, various core/shell ratios were investigated to see the effect on the formed capsules' properties. Two sets of experiments were designed in this part: in one set of experiments, the core material was kept at a constant mass ratio and the polymer mass varied; in another set of experiments, the polymer mass was constant, and the oil concentration changed.

4.4.1 The core/shell ratio influence on oil core retention

A set of microcapsule samples with 10 wt% of PMMA in the oil phase were prepared. The hexyl salicylate concentration in the oil phase varied from 10 to 30 wt%. After the capsule formation, the samples were cleaned and redispersed in 2 mL MilliQ water. 8 mL ethanol was added into the microcapsule suspension and redispersed. In the ethanol environment, the Hexyl salicylate encapsulated in PMMA capsules diffused into the ethanol-water mixture through the polymer shell along with the time, and it was detected via the GC technique. The GC samples were prepared by obtaining the supernatant of the capsules in an ethanol-

water mixture using centrifugation at different time intervals. The mass of HS

released from the polymer capsules to the supernatant was calculated via the

standard calibration curve described in Figure 3.28 in Chapter 3.2.6 . The released

HS mass was compared to the initial amount of HS in the emulsion used for

microcapsules preparation, and the percentage of the oil core released was

calculated by dividing the released HS mass by the initial HS mass in the

emulsion. The loss percentage of hexyl salicylate along the release time was

plotted in Figure 4.4-1.
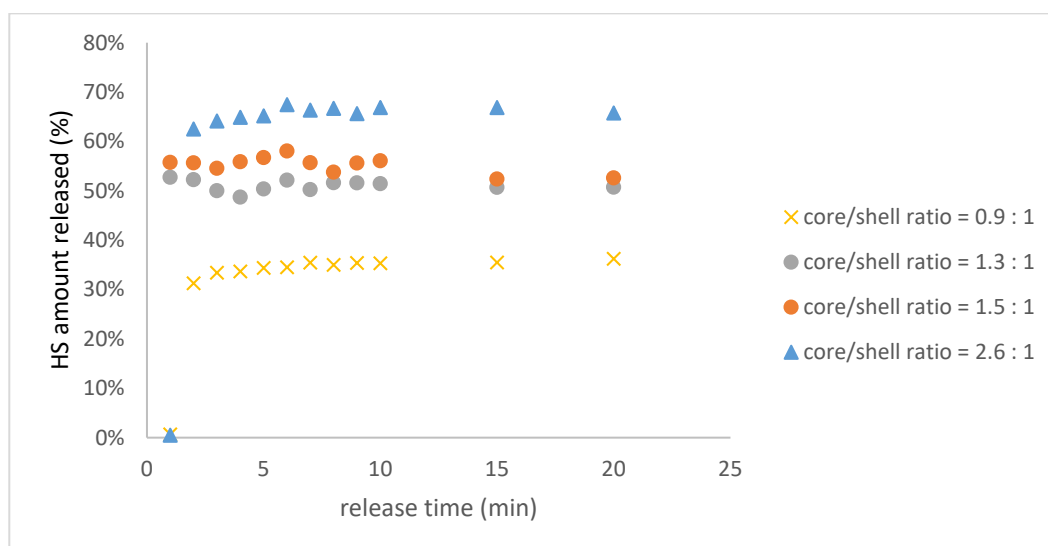
Figure 4.4-1 Percentage of hexyl salicylate core released from PMMA
microcapsules to the ethanol-water mixture at different time intervals. After
2 minutes of the PMMA capsules mixed with ethanol, the HS loss increased
rapidly and formed a plateau, indicating the full release of the HS

From above Figure 4.4-1, a rapid increase of hexyl salicylate core loss was

observed in samples with a core/shell ratio of 0.9 : 1 and 2.6 : 1 two minutes after

the ethanol was added into microcapsules suspension. After 2 minutes, the HS

loss percentage in all the samples didn't increase significantly with the release time increased. The plateau in all the curves indicated that the oil core was fully released from the PMMA capsules after 2 minutes. One of the reasons that the release percentage didn't achieve 100 per cent might be due to the loss of HS during the washing procedure. This finding coincided with the result in the previous study (Hitchcock et al., 2015) that the PMMA capsules fully released the oil core into the ethanol-water mixture within 20mins.

Interestingly, it was also found that the oil core's loss percentage was increased when the core/shell ratio was increased. This result indicated that more polymer shell content was required in the microcapsule synthesis process to achieve full coverage of the oil core.

4.4.2   The core/shell ratio influence on polymer shell thickness

The shell thickness has been shown to govern the mechanical strength of the microcapsules and the permeability of the shell. It plays a vital role in capsule-based controlled release applications (Antipov et al., 2001, Hara et al., 2003, Wang et al., 2008). A systematic study was conducted to investigate the influence of the polymer concentration in the emulsion on the shell thickness of the formed capsules and the mechanical strength.

In the experiment, polymer concentration in the oil phase was increased from 5 wt% to 20 wt%, while the total amount of the oil phase and the concentration of hexyl salicylate were maintained constant. The time for solvent evaporation was fixed at 48 hours. The core/shell ratio of the microcapsules used in the experiments was 1 : 0.6, 1 : 1.1, 1 : 1.7, and 1 : 2.3, respectively.

The microcapsules shell thickness is commonly measured using SEM combined with the microtome technique (O'Sullivan et al., 2009), or Transmission SEM (Müller et al., 2019). However, the PMMA shell thickness in this study was difficult to measure using these methods due to its material properties and the time limitation of this study.

In this study, a theoretical shell thickness calculation was designed based on the microcapsules size distribution data and surface area calculation. The assumptions made for the polymer shell thickness calculations are as follows: it's assumed that all the microcapsules are core-shell structure, as shown in Figure 4.4-2, and the total amount of polymer and oil in the emulsion is consumed in microcapsules formation.
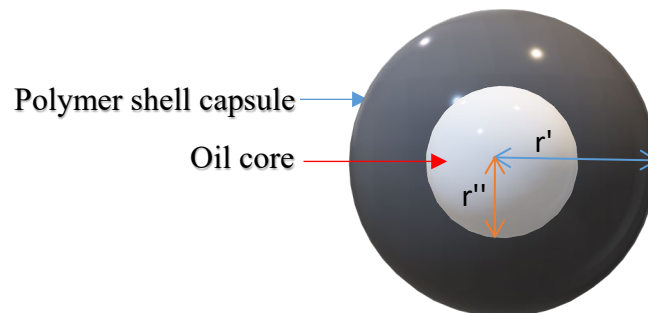
Figure 4.4-2 Ideal core-shell structured microcapsule used in the polymer shell thickness calculation

The calculated polymer shell thickness was confirmed via the measurements of the cross-section of the polymer capsules. The cross-section was obtained by cutting through sputter-coated polymer capsules via FIBSEM, and the shell thickness was measured using imageJ. The detailed calculation method was described in Chapter 3.3.5, and the method of shell thickness measurement on the cross-section was given in Chapter3.2.5 .

The size and size distribution of microcapsules with various core/shell ratios were measured using a Mastersizer. The diameter of D90 was used to calculate the shell thickness. The results of capsule diameter and shell thickness with various core/shell ratios were plotted in Figure 4.4-3.
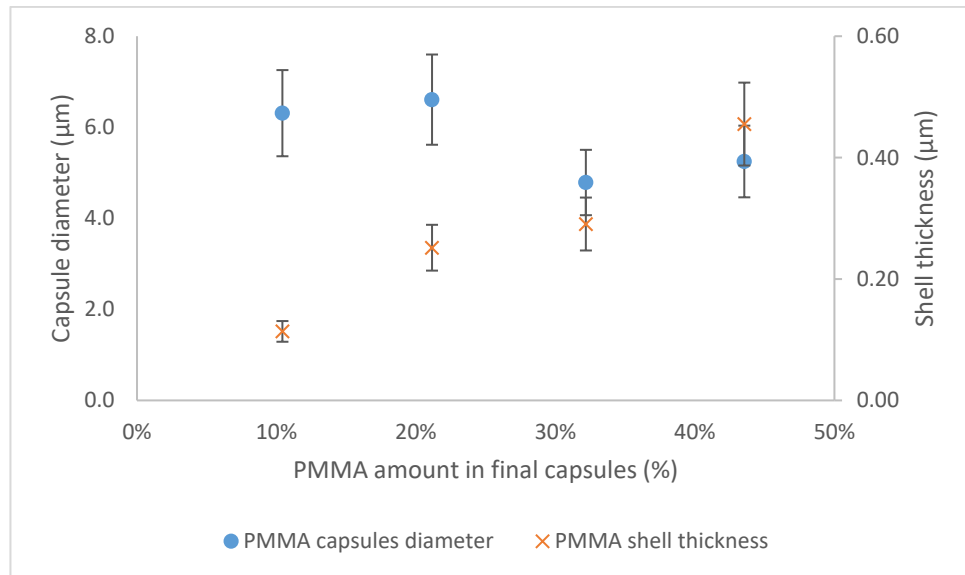
Figure 4.4-3 Diameter and shell thickness of PMMA microcapsules with increasing shell percentage in the final capsule

It was found in Figure 4.4-3, that the capsule diameter didn't vary a lot when the PMMA ratio in the final capsules increased. This is because the total amount of the PMMA and HS was kept constant regardless of the PMMA to HS ratio change. However, it can be observed that the PMMA shell thickness increases with the PMMA amount increases.

Based on the capsule diameter and shell thickness results, a 21% PMMA amount in final capsules was found to generate microcapsules with the greatest diameter and the thinnest shell thickness.

4.5 Conclusions

In this Chapter, polymer shell oil core microcapsules were prepared using solvent evaporation and extraction method.

First, a model of the microcapsules was prepared based on Loxley and Vincent's method. In this model, an oil phase, which contained polymer PEMA, good solvent DCM, and non-solvent toluene, was mixed with an equivalent amount of aqueous phase to form an oil-in-water emulsion. The cationic surfactant $C_{16}TAB$ in the aqueous phase was used to help form and stabilise the oil droplets in the water. The emulsion was stirred for 48 hours to allow the extraction and evaporation of DCM. In the process of DCM evaporation, the polymer precipitated at the oil-water interface and formed a film surrounding the oil droplets. When all the DCM was extracted and evaporated from the mixture, the polymer film solidified, and polymer shell microcapsules were obtained. The resulting microcapsules were characterised using the SEM technique, and the core-shell structure was demonstrated.

Based on the model microcapsules, a study on various oil core polymer shell combinations was conducted to investigate the relationship between microcapsule morphology and core/shell combinations. According to Torza and Mason's theory, the capsule morphology was decided by the interfacial tension and spreading coefficient between polymer, oil and aqueous phases. PMMA capsules with hexadecane, hexyl salicylate, toluene, cyclamen aldehyde and dihydromercenol core were prepared, respectively. The capsule morphology was predicted based on the interfacial tension and spreading coefficient between phases. The resulting microcapsule morphology was characterised using SEM

and FIBSEM, and it was found that most of the morphology predictions coincided with the observation. All the PMMA capsules except the ones with hexadecane core formed a core-shell structure.

On the selected PMMA shell hexyl salicylate core microcapsules, the effect of core/shell ratio on the core retention, capsule diameter, and polymer shell thickness was investigated. Two sets of experiments were designed. One set of experiments prepared PMMA microcapsules with increasing core content, and a release study was conducted on the prepared capsules. It was found that the oil content was fully released within 2 minutes in all the samples. It was also found that the greater the core/shell ratio, the higher percentage of the oil core was lost during the process. The other set prepared PMMA microcapsules with increasing polymer shell content. The diameter of the resulting capsules was measured using Mastersizer, and the shell thickness was calculated. It was found that the smaller the core/shell ratio, the narrower size distribution the microcapsules had. It was also found that at a core/shell ratio of 1 : 1.1, the resulting microcapsules demonstrated the largest diameter and the thinnest shell thickness.

Chpater 5 Adsorption of Au NPs to polymer microcapsules as the catalyst and the Au NPs adsorption density

5.1 Introduction

In Chapter 4, the polymer shell oil core microcapsules were prepared and characterised. The relationship between the microcapsules' morphology and the interfacial tension between the phases was investigated, and the core-shell structured microcapsules were formed based on the finding. The effects of core/shell ratio on the polymer capsules' dimension and shell thickness were also studied.

However, the large free volume within the polymer shell provides a low resistance pathway to the rapid diffusion of the components with small molecular weight, such as toluene and fragrance oil. These active small molecules permeated most polymeric shells through the pre-existed pores (Patchan et al., 2012, Madene et al., 2006, Brannonpeppas, 1993, Evans, 1970). Hence, a continuous layer of metal coating on the polymer shell microcapsules provides vastly improved barrier properties to avoid the evaporation of volatile core content. In the process of metal coating of the polymer shell microcapsules, the usage of catalysts facilitated forming the nucleation site for the metallic layer and accelerated the rate of coating reaction by providing a lower activation energy pathway (Kobayashi and Ishii, 2013, Inberg et al., 2012, Moshfegh, 2009b). Nanoparticles have been used as catalysts for metal deposition in electroless plating driven by various specific properties, such as more significant surface

area, increasing surface-to-volume ratio, better dispersion ability, higher reactivity, and so on. (Patchan et al., 2012, Horiuchi and Nakao, 2010, Zhu et al., 2011, Martin et al., 2010). In this study, Au NPs were used as the catalyst embedding onto polymer capsules surface to facilitate the subsequent silver coating by forming catalytic nuclei on the targeted polymer capsules surface and accelerating the reaction rate. This part of the study became the second step of the silver shell microcapsule preparation process, as indicated by the red box in Figure 5.1-1.
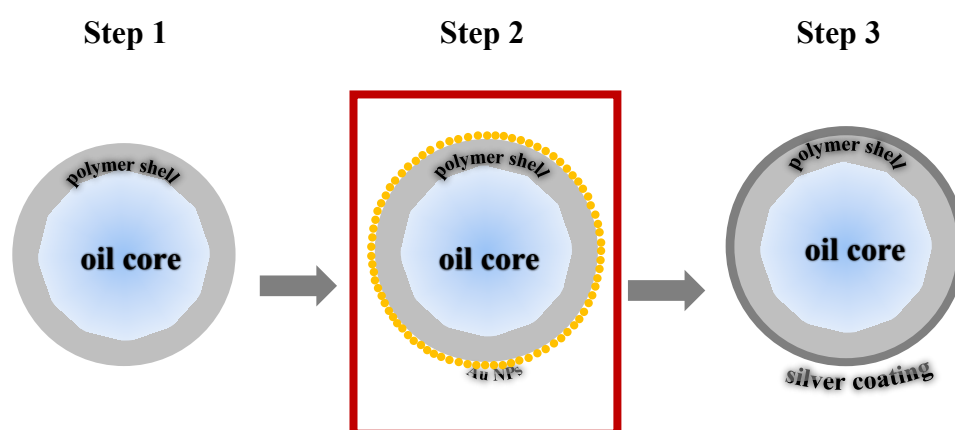
Figure 5.1-1 Schematics of silver shell microcapsules synthesis process: Step 1: Formation of polymer shell oil core microcapsule, Step 2: Au NPs adsorption to polymer microcapsule surface as the catalyst, Step 3: Silver coating on the polymer microcapsules' surface via electroless plating method

In this Chapter, a stable monodispersed colloidal gold nanoparticles system was developed using a fast chemical reaction method. The synthesised Au NPs were stabilised in water via electrostatic repulsion and were adsorbed to the polymer microcapsules surface via electrostatic attraction.

5.2 Synthesis of electrostatic stabilised Au NPs via a chemical reaction method

Au shows a pronounced catalytic activity. Au NPs are highly reactive when used as catalysts due to the distinctively small particle size and hence the large surface area. One of the simplest ways of synthesis Au NPs was studied by Turkevich et al. (1951) and refined by Frens (1973). Au NPs were made using sodium citrate as both a reducer and a stabiliser in their studies. The reaction took 30-45 minutes at 70°C, or 5 minutes at 100 °C. For the faster formation of Au NPs at room temperature, stronger reducers, such as borohydride, were used to generate Au NPs which sizes varying from 2nm to over 50nm (Wagner et al., 2008, Jana et al., 2001, Patil et al., 1999, Hohnstedt et al., 1965). Martin et al. (2010) found that the stability of Au NPs in water could be improved by adding HCl and NaOH to gold chloride stock solution and borohydride solution, respectively. Meanwhile, the size of Au NPs could be controlled between 3.2 and 5.2 nm by adjusting the ratio of BH_4^-/OH^- ions to $AuCl_4^-/H^+$ ions.

Following Martin's method, Au NPs were synthesised using the chemical reaction method. The chemical reaction of $NaBH_4$ reduction of gold salt is shown in Equation 5.2-1.

$$HAuCl_4 + 4\,NaBH_4 \ \rightarrow \ Au + 2B_2H_6 + 4NaCl + 5/2H_2 \quad \text{Equation 5.2-1}$$
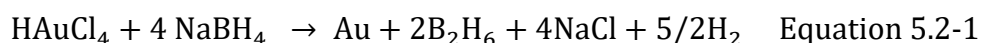
Adsorption of borohydride played a crucial role in stabilising Au NPs by providing a negative particle surface charge. It also served for the adhesion towards positively charged polymer capsules surface. Therefore, enough borohydride to allow the reaction procedure was required. The BH_4^-/OH^- ions to $AuCl_4^-/H^+$ ions ratio was set as 3: 1, which leads to stable monodispersed colloidal gold nanoparticles with the concentration of gold ions of 0.5 mmol/dm^3, as shown in Figure 5.2-1.

a)   b)
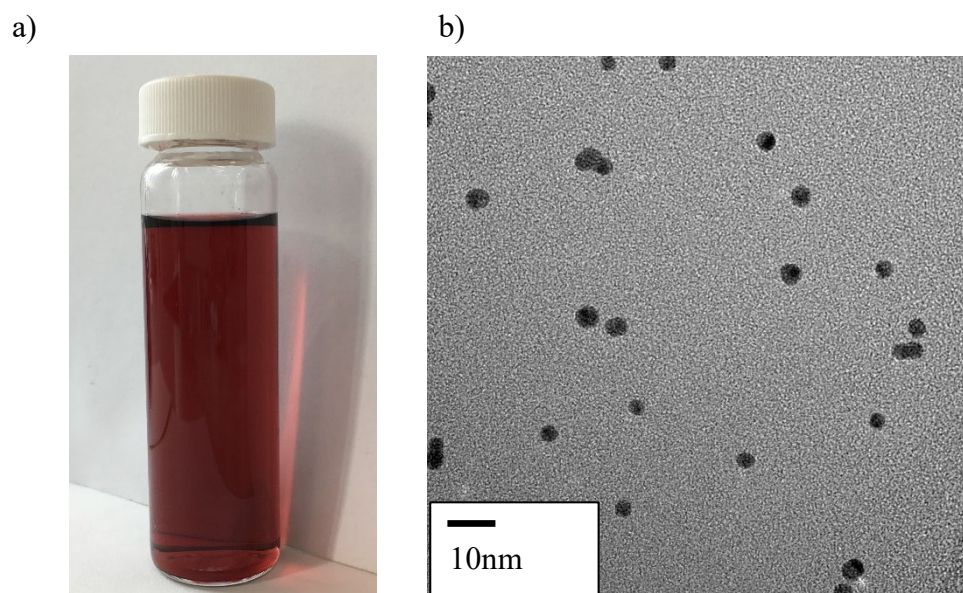
Figure 5.2-1a) Image of synthesised Au NPs in water, showing typical dark red colour and b) TEM micrograph of Au NPs with a gold concentration of 0.5 mmol/dm^3

As shown in Figure 5.2-1a), the HAuCl$_4$ solution changed colour from light yellow to dark red within 1 second at room temperature while sodium borohydride solution was added. The immediate colour change indicated that all the gold ions were reduced to neutral gold atoms and the formation of Au NPs.

The resulting Au NPs were dried in the air and examined using TEM. The monodispersed spherical Au NPs were observed and shown in Figure 5.2-1 b).

The resulting Au NPs were analysed using UV-Vis technique, and it was found that the resulting Au NPs showed the typical plasmon peak around ~510 nm, which was similar to the previous study (Zimbone et al., 2011, Zuber et al., 2016, Mohd Sultan and Johan, 2014, Martin et al., 2010). The Au NPs were dried in the air and examined using TEM. The monodispersed spherical Au NPs were observed and shown in Figure 5.2-1b). The size of the synthesised Au NPs was analysed via TEM micrographs combined with ImageJ software. The average size of Au NPs is 3.4 ±0.4 nm.

5.3   Au NPs adsorption to polymer capsules' surface

The synthesised Au NPs were stabilised by the electrostatic repulsion induced by BH_4^- and showed a negative charge. In contrast, the polymer microcapsule surface carried a positive charge because the cationic surfactant $C_{16}TAB$ was used as the stabiliser in the preparation process of polymer shell microcapsules. The surfactant sat at the oil-water interface when the polymer precipitated and formed a film layer surrounding the oil droplet. Its hydrophilic head stretched towards the aqueous phase, and its long hydrophobic tail extended to the oil core. When bromide anions in the head groups dissociated from the polymer capsules in the aqueous phase, positive charges formed on the capsules' surface.

The negatively charged Au NPs were attached to the polymer capsules' surface via electrostatic attraction, as shown in Figure 5.3-1.
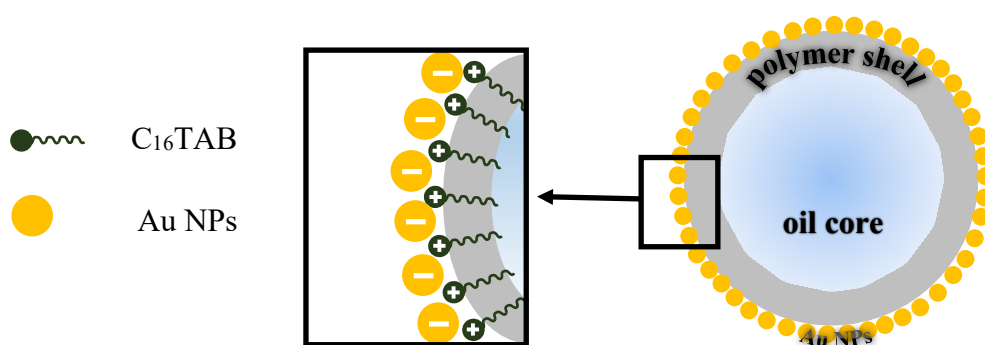
Figure 5.3-1 Schematic of negatively charged Au NPs were adsorbed to the polymer capsule surface via the positively charged head of cationic surfactant $C_{16}TAB$

The synthesised Au NPs mixed with cationic surfactant CTAB stabilised polymer capsules at a volume ratio of 6 : 1. The mixture was stirred for 1 minute, and gold NPs adsorbed capsules were obtained. The capsules were dried in air and observed using TEM. The results are shown in Figure 5.3-2.

Figure 5.3-2 TEM micrographs of Au NPs attached polymer capsules surface
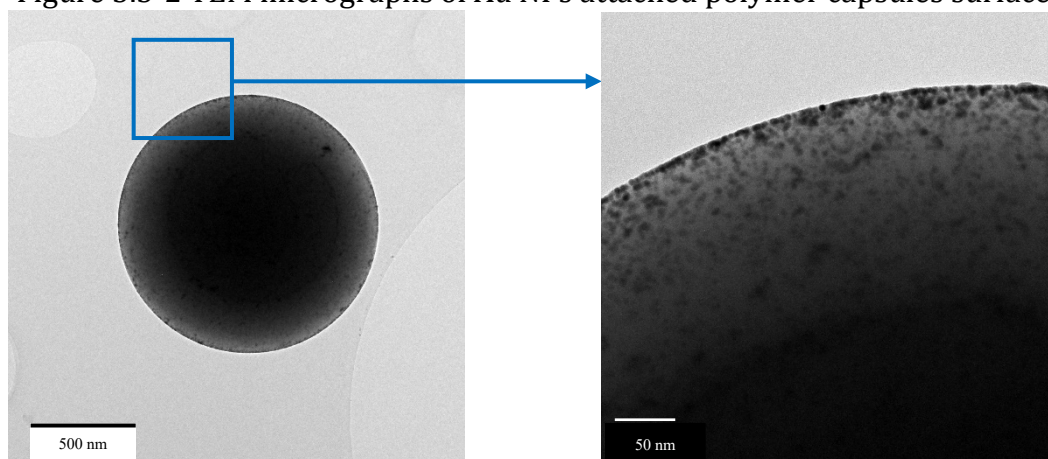
It was observed from Figure 5.3-2 that Au NPs evenly distributed on the PEMA capsule's surface and formed the catalytic site for the following on silver coating. A systematic study was conducted to investigate the influence of surfactant

concentration in the polymer capsule system and the Au NPs suspension concentration to the Au NPs adsorption on the polymer capsules surface.

5.4   Influence of surfactant concentration on Au NPs adsorption

The negatively charged Au NPs adhered to the polymer capsule surface via electrostatic attraction. The positive charge of the capsule was brought by cationic surfactant CTAB trapped on the capsule surface. Hence, a sufficient amount of CTAB present in the capsule is vital to bind the gold NPs. At the same time, an inadequate or excessive amount of CTAB leads to the aggregation of Au NPs on the polymer surface.

Chakraborty et al. (2006) reported that a difference in the degree of surfactant concentration affects the charge density of the polymer in their study of polymer-surfactant interaction with opposite charges. Perez-Juste et al. (2004) also reported that Au could be quantitatively bound to CTAB, but the CTAB : $HAuCl_2$ concentration falls in a narrow range. Therefore, the aggregation and poor coverage of Au NPs on polymer capsules' surfaces may be caused by the decrease in the ratio of CTAB to Au NPs. As shown in Figure 5.4-1, in the absence of CTAB, the Au NPs display negative charges, repel each other and remain stable. When a low concentration of CTAB is added, the negative charge is reduced due to the partial counteraction with the positively charged CTAB. However, the Au NPs can still repel each other and stay relatively stable. At the addition of a critical concentration of CTAB, the Au NPs are neutralised by CTAB; without the electrostatic repulsion between particles, aggregation occurs. With an excessive amount of CTAB, the surface of Au NPs is covered by CTAB

and the micelles, and consequently, the system presents a positively charged surface.
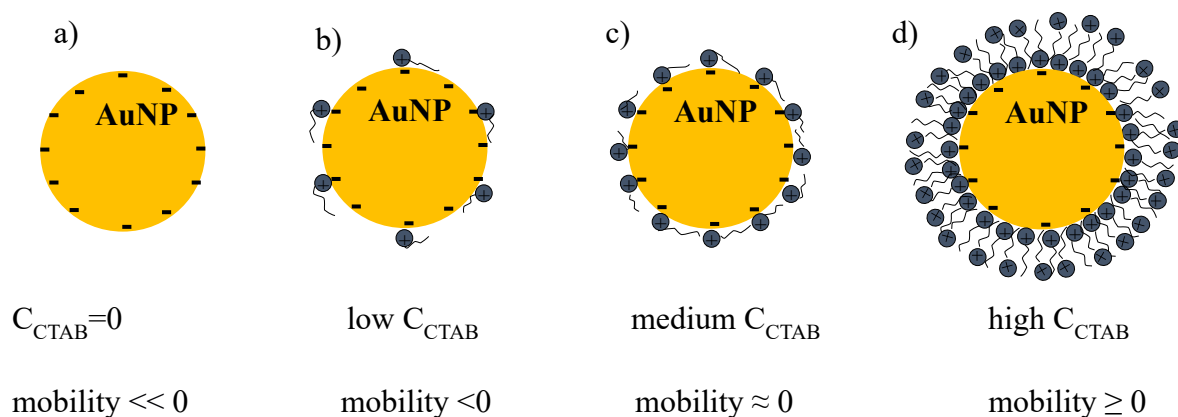
Figure 5.4-1 Schematics of electrostatics interactions between Au NPs and CTAB with different ratios: a) When there is no CTAB present, the mobility of Au NPs is negative; b) when CTAB concentration is at a low range, the Au NPs remain negative; c) when CTAB concentration increases to a higher range, the negative charge of Au NPs were neutralised; d) when excessive CTAB present, Au NPs become positive charged

In order to find out the appropriate ratio of CTAB to Au NPs for successful attraction of Au NPs and subsequent silver coating, the effect of CTAB concentration on the Au NPs aggregation behaviour was studied.

An equivalent volume of aqueous CTAB solution with various concentrations (from 0.1-1 mmol/dm^3) was added to the 6 mL Au NPs solution of 0.5 mmol/dm^3 concentration. It was found that Au NPs solution turned from dark red to black immediately following the addition of 0.1 mmol/dm^3 CTAB. Sedimentation of aggregated Au NPs formed in this sample after ~20 minutes. Au NPs and CTAB mixed samples are shown in Figure 5.4-2. It was observed that Au NPs solution

changed from transparent red to obstacle dark when CTAB solution with concentrations between 0.1 and 0.3 mmol/dm^3 was added. This colour change phenomenon indicated the aggregation of Au NPs.
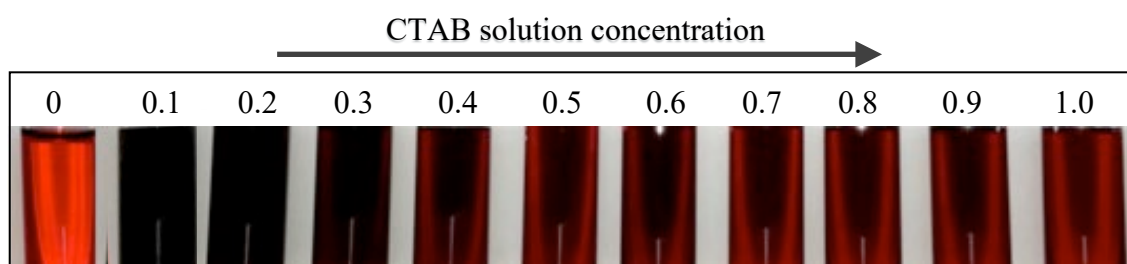
Figure 5.4-2 Digital micrographs of various AuNPs with CTAB concentration increasing from 0 to 1 mmol/dm^3 from left to right

Aggregation behaviour of Au NPs when mixed with CTAB solution. The concentration of CTAB in the Au NPs suspension increases from 0 to 1 mmol/dm^3 from left to right.

A further study of CTAB concentration effect on Au NPs aggregation behaviour was carried out on lower CTAB concentrations between 0.01 and 0.1 mmol/ dm^3. The zeta potential of the samples was measured and plotted in Figure 5.4-3.
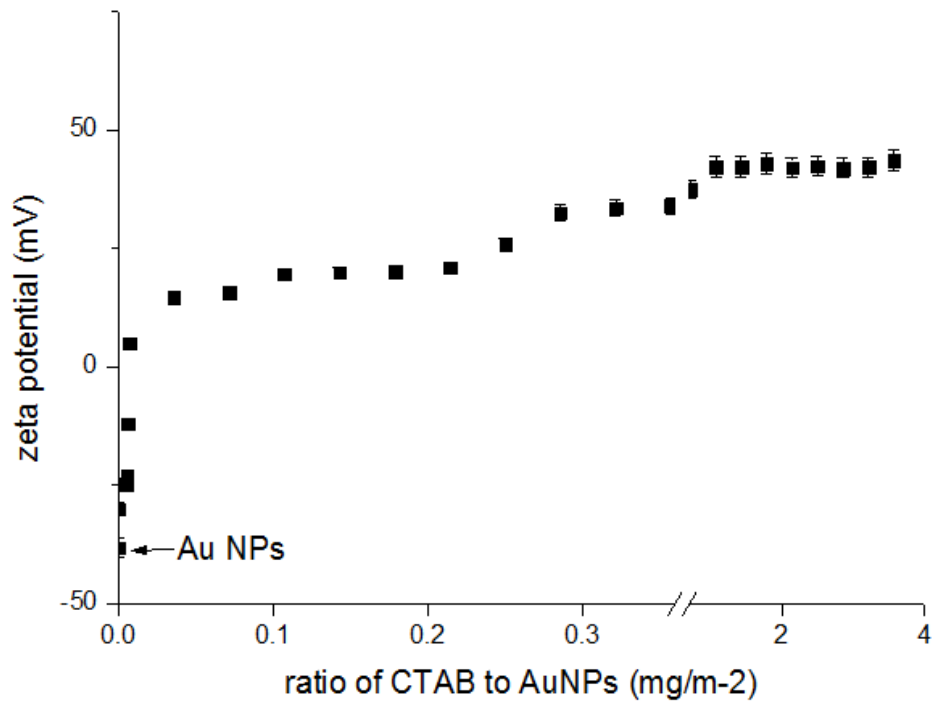
Figure 5.4-3 Zeta potential of Au NPs increased when the CTAB
concentration added into Au NPs suspension was growing

Figure 5.4-3 shows that the negative value of the *zeta* potential of Au NPs

became smaller with an increase in the concentration of added CTAB solution.

This zeta potential change indicated that the mixture became unstable. When the

ratio of CTAB mass to Au NPs surface area falls into the range 0.0046 to 0.357

mg/m^2 (C_{CTAB} = 0.0013 - 0.1 mmol/dm^3), the *zeta* potential of Au NPs is between

-24.9 and +25.9 mV. At a ratio of 0.0068 mg/m^2, the zeta potential is +5.0 mV.

At this point, the negative charge of Au NPs was counteracted by the opposite

charge of CTAB, and the repulsive force between the particles was greatly

weakened, which led to the least stable system, and aggregation occurred. When

the ratio was increased to the *zeta* potential was raised to +37.5 mV, indicating

that the system became stable again. At this stage, the positive charge is caused

by a sufficient amount of CTAB covering the surface of the Au NPs. When the ratio is greater than 1.07 mg/m^2 (Concentration$_{CTAB}$ = 0.3 mmol/dm^3), the *zeta* potential remains ~+42 mV.

The experiment results support the hypothesis that the CTAB concentration affects the Au NPs aggregation behaviour. The presence of CTAB should be controlled only at the capsule surface instead of in the bulk solution.

Initially, the experiments were conducted on microcapsules subjected to different levels of 'washing' to remove the excess surfactant from the capsules continuous phase. The prepared polymer microcapsules were centrifuged, and the aqueous supernatant (containing the excess surfactant) was replaced by fresh Milli-Q water. This "washing" was repeated three times, and the surface tension of the supernatant from each wash was measured. The concentrations of the surfactant in the system was calculated.

A calibration experiment was conducted by measuring the surface tension of the known concentration of CTAB aqueous solutions using the pendant drop tensiometer, and the data is shown in Figure 5.4-4. It is shown that the surface tension decreases along with the increase of the CTAB concentration until it reaches a concentration of 0.9 mmol/dm3. The surface tension of the CTAB solution remains relatively constant above this concentration. It indicates that 0.9 mmol/dm3 is the critical micelle concentration (CMC) of CTAB in water at room temperature, which is close to the results reported by Javadian et al. (2013) and (Kuntz and Walker, 2007). At this concentration, micelle starts to form, and all additional surfactants added to the system go to micelles. In the experiment, we

observed that the washing cycle removing excessive CTAB from the system has a vital influence on Au NPs adsorption.
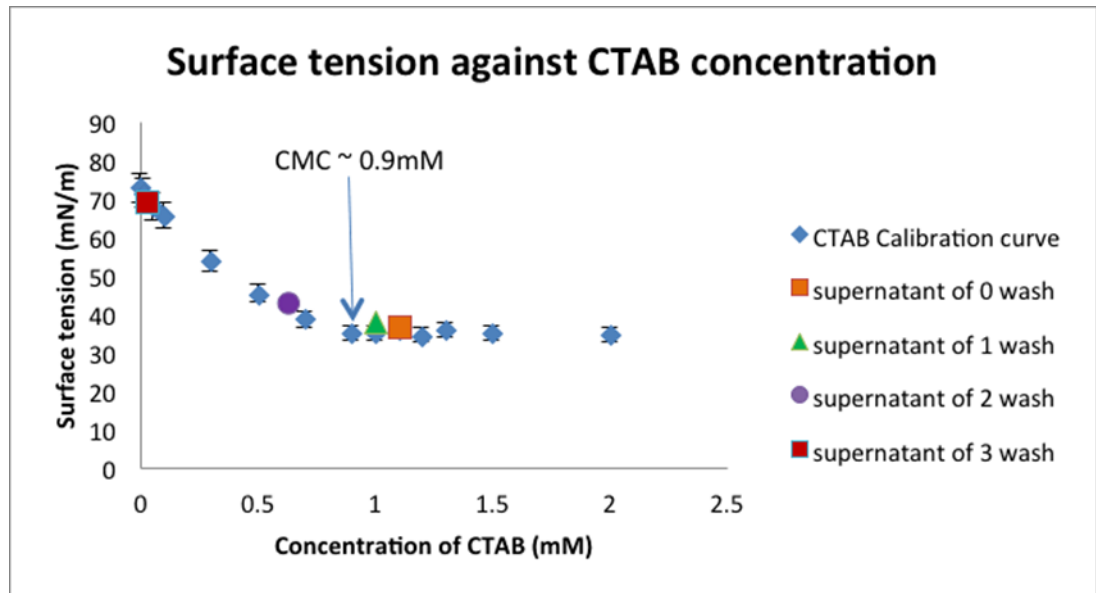
Figure 5.4-4 Surface tension against CTAB concentration

The surface tensions of supernatant after 0-3 times washes were also shown in Figure 5.4-4. The calibration curve can determine the approximate CTAB concentration in the continuous phase of capsules washed to different degrees. The CTAB concentration in the supernatant was above CMC without a wash or with only one wash. After three wash times, the surface tension of the supernatant was very low (~69.13 mN/m), which indicates that few amounts of surfactant were left in the continuous phase. More studies on investigating the effect of the ratio of CTAB to Au NPs on Au adsorption density were carried out with two or three washes.

5.5   Influence of Au NPs concentration on the adsorption density

The amount of catalyst adsorbed on the polymer capsule surface also impacts the formation of the silver shell morphology and shell thickness. Au NPs have been used to accelerate the reaction rate between silver and reducing agent HCHO and provided target sites for silver deposition. Previous research in my MSc study showed that a deficiency in Au NPs on the PEMA capsules' surfaces leads to an incomplete silver coating. An excessive amount of Au NPs in the system might broaden the size distribution of the microcapsules and result in aggregation.
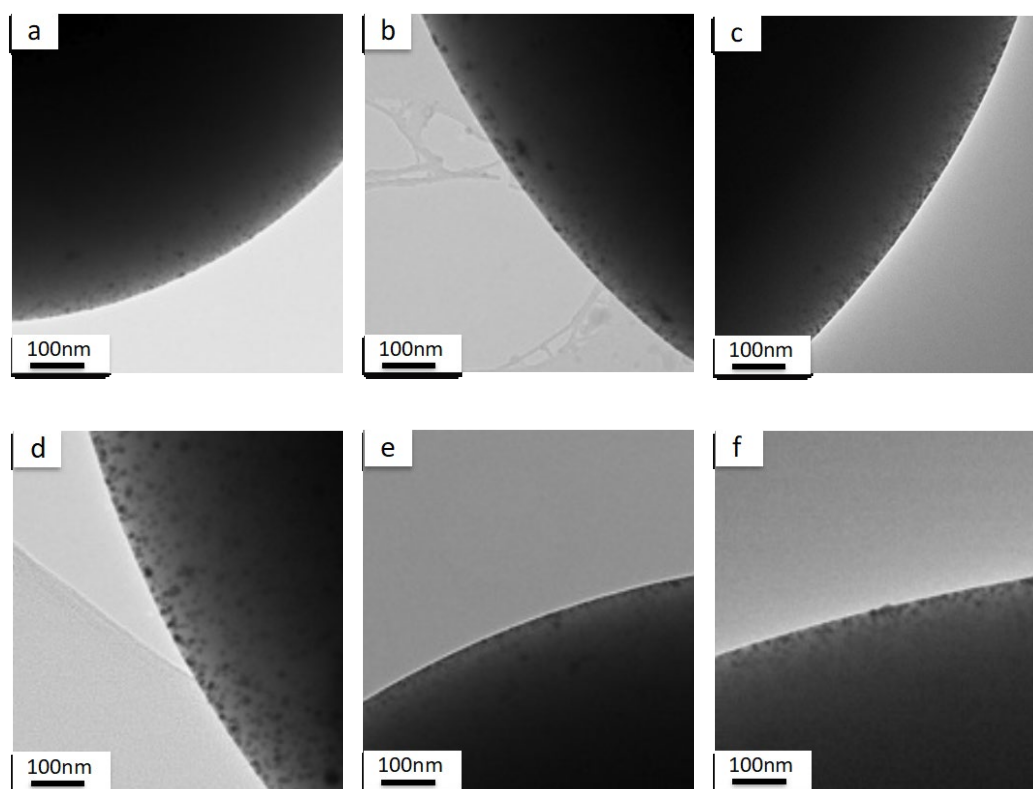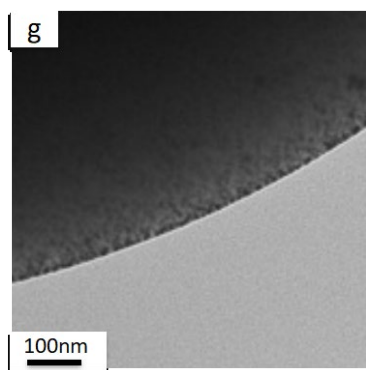
Figure 5.5-1 The adsorption density of Au NPs on polymer microcapsules surface increases as the concentration of Au NPs. The input ratio of Au NPs to polymer capsules' surface area are : a) 2.9 mg/m^2; b) 14.6 mg/m^2; c) 29.3 mg/m^2; d) 58.5 mg/m^2; e) 87.7 mg/m^2; f) 116.9 mg/m^2; g) 146.1 mg/m^2

Initially, Au NPs were varied in the system to study their effect on the adsorption density. The ratio of the mass of Au NPs to the total surface area of the polymer microcapsules was varied from 2.92-146.13 mg/m^2, and the morphology of Au NPs loaded polymer capsules is illustrated in Figure 5.5-1 through observations via TEM.

From TEM micrographs of Au NPs loaded polymer capsules in Figure 5.5-1, it could be observed that the absorption density of Au NPs attached to the polymer surface increase with the increase of the Au NPs concentration used in the process. However, it is difficult to precisely measure the amount of Au NPs adsorbed on polymer surfaces through micrographs. Therefore the adsorption density was studied using a UV-Vis spectrophotometer and a thermal analysis.

5.5.1 Adsorption density characterised via UV-Vis technique

The adsorption amount of Au NPs on the polymer capsule surface was evaluated by subtracting the amount of Au NPs in supernatant from the initial Au NPs used

for the adsorption process. A calibration curve for Au NPs suspensions with different concentrations was generated to calculate the concentration of Au NPs in the supernatant. Samples of Au NPs suspensions with different concentrations were prepared, and a calibration curve was plotted based on UV-Vis spectra. The concentration of Au NPs could be obtained via this calibration curve (the detailed method was given in Chapter 3.2.4 .

The Au NPs adsorption process was performed by mixing polymer capsules with various concentrated Au NPs suspensions, as described in Chapter 5.3. After the process, samples of polymer capsules with adsorbed Au NPs were centrifuged to separate the capsules from the aqueous supernatants. The aqueous supernatants were characterised using a UV-Vis spectrophotometer. The mass of Au NPs remaining in the supernatant was calculated according to the calibration curve of the Au NPs, which was described in Figure 3.24 in Chapter 3.2.4. The mass of Au NPs before the adsorption process and remaining in the supernatant are plotted inFigure 5.5-2, respectively.
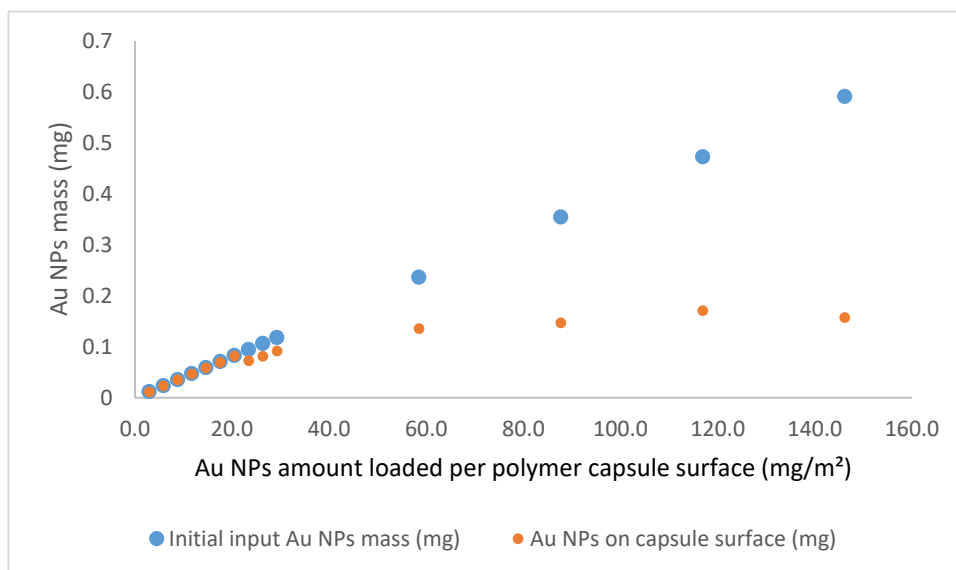
Figure 5.5-2 The mass of Au NPs on the capsule surface was calculated by deducting the Au NPs mass remaining in the supernatant from its initial input mass

From Figure 5.5-2, it was found that, at a low input ratio of Au NPs to the capsule surface area (up to 14.61 mg/ m^2), the mass of Au NPs in the supernatant was very close to the initial mass of Au NPs. This indicated that most Au NPs were adsorbed on the capsules. As the input Au NPs loading increases to 29.3 mg/ m^2, a noticeable increase of Au NPs consumed during the adsorption process was observed. When the initial ratio of Au NPs to capsules was greater than 29.23 mg/m^2, the mass of Au NPs on the capsule remained at the same level. This is likely to indicate that the capsule surface was saturated with Au NPs when the adsorption density of Au NPs to the surface exceeded 29.23mg/m^2.

5.5.2   Adsorption density characterised via thermal analysis

In addition to the UV-Vis, a Thermogravimetric analysis (TGA) was also used to analyse the adsorption density of Au NPs to the capsules surface. Polymer capsules were mixed with Au NPs aqueous suspension of different concentrations

for Au NPs adsorption. The capsules were rinsed after the Au NPs adsorption and then analysed using a TGA technique from room temperature to 900 °c. The sample's weight went through two significant losses in the process. At 100 °c, the water in the samples evaporated, and hence a massive decrease in the sample weight was observed. At the range of 200-400 °c, another weight drop was observed, where the polymer was decomposed. This observation coincided with the findings reported by Fares (2012), Zhang et al. (2012), Kaya and özdemir (1995). The final mass measured at 800 °c was the weight of Au NPs adsorbed on the PEMA capsules' surface. The sample mass at 100 and 800 °c was plotted in Figure 5.5-3, and the mass loss percentage against the initial sample weight at 100 °c.

It was observed that Au NPs adsorbed polymer capsules mass (mass at 100 °c) and Au NPs mass (mass at 800 °c) increased when the input ratio of Au to polymer surface increased from 2.9 to 29.3 mg/m^2. When the input ratio of Au to polymer surface exceeded 29.3 mg/m^2, the mass curve remained a plateau which indicates that the adsorption of Au NPs on the capsules surface reached a saturated status. The TGA results coincided with the UV-Vis results.
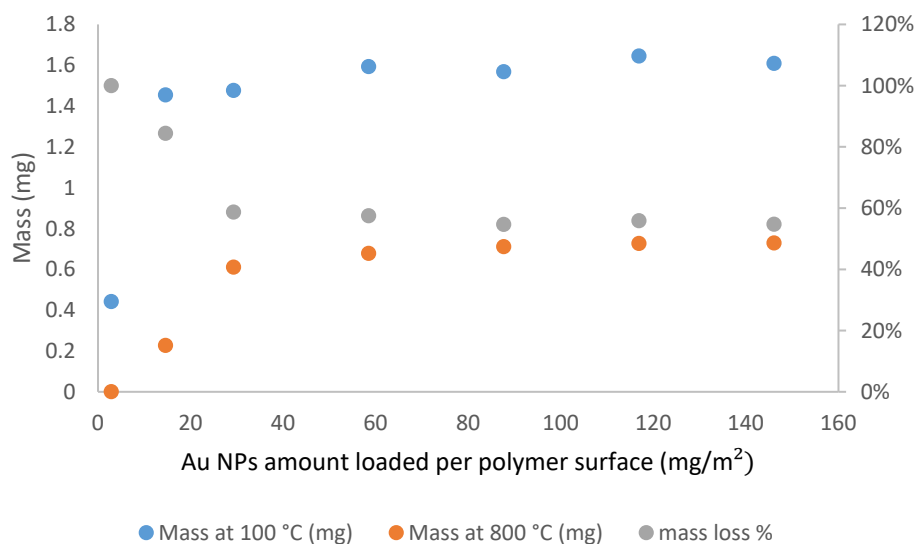
Figure 5.5-3 Mass of Au NPs on polymer capsules decreases with the decrease of adsorption density, results obtained via TGA

5.6   Conclusions

In this Chapter, Au NPs were synthesised and embedded onto the polymer shell oil core capsule surface via static electronic adsorption.

Firstly the Au NPs were synthesised using a chemical reaction method. Sodium borohydride solution was added into gold chloride stock solution at room temperature. The gold ions in the $HAuCl_4$ solution were reduced to neutral gold atoms, and Au NPs were formed within 1 second after sodium borohydride was added. The monodispersed spherical Au NPs are stable in the water. The average size of synthesised Au NPs is 3.4 ±0.4 nm, measured with a TEM combined with ImageJ technique.

The synthesised Au NPs carried a negative charge, and the polymer microcapsule surface carried a positive charge because the cationic surfactant $C_{16}TAB$ was

used as the stabiliser in the preparation process of polymer shell microcapsules. The negatively charged Au NPs were attached to the polymer capsules' surface via electrostatic attraction by mixing the Au NPs with polymer capsules.

The surfactant concentration plays an essential role in Au NPs adsorption to the polymer capsule surface. A sufficient amount of CTAB on the capsule is vital to bind the Au NPs. At the same time, an inadequate or excessive amount of CTAB leads to the aggregation of Au NPs on the polymer surface. A systematic study of the effect of CTAB concentration on Au NPs adsorption on capsule surface was conducted. It was found that the aggregation of the Au NPs occurred when the CTAB concentration in the capsule suspension was too high or low. A stable system of Au NPs adsorbed polymer capsules was achieved when the ratio of input CTAB mass to Au NPs surface area remained from 0.0046 to 0.357 mg/m^2 (2 wash cycles after the Au NPs adsorption).

The amount of catalyst adsorbed on the polymer capsule surface also impacts the formation of the silver shell morphology and shell thickness. Therefore a systematic study of the effect of Au NPs concentration on the adsorption density was also conducted. Au NPs suspensions with various concentrations were mixed with fix amount of capsule suspension for Au NPs adsorption. The input Au NPs mass ratio to the total capsules surface area of the samples was 2.92 - 146.13 mg/m^2. The absorption density of Au NPs on the capsules surface was characterised using TEM, UV-Vis, and TGA techniques. It was found that the higher concentration of the Au NPs suspension added into the capsules, the more Au NPs were adsorbed onto the capsules surface. However, when the input Au NPs mass ratio to the capsules surface area reaches 29.23mg/m^2 (the input Au

NPs concentration reaches 0.1 mM), the amount of Au NPs adsorbed on the

surface saturated and stops increasing.

Chpater 6 Silver shell microcapsules formation and the capsules mechanical strength

6.1 Introduction

In Chapter 4, the preparation and characterisation of polymer shell oil core microcapsules were discussed. In Chapter 5, the discussion focuses on the synthesis of the Au NPs and attaching the Au NPs onto the polymer capsules surface as a catalyst to facilitate the growth of the silver layer on the polymer capsules surface. In Chapter 5, the synthesis method of Au NPs and the process of embedding the synthesised Au NPs to the polymer capsules surface via electrostatic attraction were explained. Systematic studies were also carried out to investigate the effect of surfactant CTAB in the system and the concentration of Au NPs suspension to the Au NPs adsorption density on the polymer capsules surface. It was found that the best Au NPs adsorption density in a stable system was achieved when the ratio of input CTAB mass to Au NPs surface area falls in the range of 0.0046 to 0.357 mg/m^2 (2 wash cycles after the Au NPs adsorption), and when the input Au NPs mass ratio to the capsules surface area reaches 29.23mg/m^2 (the input Au NPs concentration reaches 0.1 mM).

In this Chapter, the discussion focuses on the preparation and characterisation of the silver shell of the microcapsules. As shown in Figure 6.1-1, to encapsulate the low vapour pressure fragrant oil with no release in a continuous phase that dissolves the oil, a continuous layer of metallic coating on the polymer shell of the microcapsule was created to improve the resistance of the shell to the leakage of core content, the fragrance oil.
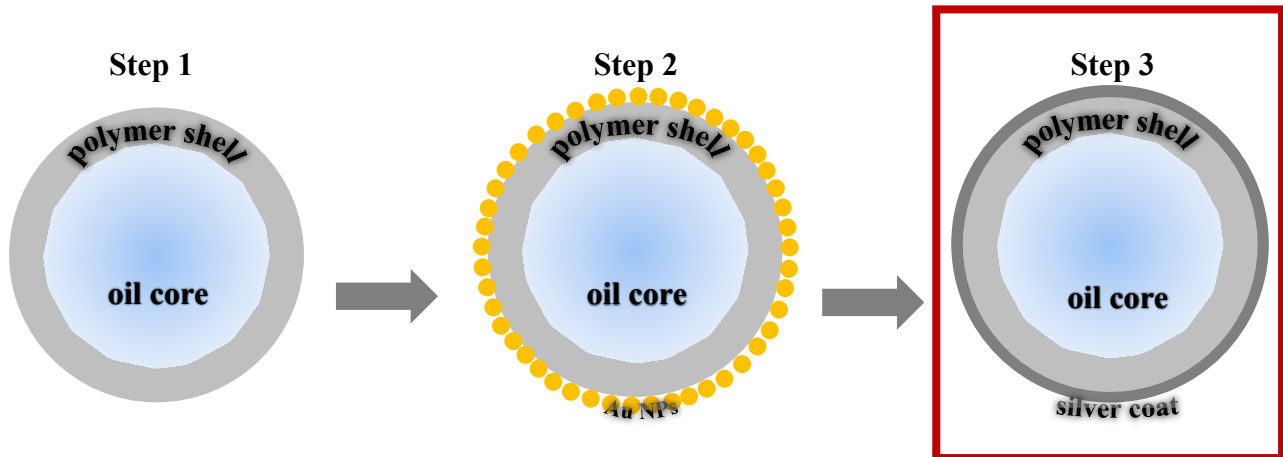
Figure 6.1-1 Schematics of silver shell microcapsules synthesis process: Step 1: Formation of polymer shell microcapsule· Step 2: Au NPs catalyst adsorption· Step 3: Silver coating via electroless plating

In this Chapter, a thin layer of silver film was grown onto catalytic sites created by Au NPs adsorbed on the polymer capsule and thus formed the secondary silver shell of the microcapsules. The silver shell was produced through the electroless plating method, which is essentially a metal deposition process brought about through a chemical reaction between metal ions and reducing agents. Electroless plating has the advantages of being a simple process and providing a uniform thickness of coating deposited.

The influence of silver salt concentration of the plating bath and the Au NPs adsorption on the polymer capsule surface on the silver shell thickness was investigated in this Chapter.

The mechanical strength of formed silver shell microcapsules was studied in relation to the microcapsule diameter and shell thickness.

6.2 Preparation of silver shell microcapsules via electroless metal plating method

The term 'electroless metal plating (ELP)' was first introduced by Brenner and Riddell (1946b) and was used in various metal coating processes (Patchan et al., 2012). It is an electrochemical process, which involves electron donor-acceptor reactions. In this study, the Au NPs attached polymer capsules were mixed with an aqueous $AgNO_3$ solution under gentle agitation. Formaldehyde (HCHO) was used to reduce the Ag ions into Ag coating on the catalytic site created by Au NPs. The solution mixture was alkaline by adding a tiny amount of ammonia solution. The pH value was controlled at 10. The plating bath consisting of $AgNO_3$ changed its colour from yellow to dark brown after adding ammonia solution, which indicates the formation of the silver coating. The chemical equation of the silver ELP is described in Equation 6.2-1.

$$4AgNO_3 + 9HCHO \rightarrow 4Ag + 9CO_2 + 4NH_3 + 3H_2O \qquad \text{Equation 6.2-1}$$
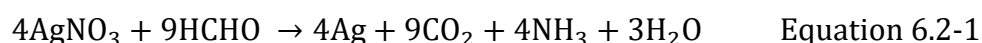
The silver-coated microcapsules were centrifuged to remove the supernatant and observed using an SEM, as illustrated in Figure 6.1-1. A continuous layer of silver coating was observed when the input ratio of Ag to capsule surface reached 93.95 mg/m^2. The Energy Dispersive X-Ray Analysis (EDX) was carried out with SEM. The results showed that the main component detected was silver.
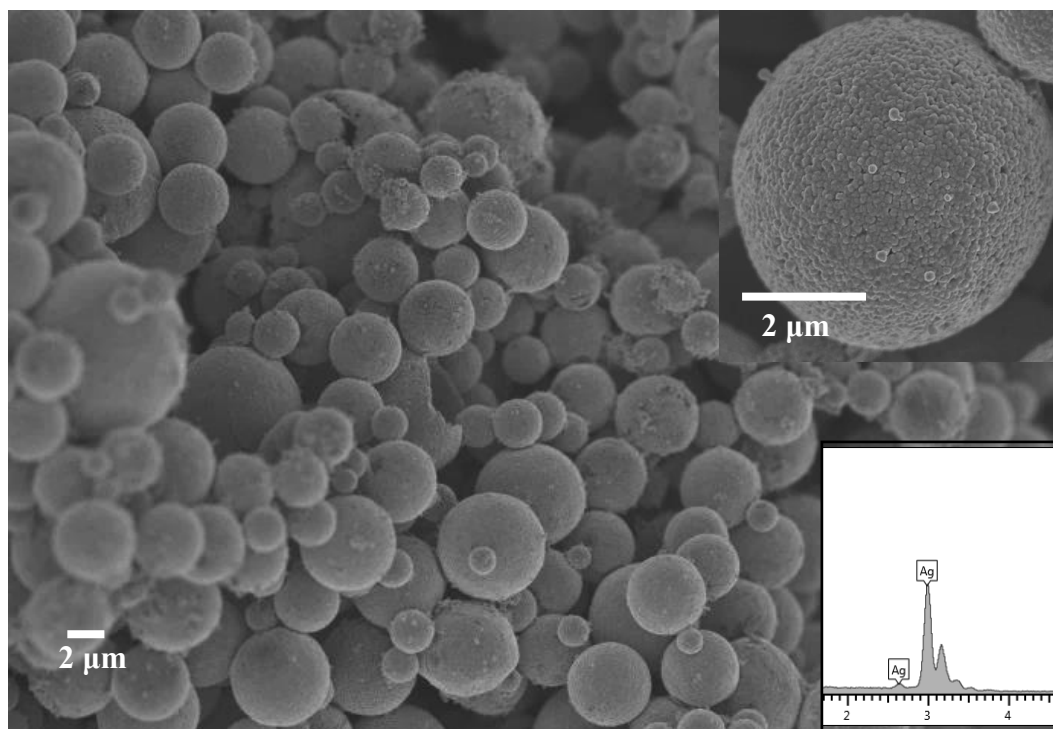
Figure 6.2-1 SEM micrograph of silver-coated microcapsules with EDX analysis. The input ratio of Ag to capsule surface is 93.95 mg/m^2. The AuNPs adsorbed on the polymer capsule surface before Ag coating can't be detected via EDX due to its limited amount

Silver microcapsules samples were prepared with different oil core concentrations of 10 wt% hexylsalicylate (HS). The obtained silver capsules were centrifuged and redispersed into the ethanol and water mixture for 0-20 minutes. Then the silver capsules were centrifuged and air-dried before crushing with a glass slide. The crushed silver microcapsules and hexadecane oil core were washed back into ethanol and then centrifuged to get the supernatant. The supernatant was analysed using a GC technique. The loss of HS was calculated by comparing the HS detected in the supernatant to the initial input weight. The core content release was compared between PMMA shell HS core capsules and silver-coated PMMA shell HS core capsules before and after crushing. The same analysis was carried

out between PEMA shell toluene core capsules and silver-coated PEMA toluene

core capsules before and after crushing. The results are shown in Figure 6.2-2.
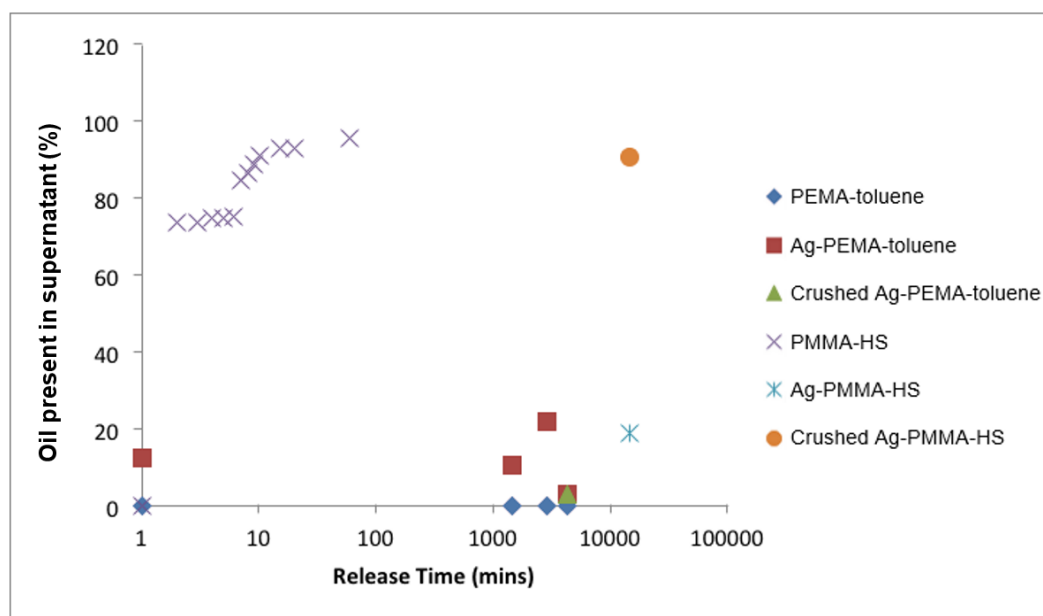
Figure 6.2-2 Core content release of polymer shell and silver shell
microcapsules using Gas Chromatography

From Figure 6.2-2, it was found that among three sets of HS core microcapsules,

the PMMA shell ones showed a 72% loss of core content within 10 minutes after

they were added to the ethanol/water mixture. The loss percentage of core content

increased to 100% in 100 minutes. On the other hand, silver-coated HS core

capsules showed no loss of core content within two weeks after the capsules were

added to the ethanol/water mixture and less than 20% of core content loss after

two weeks. At the same time, the crushed silver-coated showed 90% of core

release. These results prove that the silver coating of the polymer capsules

provided significant protection of its oil core content in a miscible solvent

environment than the polymer shell.

Another interesting finding was that all toluene core capsules presented a low core content loss percentage, no matter with polymer shell, metal shell, or crushed silver shell. It was assumed that the toluene core in the microcapsules might have already evaporated during the capsule formation stage, leading to lower toluene core detection in GC analysis. This assumption was proved by SEM analysis of microtomed silver-coated toluene core microcapsules, as shown in Figure 6.2-3 and Figure 6.2-4.
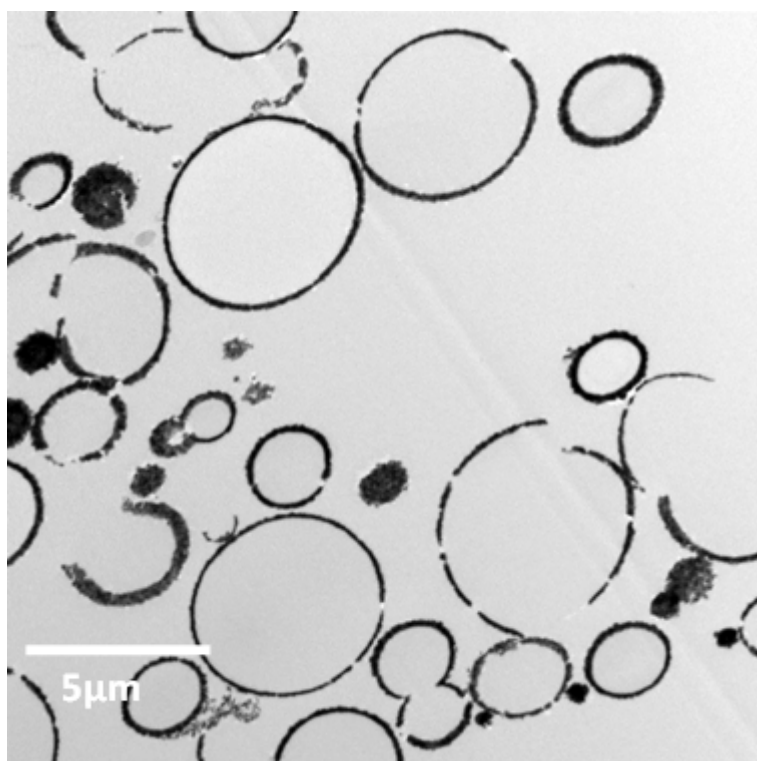
Figure 6.2-3 SEM micrograph of Cross-section of silver shell toluene core microcapsules
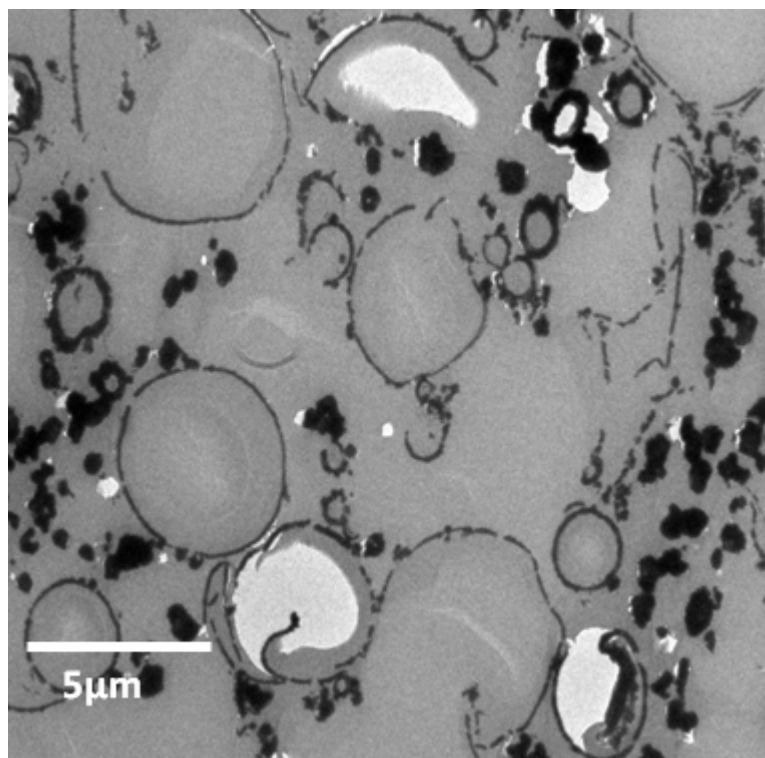
Figure 6.2-4 SEM micrograph of Cross-section of silver shell hexylsalicylate core microcapsules

Compare Figure 6.2-3 to Figure 6.2-4, the oil can be observed clearly in HS core capsules but not found in toluene core capsules.

In this Chapter, not only the preparation of silver shell microcapsules was discussed, but also the influence of silver salt concentration and Au NPs adsorption density on the silver shell thickness was studied.

6.2.1 Influence of silver salt concentration on the silver shell thickness

The influence of silver salt concentration on the properties of the silver shell of toluene core microcapsules, particularly the silver shell thickness, was studied in my previous MSc study. In the preparation of silver-shell toluene core microcapsules, the coating bath concentration of $AgNO_3$ was increased from

0.125 to 1.25 mmol/L. It was found that the coverage of silver coating was improved with the increase of the silver salt concentration. A continuous silver shell formed when the $AgNO_3$ concentration reached 1mmol/L. When the $AgNO_3$ concentration exceeded 1 mmol/L, the silver shell thickness stopped increasing, and aggregation was observed on the capsules surface (He et al., 2013).

In this study, the influence of silver salt concentration on the silver shell thickness was studied with hexylsalicylate core microcapsules. $AgNO_3$ solutions with concentrations from 0.01-1 mmol/L were used in the study. The resulting silver shell microcapsules were cut into half using the microtome technique, and the cross-section of the microcapsule was observed using a Field Emission Gun Transmission Electron Microscope (FEGTEM), as shown in Figure 6.2-5.
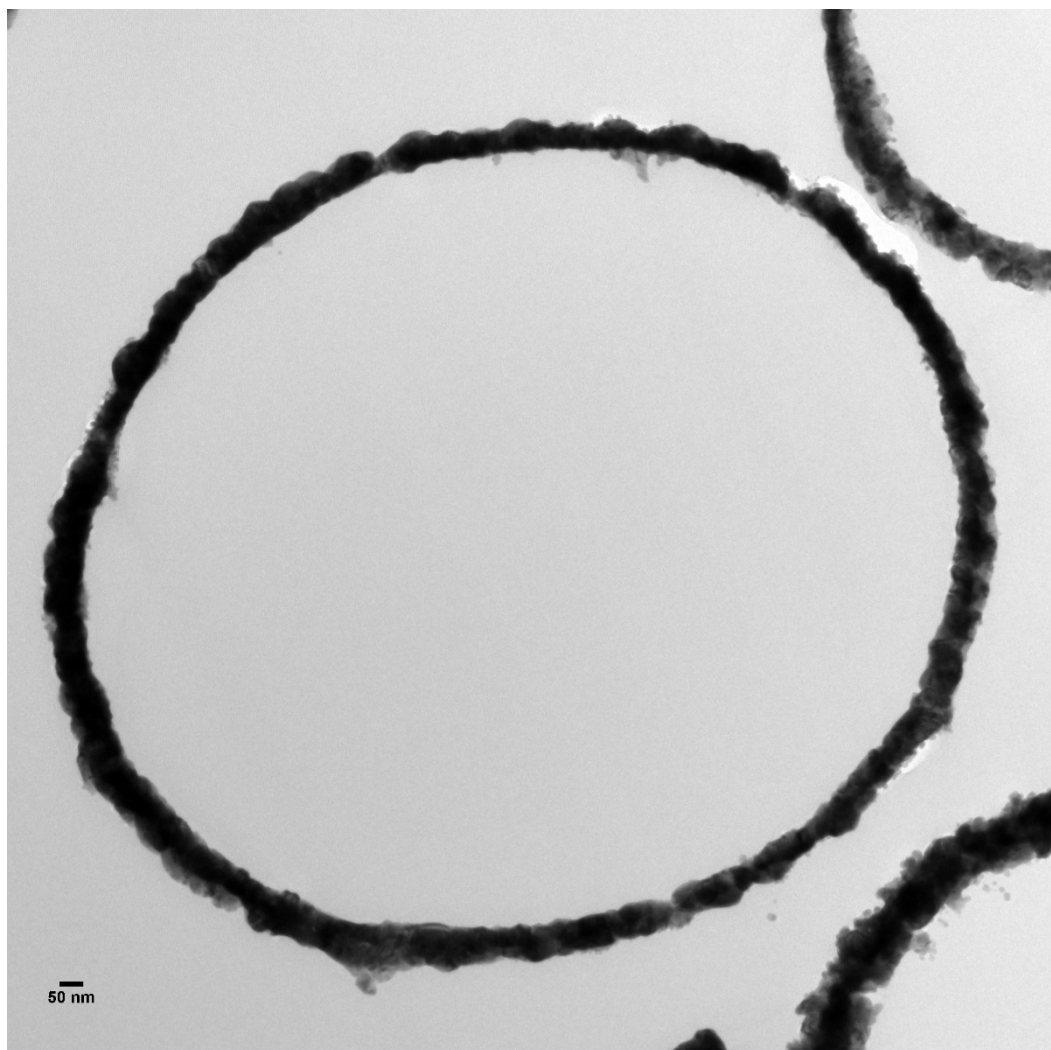
Figure 6.2-5 FEGTEM micrograph of the cross-section of silver-coated microcapsules with silver salt concentration at 1.0 mmol/L

The silver shell thickness was analysed using the FEGTEM micrographs combined with ImageJ software. An average silver shell thickness was obtained for the samples prepared with various silver salt concentrations. The shell thickness was plotted against the ratio of input silver salt to the microcapsules surface area and shown in Figure 6.2-6.
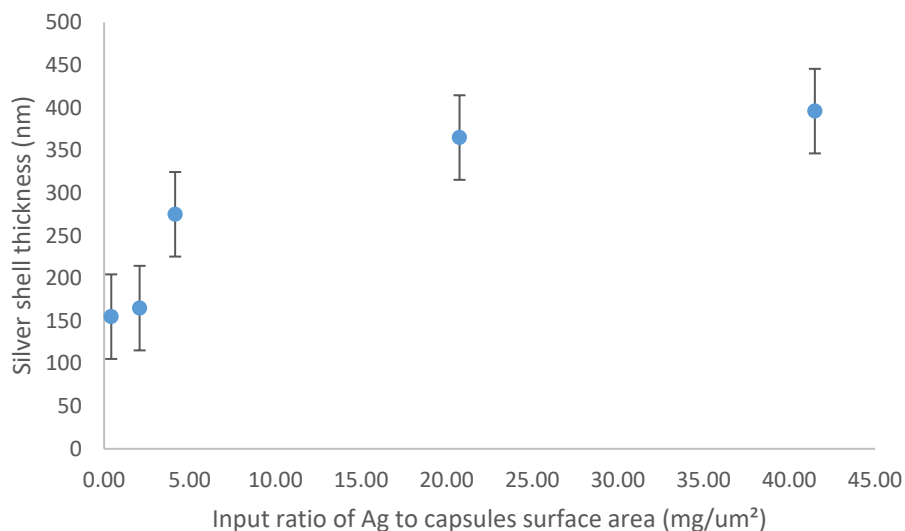
Figure 6.2-6 Silver shell thickness against the input ratio of silver salt to the microcapsule surface area

It was observed from Figure 6.2-6 that the silver shell thickness increased with the increase of the input ratio of silver salt to the capsule surface area, i.e. the more silver salt in the plating bath, the greater the silver shell thickness. However, it is notable that the thickness of the silver coating did not increase significantly when the silver to capsule surface area was greater than 20.74 mg/um² (AgNO$_3$ concentration is 0.5 mmol/L). As the shell thickness increases, it is accompanied by an increase in the surface area of the microcapsules, and consequently, a greater amount of Ag is required to increase the shell thickness than when smaller microcapsules are present. This accounts for the observation that the increase in shell thickness was slower when the microcapsules reached a specific size.

6.2.2 Influence of Au NPs adsorption density on the silver shell thickness

The amount of Au NPs catalyst adsorbed on the polymer capsule surface also impacts the silver shell formation and shell thickness. As shown in Figure 6.2-7, when the Au NPs adsorption is as lower as 2.92 mg/m^2, the Au NPs did not achieve a homogeneous cover of the polymer capsule surface, and as a result, the silver layer did not form a continuous layer on the capsule due to the lack of Au NPs.
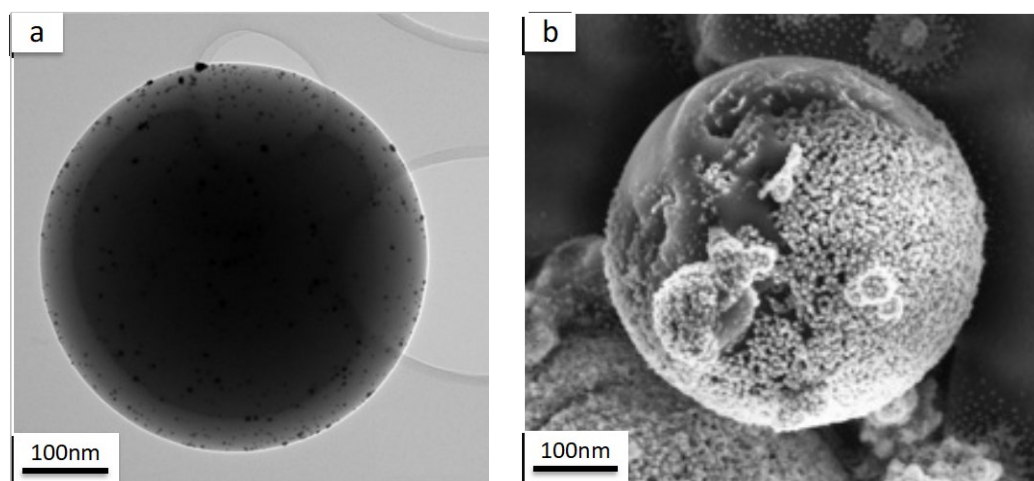
Figure 6.2-7 a) TEM micrograph of Au NPs loaded polymer microcapsules which Au NPs adsorption density is 2.92 mg/m²; b) SEM micrographs of corresponding silver-coated microcapsules

Samples of Au NPs loaded PMMA capsules were prepared with the Au NPs adsorption density from 29.3 – 584.4 mg/m². The same amount of AgNO$_3$ solution with the same concentration was used in the silver electroless plating process. The obtained silver microcapsules shell thickness was analysed using

FEGTEM combined with the microtome and ImageJ techniques. The results are shown in Figure 6.2-8.
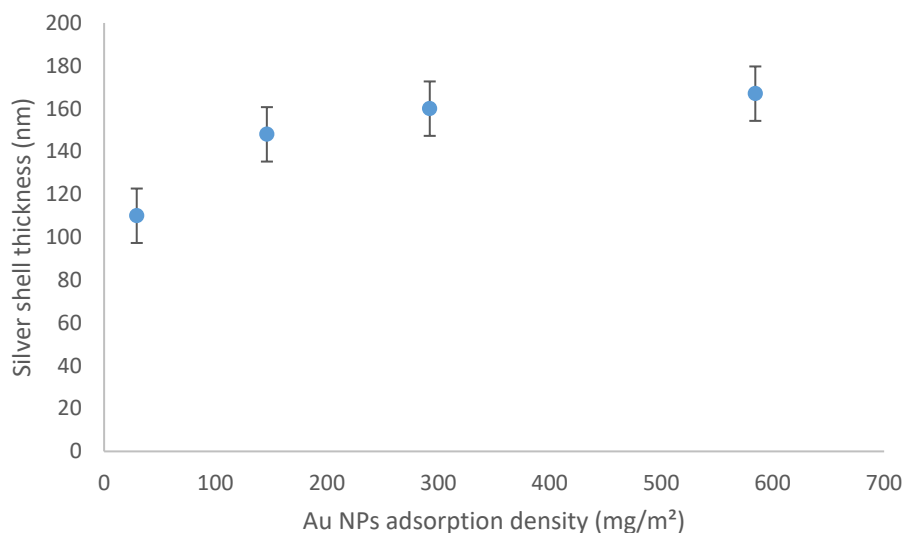
Figure 6.2-8 Silver shell thickness against the input ratio of Au NPs to the microcapsule surface area

It was found that silver shell thickness increases when the Au NPs adsorption density increases. However, the silver shell thickness grows slowly when the Au NPs adsorption density exceeds 146.1 mg/m² and stops growing when the Au NPs adsorption density exceeds 292.2 mg/m².

6.3 Factors affecting the silver shell microcapsules' mechanical strength

The silver shell microcapsule was achieved by forming capsules with PMMA shell and hexylsalicylate core, followed by growing a thin layer of silver coating

on the polymer surface. In this way, long term storage of the volatile fragrance oil core in the ethanol environment was achieved.

In this study, the controlled release of the core content is realised through the shell rupture mechanism. The mechanical strength of synthesised microcapsules was investigated via a micromanipulation technique. This technique is based on diametrical compression and was used to measure the bursting force and deformation at the bursting of single microcapsules and to determine the elastic, visco-elastic or plastic behaviours of single microcapsules (Zhang et al., 2009, Sun and Zhang, 2002, Zhang et al., 1999, Liu et al., 1996).

Rupture stress is the maximum stress the microcapsule can withstand before fracturing under pressure. It depends on the force applied, dimension, and shell thickness of the microcapsules and can be calculated. The nominal rupture stress was used to indicate the mechanical strength of the microcapsules in this study. It was calculated based on the compression force and deformation at the rupture point of a single microcapsule measured using a micromanipulator. Average nominal rupture stress was obtained based on five single capsules with a similar diameter. The main factors that influenced the shell thickness and hence the mechanical strength of the capsules include the capsules diameter, core/shell ratio of the polymer capsules, Au NPs adsorption density, silver salt concentration, and silver shell thickness.

6.3.1 Influence of capsules diameter on the microcapsule mechanical strength

PMMA shell hexylsalicylate core microcapsules with a core/shell ratio of 1:1 were analysed using the micromanipulation technique. The rupture force for

compressing each microcapsule was measured, and the average nominal rupture

stress was calculated based on five microcapsules of similar diameters. The

silver-coated PMMA microcapsules prepared using the same batch of PMMA

shell capsules were also crushed using micromanipulation, and the average

nominal rupture stress was calculated and plotted in Figure 6.1-1.
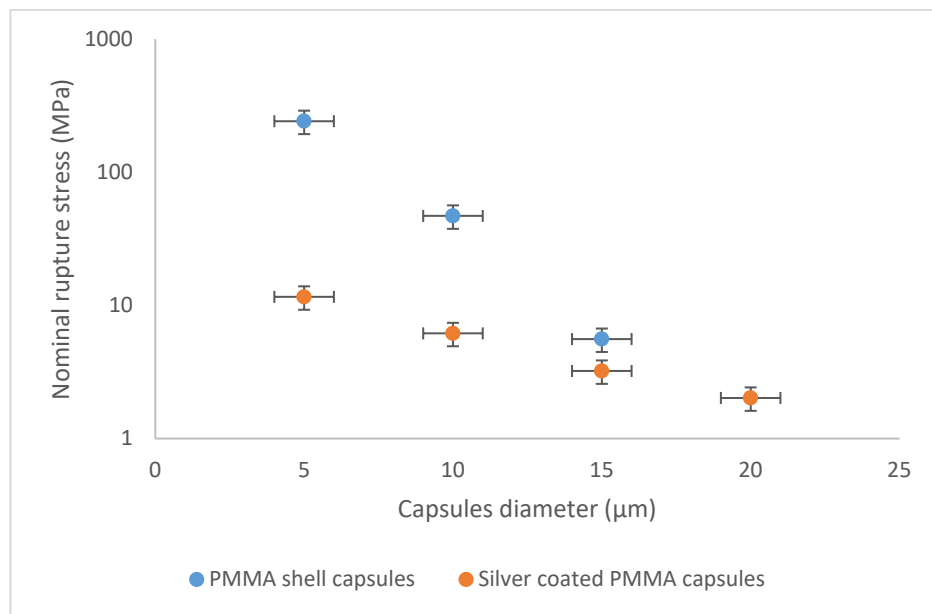
Figure 6.3-1 Nominal rupture stress versus diameter for PMMA shell
hexylsalicylate core capsules with core/shell ratio of 1:1 and silver shell
microcapsules prepared using the same batch of PMMA shell capsules

From Figure 6.3-1, it was found that PMMA shell capsules require greater force

to rupture than silver shell capsules. This is related to the different stress-strain

behaviour of PMMA shell and silver shell microcapsules. The stress-strain

behaviour describes the deformation characteristics of microcapsules upon

compression, which may be elastic, viscoelastic or plastic and may involve

fracture or a combination of these deformation mechanisms. PMMA shell

microcapsules showed a typical viscoelastic deformation, and the deformation

that occurred at the rupture point was more significant than the silver-coated capsules. Silver-coated PMMA microcapsule showed plastic deformation.

The silver-coated PMMA shell capsules shown in Figure 6.3-1 were coated with the same amount of silver; the silver shell thickness was 165±15 nm, while their PMMA shell thickness was 250±37 nm. It was found that the nominal rupture stress decreases with the increase of capsule size in both PMMA and silver shell microcapsules. As described in Chapter 3.3.6 , the rupture force (F_r) and the capsule diameter (D_{cap}) were used to calculate the nominal rupture stress ($\sigma_r = F_r / \pi D_{cap}^2$). Hence the larger diameter of the capsule, the greater the rupture force is required to rupture the shell; meanwhile, the smaller the nominal rupture stress.

6.3.2 Influence of polymer shell thickness on the microcapsule mechanical strength

The mechanical strength of PMMA shell hexylsalicylate core microcapsules with different core/shell ratios, i.e. 1:0.5, 1:1, and 1:1.5, was analysed using the micromanipulator. The average nominal rupture stress was obtained for each batch of samples against the polymer shell thickness and was plotted in Figure 6.3-2.
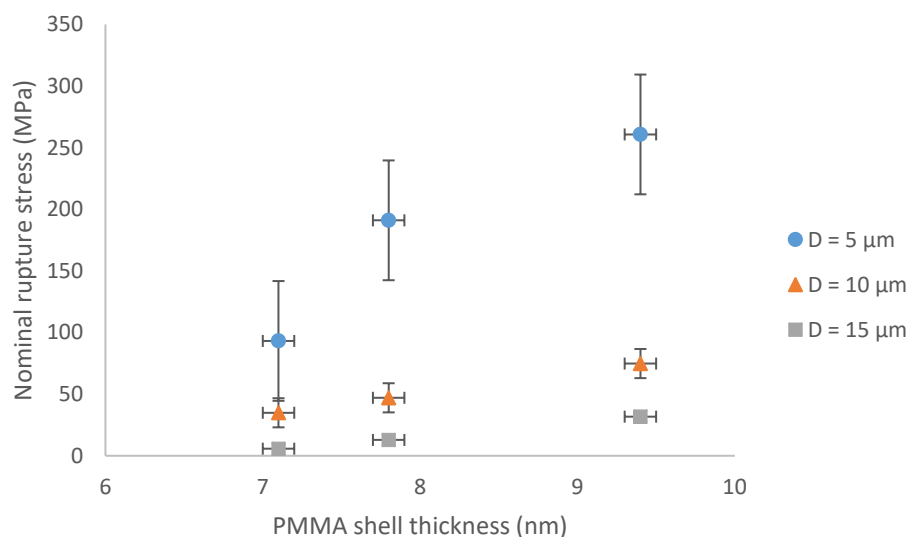
Figure 6.3-2 Nominal rupture stress versus polymer shell thickness for PMMA shell hexylsalicylate core capsules with different diameters

It was found that the capsules mechanical strength increases with the polymer shell thickness in all the PMMA capsules regardless of the diameter. The rupture stress for capsules with smaller diameters is less than the larger capsules. This finding is in accordance with the results in Chapter 6.3.1

6.3.3 Influence of silver shell thickness on the microcapsule mechanical strength

The mechanical strength of the silver shell microcapsules prepared with various Au NPs adsorption densities and silver salt concentrations was analysed using the micromanipulator. As discussed in Chapters 6.2.1and 6.2.2, the silver shell thickness of the formed microcapsules depended on the Au NPs adsorbed on the polymer capsule surface and the concentration of the silver plating bath. The nominal rupture stress of the silver shell microcapsules was plotted against the silver shell thickness in Figure 6.3-3.
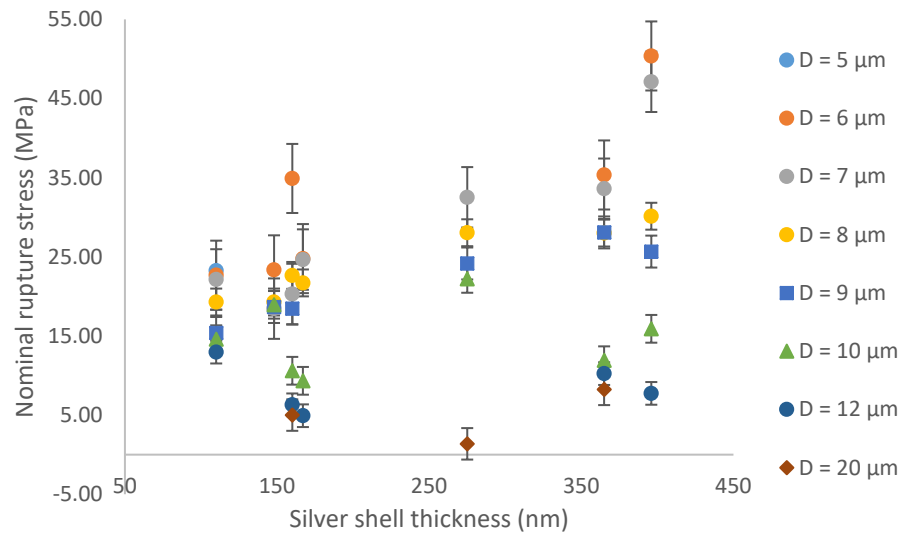
Figure 6.3-3 Nominal rupture stress versus silver shell thickness for the silver shell hexylsalicylate core capsules with different diameters

From Figure 6.3-4, it was found that the nominal rupture stress of all the silver shell microcapsules increases with the silver shell thickness, except the capsules with a diameter of 12 μm. Capsules with a diameter of 6 μm required the greatest rupture stress among all the capsules with the same silver shell thickness, and the capsules with a diameter of 20 μm required the least rupture stress.

Once the silver shell was ruptured, the underneath polymer shell was revealed. The microencapsulated oil was able to release.

6.4 Conclusions

In this Chapter, silver-shell hexylsalicylate core microcapsules were produced via the silver electroless plating method. AgNO₃ aqueous solution was used as the metal salt, and formaldehyde was used to reduce the Ag ions into Ag coating on

the catalytic site created by Au NPs on the PMMA capsule surface. The pH was adjusted to 10 by adding a tiny amount of ammonia solution. The morphology of the obtained silver microcapsules was analysed via SEM, and the encapsulated hexylsalicylate was detected using the GC analysis.

Through GC analysis, it was found that PMMA shell microcapsule released most of the encapsulated core content hexylsalicylate to the ethanol/water mixture within 10 minutes. Compared to the rapid loss of core content with the polymer shell, the silver-coated hexylsalicylate core capsules showed no loss of core content within two weeks after the capsules were added to the ethanol/water mixture and less than 20% of core content loss after two weeks. After two weeks, 90% of core release was observed when the silver-coated microcapsules were crushed. These results prove that the silver coating of the polymer capsules provided significant protection of its oil core content in a miscible solvent environment than the polymer shell.

The silver shell thickness was analysed based on the TEM micrographs of the microtomed capsules, combined with ImageJ software. It was found that the silver shell thickness increased with the increase of the input ratio of silver salt to the capsule surface area, i.e. the more silver salt in the plating bath, the greater the silver shell thickness. However, it is notable that the thickness of the silver coating did not increase significantly when the silver to capsule surface area was greater than 20.74 mg/um² ($AgNO_3$ concentration is 0.5 mmol/L).

It was also found that silver shell thickness increases when the Au NPs adsorption density increases. However, the silver shell thickness grows slowly when the Au

NPs adsorption density exceeds 146.1 mg/m² and stops growing when the Au NPs adsorption density exceeds 292.2 mg/m².

The mechanical strength of the capsules was analysed using the micromanipulation technique. The nominal rupture stress of the single microcapsules was calculated based on the compression force and capsule surface deformation at the rupture point of a single microcapsule measured. Average nominal rupture stress was obtained based on five single capsules with a similar diameter. The main factors that influenced the microcapsules' mechanical strength were investigated, including capsule diameter, polymer shell thickness, and silver shell thickness.

The nominal rupture stress decreases with the increase of capsule size in both PMMA and silver shell microcapsules. PMMA shell capsules require greater force to rupture than silver shell capsules. This is related to the different stress-strain behaviour of PMMA shell and silver shell microcapsules, as it was observed that the deformation that occurred at the rupture point of the PMMA shell capsules was more significant than the silver shell capsules. The capsules mechanical strength increases with the shell thickness in all the PMMA and silver shell capsules regardless of the diameter.

Chpater 7 Conclusions and future work

7.1 Conclusion

Silver shell microcapsules containing volatile fragrance oil as core content were prepared in this study. A three-step method was developed for the fabrication of such microcapsules, i.e. step 1: synthesis of polymer shell oil core microcapsules; step 2: synthesis of electrostatically stabilised negatively charged Au NPs, and the adsorption of Au NPs to the polymer capsules as the catalyst for the following reaction; step 3: a continuous layer of silver coating was applied on the polymer capsule surface via electroless plating method.

The morphology of the polymer microcapsules was predicted by studying the interfacial tensions between oil, polymer and aqueous phases based on Torza and Mason (1970)'s theory. The morphology was confirmed via SEM and FIBSEM. All the synthesised polymer capsules were in a core-shell structure except those with PMMA shell hexadecane core. The influence of the core/shell ratio on oil core retention and polymer shell thickness was studied. The retention and release of the oil core were studied via GC technique, and polymer shell thickness was obtained via theoretical calculation and confirmed via FIBSEM cross-section measurement. It was found that at a core/shell ratio of 1:1.1, the resulting microcapsules showed the biggest dimension, thinnest shell thickness, and the least loss of the core content.

Electrostatic stabilised negative charged Au NPs were synthesised and adsorbed to the polymer capsule surface to create a catalytic site for following on silver reduction reaction. The Au NPs were adsorbed to the polymer surface via

electrostatic, and the adsorption density was influenced by the amount of the cationic surfactant in the capsules suspension. It was found that the adsorption density was also affected by the Au NPs concentration. The Au NPs adsorbed on the polymer surface saturated when the input ratio of Au NPs to the polymer surface was $29.23 mg/m^2$.

AgNO3 aqueous solution was reduced by formaldehyde (HCHO) and formed a layer of silver shell on the polymer capsules surface. Full retention of the oil core was achieved when a continuous layer of silver was formed. Silver shell thickness increased with the input ratio of silver salt to the capsule surface area but stopped increasing when the silver to capsule surface area was greater than 20.74 mg/um².

The mechanical strength of the capsules was studied using the micromanipulation technique. The nominal rupture stress decreases with capsule size in both PMMA and silver shell microcapsules. The capsules mechanical strength increases with the shell thickness in all the PMMA and silver shell capsules regardless of the diameter.

7.2   Future work

Due to the time constraints, it is not possible to give an experimental prediction of the controlled-release of the silver-coated PEMA capsules at this stage. Further study could be focused on generating a prediction system from the data sets of the controlled release of the capsules based on mechanical strength, shell thickness and relevant factors.

This work could be extended to other metal pairings (such as Ag NPs catalyst and Cu coating, Ni NPs catalyst and Ag coating, *etc.*) to study the influence of the metal type on mechanical strength and release properties.

References

ABDERRAHMEN, R., GAVORY, C., CHAUSSY, D., BRIANCON, S., FESSI, H. & BELGACEM, M. N. 2011. Industrial pressure sensitive adhesives suitable for physicochemical microencapsulation. *International Journal of Adhesion and Adhesives,* 31**,** 629-633.

AGARWALA, R. C. & AGARWALA, V. 2003. Electroless alloy/composite coatings: A review. *Sadhana-Academy Proceedings in Engineering Sciences,* 28**,** 475-493.

ANDERSSON TROJER, M., NORDSTIERNA, L., NORDIN, M., NYDEN, M. & HOLMBERG, K. 2013. Encapsulation of actives for sustained release. *Physical chemistry chemical physics : PCCP,* 15**,** 17727-41.

ANTHONY, N. & BERLAND, K. 2013. Chapter Seven - Global Analysis in Fluorescence Correlation Spectroscopy and Fluorescence Lifetime Microscopy. *In:* TETIN, S. Y. (ed.) *Methods in Enzymology.* Academic Press.

ANTIPOV, A. A., SUKHORUKOV, G. B., DONATH, E. & MOHWALD, H. 2001. Sustained release properties of polyelectrolyte multilayer capsules. *Journal of Physical Chemistry B,* 105**,** 2281-2284.

APPARAO, B., SHIVALINGAM, M. R., REDDY, Y. V. K., SUNITHA, N., JYOTHIBASU, T. & SHYAM, T. 2010. Design and evaluation of sustained release microcapsules containing diclofenac sodium. *International Journal of PHARMACEUTICAL AND BIOMEDICAL RESEARCH,* 1**,** 90-93.

ASTRUC, D. 2008. Transition-metal Nanoparticles in Catalysis: From Historical Background to the State-of-the Art. *Nanoparticles and Catalysis.* Wiley-VCH Verlag GmbH & Co. KGaA.

ASTRUC, D., LU, F. & ARANZAES, J. R. 2005. Nanoparticles as recyclable catalysts: The frontier between homogeneous and heterogeneous catalysis. *Angewandte Chemie-International Edition,* 44**,** 7852-7872.

ATKIN, R., DAVIES, P., HARDY, J. & VINCENT, B. 2004. Preparation of aqueous core/polymer shell microcapsules by internal phase separation. *Macromolecules,* 37**,** 7979-7985.

BACHTSI, A. R. & KIPARISSIDES, C. 1995. AN EXPERIMENTAL INVESTIGATION OF ENZYME-RELEASE FROM POLY(VINYL ALCOHOL) CROSS-LINKED MICROSPHERES. *Journal of Microencapsulation,* 12**,** 23-35.

BASARIR, F. 2012. Fabrication of Gold Patterns via Multilayer Transfer Printing and Electroless Plating. *Acs Applied Materials & Interfaces,* 4**,** 1324-1329.

BERGER, R. G. 2007. *Flavours and Fragrances: Chemistry, Bioprocessing and Sustainability*, Springer.

BHANDARI, B. R., D'ARCY, B. R. & PADUKKA, I. 1999. Encapsulation of lemon oil by paste method using beta-cyclodextrin: Encapsulation efficiency and profile of oil volatiles. *Journal of Agricultural and Food Chemistry,* 47**,** 5194-5197.

2

BINDRA, P. W., J. R. 1990. Fundamental aspects of electroless copper plating. *In:* MALLORY, G. O. H., J.B. (ed.) *Electroless plating-fundamentals and applications.* Noyes: William Andrew.

BLAKE, P., AHN, W. & ROPER, D. K. 2010. Enhanced Uniformity in Arrays of Electroless Plated Spherical Gold Nanoparticles Using Tin Presensitization. *Langmuir,* 26**,** 1533-1538.

BODMEIER, R., CHEN, H., DAVIDSON, R. G. W. & HARDEE, G. E. 1997. Microencapsulation of Antimicrobial Ceftiofur Drugs. *Pharmaceutical Development and Technology,* 2**,** 323-334.

BOEHM, A. L., MARTINON, I., ZERROUK, R., RUMP, E. & FESSI, H. 2003. Nanoprecipitation technique for the encapsulation of agrochemical active ingredients. *Journal of Microencapsulation,* 20**,** 433-441.

BOHREN, C. F. & HUFFMAN, D. R. 2007. Angular Dependence of Scattering. *Absorption and Scattering of Light by Small Particles.* Wiley-VCH Verlag GmbH.

BOND, G. C. 1974. *Heterogeneous catalysis: principles and applications*, Clarendon Press.

BOWKER, M. 1998. *The Basis and Applications of Heterogeneous Catalysis*, Oxfor University Press.

BRANNONPEPPAS, L. 1993. CONTROLLED-RELEASE IN THE FOOD AND COSMETICS INDUSTRIES. *Acs Symposium Series,* 520**,** 42-52.

BRENNER, A. & RIDDELL, G. 1946a. *Research Natl. US Bur. Stand.,* 37: 31.

BRENNER, A. & RIDDELL, G. E. 1946b. Nickel plating on steel by chemical reduction. *Plating and Surface Finishing,* 85**,** 54-56.

BROWN, E. N., KESSLER, M. R., SOTTOS, N. R. & WHITE, S. R. 2003. In situ poly(urea-formaldehyde) microencapsulation of dicyclopentadiene. *Journal of Microencapsulation,* 20**,** 719-730.

BRYDSON, R. Class handout of 'Microscopy and analysis techniques'.

BRYDSON, R. M. & HAMMOND, C. 2005. Generic Methodologies for Nanotechnology: Characterization. *Nanoscale Science and Technology.* John Wiley & Sons, Ltd.

CAO, X. G. & ZHANG, H. Y. 2013. Investigation into conductivity of silver-coated cenosphere composites prepared by a modified electroless process. *Applied Surface Science,* 264**,** 756-760.

CARUSO, F., NIIKURA, K., FURLONG, D. N. & OKAHATA, Y. 1997. 2. Assembly of Alternating Polyelectrolyte and Protein Multilayer Films for Immunosensing. *Langmuir,* 13**,** 3427-3433.

CHAMPAGNE, C. P. & FUSTIER, P. 2007. Microencapsulation for the improved delivery of bioactive compounds into foods. *Current Opinion in Biotechnology,* 18**,** 184-190.

CHEN, D., LIU, H. Y., LIU, J. S., REN, X. L., MENG, X. W., WU, W. & TANG, F. Q. 2008a. A general method for synthesis continuous silver nanoshells on dielectric colloids. *Thin Solid Films,* 516**,** 6371-6376.

CHEN, M., KIM, Y. N., LEE, H. M., LI, C. & CHO, S. O. 2008b. Multifunctional magnetic silver nanoshells with sandwichlike nanostructures. *Journal of Physical Chemistry C,* 112**,** 8870-8874.

CHU, L. Y., PARK, S. H., YAMAGUCHI, T. & NAKAO, S. 2001. Preparation of thermo-responsive core-shell microcapsules with a porous membrane and poly(N-isopropylacrylamide) gates. *Journal of Membrane Science,* 192**,** 27-39.

DAI, J. H. & BRUENING, M. L. 2002. Catalytic nanoparticles formed by reduction of metal ions in multilayered polyelectrolyte films. *Nano Letters,* 2**,** 497-501.

DEJUGNAT, C. & SUKHORUKOV, G. B. 2004. PH-responsive properties of hollow polyelectrolyte microcapsules templated on various cores. *Langmuir,* 20**,** 7265-7269.

DELANEY, J. A., SCHNEIDER-LINDNER, V., BRASSARD, P. & SUISSA, S. 2008. Mortality after infection with methicillin-resistant Staphylococcus aureus (MRSA) diagnosed in the community. *BMC Med,* 6**,** 2.

DENNIS, J. K. & SUCH, T. E. 1993. Autocatalytic deposition of nickel. *Nickel and Chromium Plating.* Woodhead Pub.

DESAI, K. G. H. & PARK, H. J. 2005. Encapsulation of vitamin C in tripolyphosphate cross-linked chitosan microspheres by spray drying. *Journal of Microencapsulation,* 22**,** 179-192.

DESHPANDE, K., DAVE, B. C. & GEBERT, M. S. 2006. Controlled dissolution of organosilica sol-gels as a means for water-regulated release/delivery of actives in fabric care applications. *Chemistry of Materials,* 18**,** 4055-4064.

DÍAZ, D. J., WILLIAMSON, T. L., GUO, X., SOOD, A. & BOHN, P. W. 2006. Electroless deposition of gold and platinum for metallization of the intrapore space in porous gallium nitride. *Thin Solid Films,* 514**,** 120-126.

DOWDING, P. J., ATKIN, R., VINCENT, B. & BOUILLOT, P. 2004. Oil core-polymer shell microcapsules prepared by internal phase separation from emulsion droplets. I. Characterization and release rates for microcapsules with polystyrene shells. *Langmuir,* 20**,** 11374-11379.

DOWDING, P. J., ATKIN, R., VINCENT, B. & BOUILLOT, P. 2005. Oil core/polymer shell microcapsules by internal phase separation from emulsion droplets. II: Controlling the release profile of active molecules. *Langmuir,* 21**,** 5278-5284.

DOWLER, C. C., DAILEY, O. D. & MULLINIX, B. G. 1999. Polymeric microcapsules of alachlor and metolachlor: Preparation and evaluation of controlled-release properties. *Journal of Agricultural and Food Chemistry,* 47**,** 2908-2913.

DUBEY, R., SHAMI, T. C. & RAO, K. U. B. 2009. Microencapsulation Technology and Applications. *Defence Science Journal,* 59**,** 82-95.

DUCKER, W. A., SENDEN, T. J. & PASHLEY, R. M. 1991. DIRECT MEASUREMENT OF COLLOIDAL FORCES USING AN ATOMIC FORCE MICROSCOPE. *Nature,* 353**,** 239-241.

EDELMAN, E. R., MATHIOWITZ, E., LANGER, R. & KLAGSBRUN, M. 1991. CONTROLLED AND MODULATED RELEASE OF BASIC FIBROBLAST GROWTH-FACTOR. *Biomaterials,* 12**,** 619-626.

ENDERLE, J. D. 2012. Chapter 7 - Compartmental Modeling. *In:* ENDERLE, J. D. & BRONZINO, J. D. (eds.) *Introduction to Biomedical Engineering (Third Edition).* Boston: Academic Press.

EVANS, R. L. 1970. Process of forming metal coating on filled microcapsules. Google Patents.

FALDT, P. & BERGENSTAHL, B. 1995. FAT ENCAPSULATION IN SPRAY-DRIED FOOD POWDERS. *Journal of the American Oil Chemists Society,* 72**,** 171-176.

FARES, S. 2012. Influence of gamma-ray irradiation on optical and thermal degradation of poly(ethyl-methacrylate) (PEMA) polymer. *Natural Science,* 2012**,** 499-507.

FERRANDO, R. 2006. Surface Diffusion: Simulations. *In:* BUSCHOW, K. H. J., CAHN, R. W., FLEMINGS, M. C., ILSCHNER, B., KRAMER, E. J., MAHAJAN, S. & VEYSSIÈRE, P. (eds.) *Encyclopedia of Materials: Science and Technology.* Oxford: Elsevier.

FIDDES, L. K., CHAN, H. K. C., WYSS, K., SIMMONS, C. A., KUMACHEVA, E. & WHEELER, A. R. 2009. Augmenting microgel flow via receptor-ligand binding in the constrained geometries of microchannels. *Lab on a Chip,* 9**,** 286-290.

FRENS, G. 1973. Controlled Nucleation for the Regulation of the Particle Size in Monodisperse Gold Suspensions. *Nature Physical Science***,** 20-22.

FUJIWARA, Y., KOBAYASHI, Y., SUGAYA, T., KOISHIKAWA, A., HOSHIYAMA, Y. & MIYAKE, H. 2010. Adsorption Promotion of Ag Nanoparticle Using Cationic Surfactants and Polyelectrolytes for Electroless Cu Plating Catalysts. *Journal of the Electrochemical Society,* 157**,** D211-D216.

GE, S. H., WU, Z. J., ZHANG, M. H., LI, W. & TAO, K. Y. 2006. Sulfolene hydrogenation over an amorphous Ni-B alloy catalyst on MgO. *Industrial & Engineering Chemistry Research,* 45**,** 2229-2234.

GE, X. B., YAN, X. L., WANG, R. Y., TIAN, F. & DING, Y. 2009. Tailoring the Structure and Property of Pt-Decorated Nanoporous Gold by Thermal Annealing. *Journal of Physical Chemistry C,* 113**,** 7379-7384.

GHARSALLAOUI, A., ROUDAUT, G., CHAMBIN, O., VOILLEY, A. & SAUREL, R. 2007. Applications of spray-drying in microencapsulation of food ingredients: An overview. *Food Research International,* 40**,** 1107-1121.

GHODBANE, O., ROUE, L. & BELANGER, D. 2008. Study of the electroless deposition of Pd on Cu-modified graphite electrodes by metal exchange reaction. *Chemistry of Materials,* 20**,** 3495-3504.

GHOSH, P. 2008. Coatings: principles and practice. *Adhesive And Coating Technology.* McGraw-Hill Education (India) Pvt Limited.

GHOSH, S. K. 2006. *Functional Coatings: By Polymer Microencapsulation*, Wiley.

GIBBS, B. F., KERMASHA, S., ALLI, I. & MULLIGAN, C. N. 1999. Encapsulation in the food industry: a review. *International Journal of Food Sciences and Nutrition,* 50**,** 213-224.

GOGOTSI, Y. 2006. *Nanomaterials Handbook*, Taylor & Francis.

GOODHEW, P. J., HUMPHREYS, J. & BEANLAND, R. 2000. *Electron Microscopy and Analysis, Third Edition*, Taylor & Francis.

GOUIN, S. 2004. Microencapsulation: industrial appraisal of existing technologies and trends. *Trends in Food Science & Technology,* 15**,** 330-347.

GREEN, B. K. & LOWELL, S. 1957. Oil-containing microscopic capsules and method of making them. Google Patents.

GREEN, B. K., LOWELL, SCHLEICHER. 1957. *Oil-containing microscopic capsules and method of making them*. United States patent application 2800457.

GUO, R. H., JIANG, S. X., ZHENG, Y. D. & LAN, J. W. 2013. Electroless nickel deposition of a palladium-activated self-assembled monolayer on polyester fabric. *Journal of Applied Polymer Science,* 127**,** 4186-4193.

HANCU, G., SIMON, B., KELEMEN, H., RUSU, A., MIRCIA, E. & GYERESI, A. 2013. Thin layer chromatographic analysis of Beta-lactam antibiotics. *Adv Pharm Bull,* 3**,** 367-71.

HARA, K., SATO, T., KATOH, R., FURUBE, A., OHGA, Y., SHINPO, A., SUGA, S., SAYAMA, K., SUGIHARA, H. & ARAKAWA, H. 2003. Molecular design of coumarin dyes for efficient dye-sensitized solar cells. *Journal of Physical Chemistry B,* 107**,** 597-606.

HE, L., BIGGS, S. & CAYRE, O. 2013. *RE: Preparation and Characterisation of Silver Coated Microcapsules Using Electroless Plating Routes.*

HEJZE, T., GOLLAS, B. R., SAUERBREY, R. K., SCHMIED, M., HOFER, F. & BESENHARD, J. O. 2005. Preparation of Pd-coated polymer electrolyte membranes and their application in direct methanol fuel cells. *Journal of Power Sources,* 140**,** 21-27.

HENTZE, H. P. & KALER, E. W. 2003. Polymerization of and within self-organized media. *Current Opinion in Colloid & Interface Science,* 8**,** 164-178.

HERRMANN, J. & BODMEIER, R. 1995. THE EFFECT OF PARTICLE MICROSTRUCTURE ON THE SOMATOSTATIN RELEASE FROM POLY(LACTIDE) MICROSPHERES PREPARED BY A W/O/W SOLVENT EVAPORATION METHOD. *Journal of Controlled Release,* 36**,** 63-71.

HITCHCOCK, J. P., TASKER, A. L., BAXTER, E. A., BIGGS, S. & CAYRE, O. J. 2015. Long-Term Retention of Small, Volatile Molecular Species within Metallic Microcapsules. *ACS Applied Materials & Interfaces,* 7**,** 14808-14815.

HOCHMUTH, R. M. 2000. Micropipette aspiration of living cells. *Journal of Biomechanics,* 33**,** 15-22.

HOHNSTEDT, L. F., MINIATAS, B. O. & WALLER, S. M. C. 1965. Aqueous Sodium Borohydride Chemistry. The Colnage Metals, Copper, Silver, and Gold. *Analytical Chemistry,* 37**,** 1163-1164.

HORIUCHI, S. & NAKAO, Y. 2010. Platinum colloid catalyzed etchingless gold electroless plating with strong adhesion to polymers. *Surface & Coatings Technology,* 204**,** 3811-3817.

HUANG, H. Y., REMSEN, E. E., KOWALEWSKI, T. & WOOLEY, K. L. 1999. Nanocages derived from shell cross-linked micelle templates. *Journal of the American Chemical Society,* 121**,** 3805-3806.

HUANG, Y. & DITTMEYER, R. 2006. Preparation and characterization of composite palladium membranes on sinter-metal supports with a ceramic barrier against intermetallic diffusion. *Journal of Membrane Science,* 282**,** 296-310.

HULST, H. C. & VAN DE HULST, H. C. 1957. *Light scattering: by small particles*, Dover Publications, Incorporated.

HWANG, Y. K., JEONG, U. & CHO, E. C. 2008. Production of uniform-sized polymer core-shell microcapsules by coaxial electrospraying. *Langmuir,* 24**,** 2446-2451.

ICHIKAWA, H. & FUKUMORI, Y. 2000. A novel positively thermosensitive controlled-release microcapsule with membrane of nano-sized poly(N-

isopropylacrylamide) gel dispersed in ethylcellulose matrix. *Journal of Controlled Release,* 63**,** 107-119.

IM, S. H., JEONG, U. Y. & XIA, Y. N. 2005. Polymer hollow particles with controllable holes in their surfaces. *Nature Materials,* 4**,** 671-675.

INBERG, A., LIVSHITS, P., ZALEVSKY, Z. & SHACHAM-DIAMAND, Y. 2012. Electroless deposition of silver thin films on gold nanoparticles catalyst for micro and nanoelectronics applications. *Microelectronic Engineering,* 98**,** 570-573.

ITOH, Y., MATSUSAKI, M., KIDA, T. & AKASHI, M. 2006. Enzyme-responsive release of encapsulated proteins from biodegradable hollow capsules. *Biomacromolecules,* 7**,** 2715-2718.

JAFARI, S. M., ASSAIDPOOR, E., BHANDARI, B. & HE, Y. H. 2008. Nano-particle encapsulation of fish oil by spray drying. *Food Research International,* 41**,** 172-183.

JAIN, P., S.ARORA & T.RAI 1997. Flavour encapsulation and its applications. *Beverage and food world,* July**,** 27-24.

JANA, N. R., GEARHEART, L. & MURPHY, C. J. 2001. Seeding Growth for Size Control of 5−40 nm Diameter Gold Nanoparticles. *Langmuir,* 17**,** 6782-6786.

JANG, J. S., KIM, S. & LEE, K. J. 2007. Fabrication of CdS/PMMA core/shell nanoparticles by dispersion mediated interfacial polymerization. *Chemical Communications***,** 2689-2691.

JONSSON, J. E., HASSANDER, H. & TORNELL, B. 1994. POLYMERIZATION CONDITIONS AND THE DEVELOPMENT OF A CORE-SHELL MORPHOLOGY IN PMMA PS LATEX-PARTICLES .1. INFLUENCE OF INITIATOR PROPERTIES AND MODE OF MONOMER ADDITION. *Macromolecules,* 27**,** 1932-1937.

KARUKSTIS, K. K. & VAN HECKE, G. R. 2003. *Chemistry Connections: The Chemical Basis of Everyday Phenomena*, Academic Press.

KAYA, İ. & ÖZDEMIR, E. 1995. Thermodynamic Interactions and Characterization of Poly(Ethyl Methacrylate) by Inverse Gas Chromatography. *Journal of Macromolecular Science, Part A,* 32**,** 377-383.

KIM, Y. D. & MORR, C. V. 1996. Microencapsulation properties of gum Arabic and several food proteins: Spray-dried orange oil emulsion particles. *Journal of Agricultural and Food Chemistry,* 44**,** 1314-1320.

KLAYPRADIT, W. & HUANG, Y. W. 2008. Fish oil encapsulation with chitosan using ultrasonic atomizer. *Lwt-Food Science and Technology,* 41**,** 1133-1139.

KO, J. W., KOO, H. C., KIM, D. W., SEO, S. M., KANG, T. J., KWON, Y., YOON, J. L., CHEON, J. H., KIM, Y. H., KIM, J. J. & PARK, Y. J. 2010. Electroless Gold Plating on Aluminum Patterned Chips for CMOS-Based Sensor Applications. *Journal of the Electrochemical Society,* 157**,** D46-D49.

KOBAYASHI, Y. & ISHII, Y. 2013. Electroless Deposited Gold Nanoparticles on Glass Plates as Sensors for Measuring the Dielectric Constant of Solutions. *Journal of Nanoparticles,* 2013**,** 5.

KOBAYASHI, Y., SALGUEIRINO-MACEIRA, V. & LIZ-MARZAN, L. M. 2001. Deposition of sliver nanoparticles on silica spheres by pretreatment steps in electroless plating. *Chemistry of Materials,* 13**,** 1630-1633.

KRUYT, H. R. 1949. *Colloid Science: Reversible systems, 1949*, Elsevier Publishing Company.

L, E. R. 1970. Process of forming metal coating on filled microcapsules. Google Patents.

LACASSE, K. & BAUMANN, W. 2004. *Textile Chemicals: Environmental Data and Facts*, U.S. Government Printing Office.

LAM, X. M., DUENAS, E. T. & CLELAND, J. L. 2001. Encapsulation and stabilization of nerve growth factor into poly(lactic-co-glycolic) acid microspheres. *Journal of Pharmaceutical Sciences,* 90**,** 1356-1365.

LANCE M. BAIRD, J. J. B., JENNIFER L. BREIDENICH, RYAN M. DEACON, ERIN D. LABARRE, ADAM J. MAISANO, EDWARD W. OTT, MARCIA W. PATCHAN, AND YO-RHIN RHIM. 2012. *Self-Healing Coatings with Galvanic Protection* [Online]. Available: http://www.pcimag.com/articles/96150-self-healing-coatings-with-galvanic-protection- [Accessed].

LAPIDOT, N., GANS, O., BIAGINI, F., SOSONKIN, L. & ROTTMAN, C. 2003. Advanced sunscreens: UV absorbers encapsulated in sol-gel glass microcapsules. *Journal of Sol-Gel Science and Technology,* 26**,** 67-72.

LI, Y., HONG, X. M., COLLARD, D. M. & EL-SAYED, M. A. 2000. Suzuki cross-coupling reactions catalyzed by palladium nanoparticles in aqueous solution. *Organic Letters,* 2**,** 2385-2388.

LIM, C. T., ZHOU, E. H., LI, A., VEDULA, S. R. K. & FU, H. X. 2006. Experimental techniques for single cell and single molecule biomechanics. *Materials Science & Engineering C-Biomimetic and Supramolecular Systems,* 26**,** 1278-1288.

LIN, K.-Y., TSAI, W.-T. & CHANG, J.-K. 2010. Decorating carbon nanotubes with Ni particles using an electroless deposition technique for hydrogen storage applications. *International Journal of Hydrogen Energy,* 35**,** 7555-7562.

LIN, K. J., WU, H. M., YU, Y. H., HO, C. Y., WEI, M. H., LU, F. H. & TSENG, W. J. 2013. Preparation of PMMA-Ni core-shell composite particles by electroless plating on polyelectrolyte-modified PMMA beads. *Applied Surface Science,* 282**,** 741-745.

LIU, J. B., DONG, W., ZHAN, P., WANG, S. Z., ZHANG, J. H. & WANG, Z. L. 2005. Synthesis of bimetallic nanoshells by an improved electroless plating method. *Langmuir,* 21**,** 1683-1686.

LIU, K. K., WILLIAMS, D. R. & BRISCOE, B. J. 1996. Compressive deformation of a single microcapsule. *Physical Review E,* 54**,** 6673-6680.

LIU, T., LI, D., YANG, D. & JIANG, M. 2011. An improved seed-mediated growth method to coat complete silver shells onto silica spheres for surface-enhanced Raman scattering. *Colloids and Surfaces A: Physicochemical and Engineering Aspects,* 387**,** 17-22.

LORENCEAU, E., UTADA, A. S., LINK, D. R., CRISTOBAL, G., JOANICOT, M. & WEITZ, D. A. 2005. Generation of polymerosomes from double-emulsions. *Langmuir,* 21**,** 9183-9186.

LOXLEY, A. & VINCENT, B. 1998. Preparation of poly(methylmethacrylate) microcapsules with liquid cores. *Journal of Colloid and Interface Science,* 208**,** 49-62.

LU, G. Z., THOMPSON, B. G. & GRAY, M. R. 1992. PHYSICAL MODELING OF ANIMAL-CELL DAMAGE BY HYDRODYNAMIC-FORCES IN

SUSPENSION-CULTURES. *Biotechnology and Bioengineering,* 40**,** 1277-1281.

LUKEHART, C. M. & SCOTT, R. A. 2007. *Nanomaterials: Inorganic and Bioinorganic Perspectives*, John Wiley & Sons.

LULEVICH, V. V., RADTCHENKO, I. L., SUKHORUKOV, G. B. & VINOGRADOVA, O. I. 2003. Mechanical properties of polyelectrolyte microcapsules filled with a neutral polymer. *Macromolecules,* 36**,** 2832-2837.

MA, Y. & ZHANG, Q. 2012. Preparation and characterization of monodispersed PS/Ag composite microspheres through modified electroless plating. *Applied Surface Science,* 258**,** 7774-7780.

MACRITCH.F 1969. MECHANISM OF INTERFACIAL POLYMERIZATION. *Transactions of the Faraday Society,* 65**,** 2503-&.

MADENE, A., JACQUOT, M., SCHER, J. & DESOBRY, S. 2006. Flavour encapsulation and controlled release - a review. *International Journal of Food Science and Technology,* 41**,** 1-21.

MANDAL, T. K. 1999. Effect of solvent on the characteristics of pentamidine loaded microcapsule. *Journal of Biomaterials Science, Polymer Edition,* 10**,** 1-17.

MARTIN, M. N., BASHAM, J. I., CHANDO, P. & EAH, S.-K. 2010. Charged Gold Nanoparticles in Non-Polar Solvents: 10-min Synthesis and 2D Self-Assembly. *Langmuir,* 26**,** 7410-7417.

MAURER, K. H. 2004. Detergent proteases. *Current Opinion in Biotechnology,* 15**,** 330-334.

MEI, Y., LU, Y., POLZER, F., BALLAUFF, M. & DRECHSLER, M. 2007. Catalytic activity of palladium nanoparticles encapsulated in spherical polyelectrolyte brushes and core-shell microgels. *Chemistry of Materials,* 19**,** 1062-1069.

MITCHISON, J. M. & SWANN, M. M. 1954. THE MECHANICAL PROPERTIES OF THE CELL SURFACE .1. THE CELL ELASTIMETER. *Journal of Experimental Biology,* 31**,** 443-&.

MOHD SULTAN, N. & JOHAN, M. R. 2014. Synthesis and Ultraviolet Visible Spectroscopy Studies of Chitosan Capped Gold Nanoparticles and Their Reactions with Analytes. *The Scientific World Journal,* 2014**,** 184604.

MONLLOR, P., BONET, M. A. & CASES, F. 2007. Characterization of the behaviour of flavour microcapsules in cotton fabrics. *European Polymer Journal,* 43**,** 2481-2490.

MOSHFEGH, A. Z. 2009a. Nanoparticle catalysts. *Journal of Physics D-Applied Physics,* 42.

MOSHFEGH, A. Z. 2009b. Nanoparticle catalysts. *Journal of Physics D: Applied Physics,* 42**,** 233001.

MÜLLER, A., HEINRICH, T., TOUGAARD, S., WERNER, W. S. M., HRONEK, M., KUNZ, V., RADNIK, J., STOCKMANN, J. M., HODOROABA, V.-D., BENEMANN, S., NIRMALANANTHAN-BUDAU, N., GEISSLE, D., SPARNACCI, K. & UNGER, W. E. S. 2019. Determining the Thickness and Completeness of the Shell of Polymer Core–Shell Nanoparticles by X-ray Photoelectron Spectroscopy, Secondary Ion Mass Spectrometry, and Transmission Scanning Electron Microscopy. *The Journal of Physical Chemistry C,* 123**,** 29765-29775.

MUNIN, A. & EDWARDS-LÉVY, F. 2011. Encapsulation of Natural Polyphenolic Compounds; a Review. *Pharmaceutics,* 3**,** 793-829.

NARAYANAN, R. & EL-SAYED, M. A. 2005. Catalysis with transition metal nanoparticles in colloidal solution: Nanoparticle shape dependence and stability. *Journal of Physical Chemistry B,* 109**,** 12663-12676.

NEUBAUER, M. P., POEHLMANN, M. & FERY, A. 2014. Microcapsule mechanics: From stability to function. *Advances in Colloid and Interface Science,* 207**,** 65-80.

O'SULLIVAN, M., ZHANG, Z. B. & VINCENT, B. 2009. Silica-Shell/Oil-Core Microcapsules with Controlled Shell Thickness and Their Breakage Stress. *Langmuir,* 25**,** 7962-7966.

O'SULLIVAN, M., ZHANG, Z. & VINCENT, B. 2009. Silica-Shell/Oil-Core Microcapsules with Controlled Shell Thickness and Their Breakage Stress. *Langmuir,* 25**,** 7962-7966.

OBEY, T. M. & VINCENT, B. 1994. Novel Monodisperse "Silicone Oil"/Water Emulsions. *Journal of Colloid and Interface Science,* 163**,** 454-463.

PADMAVATHY, N. & VIJAYARAGHAVAN, R. 2008. Enhanced bioactivity of ZnO nanoparticles-an antimicrobial study. *Sci Technol Adv Mater,* 9**,** 035004.

PAN, X. M., MERCADE-PRIETO, R., YORK, D., PREECE, J. A. & ZHANG, Z. B. 2013. Structure and Mechanical Properties of Consumer-Friendly PMMA Microcapsules. *Industrial & Engineering Chemistry Research,* 52**,** 11253-11265.

PANDEY, S., DE KLERK, C., KIM, J., KANG, M. & FOSSO-KANKEU, E. 2020. Eco Friendly Approach for Synthesis, Characterization and Biological Activities of Milk Protein Stabilized Silver Nanoparticles. *Polymers (Basel),* 12.

PARK, K. M., SUNG, H., CHOI, S. J., CHOI, Y. J. & CHANG, P. S. 2014. Double-layered microparticles with enzyme-triggered release for the targeted delivery of water-soluble bioactive compounds to small intestine. *Food Chemistry,* 161**,** 53-59.

PASTINE, S. J., OKAWA, D., ZETTL, A. & FRECHET, J. M. J. 2009. Chemicals On Demand with Phototriggerable Microcapsules. *Journal of the American Chemical Society,* 131**,** 13586-+.

PASTORIZA-SANTOS, I. & LIZ-MARZAN, L. M. 2002. Formation of PVP-protected metal nanoparticles in DMF. *Langmuir,* 18**,** 2888-2894.

PATCHAN, M. W., BAIRD, L. M., RHIM, Y. R., LABARRE, E. D., MAISANO, A. J., DEACON, R. M., XIA, Z. Y. & BENKOSKI, J. J. 2012. Liquid-Filled Metal Microcapsules. *Acs Applied Materials & Interfaces,* 4**,** 2406-2412.

PATIL, V., MALVANKAR, R. B. & SASTRY, M. 1999. Role of Particle Size in Individual and Competitive Diffusion of Carboxylic Acid Derivatized Colloidal Gold Particles in Thermally Evaporated Fatty Amine Films. *Langmuir,* 15**,** 8197-8206.

PENA, B., PANISELLO, C., ARESTE, G., GARCIA-VALLS, R. & GUMI, T. 2012. Preparation and characterization of polysulfone microcapsules for perfume release. *Chemical Engineering Journal,* 179**,** 394-403.

PONCELET, D. & NEUFELD, R. J. 1989. SHEAR BREAKAGE OF NYLON MEMBRANE MICROCAPSULES IN A TURBINE REACTOR. *Biotechnology and Bioengineering,* 33**,** 95-103.

PRINS, W. & HERMANS, J. J. 1959. THEORY OF PERMEATION THROUGH METAL COATED POLYMER FILMS. *Journal of Physical Chemistry,* 63**,** 716-722.

PUTNEY, S. D. & BURKE, P. A. 1998. Improving protein therapeutics with sustained-release formulations. *Nature Biotechnology,* 16**,** 153-157.

QIU, T. & CHU, P. K. 2008. Self-selective electroless plating: An approach for fabrication of functional 1D nanomaterials. *Materials Science and Engineering: R: Reports,* 61**,** 59-77.

RAO, K. B. 2005. *Frontiers in Materials Science*, Universities Press Limited.

RIBEIRO, A. J., NEUFELD, R. J., ARNAUD, P. & CHAUMEIL, J. C. 1999. Microencapsulation of lipophilic drugs in chitosan-coated alginate microspheres. *International Journal of Pharmaceutics,* 187**,** 115-123.

RODRIGUES, S. N., MARTINS, I. M., FERNANDES, I. P., GOMES, P. B., MATA, V. G., BARREIRO, M. F. & RODRIGUES, A. E. 2009. Scentfashion (R): Microencapsulated perfumes for textile application. *Chemical Engineering Journal,* 149**,** 463-472.

SA, F., SM, S., S, S., M, S. & L., N. 2010. Sustained release of verapamil hydrochloride from sodium alginate microcapsules. *Curr Drug Deliv,* 7**,** 98-108.

SAMIMI, A., HASSANPOUR, A. & GHADIRI, A. 2005. Single and bulk compressions of soft granules: Experimental study and DEM evaluation. *Chemical Engineering Science,* 60**,** 3993-4004.

SANEMASA, I., ARAKI, M., DEGUCHI, T. & NAGAI, H. 1982. SOLUBILITY MEASUREMENTS OF BENZENE AND THE ALKYLBENZENES IN WATER BY MAKING USE OF SOLUTE VAPOR. *Bulletin of the Chemical Society of Japan,* 55**,** 1054-1062.

SANSDRAP, P. & MOES, A. J. 1993. INFLUENCE OF MANUFACTURING PARAMETERS ON THE SIZE CHARACTERISTICS AND THE RELEASE PROFILES OF NIFEDIPINE FROM POLY(DL-LACTIDE-CO-GLYCOLIDE) MICROSPHERES. *International Journal of Pharmaceutics,* 98**,** 157-164.

SAU, T. K., PAL, A. & PAL, T. 2001. Size regime dependent catalysis by gold nanoparticles for the reduction of eosin. *Journal of Physical Chemistry B,* 105**,** 9266-9272.

SCHAEFERS, S., RAST, L. & STANISHEVSKY, A. 2006. Electroless silver plating on spin-coated silver nanoparticle seed layers. *Materials Letters,* 60**,** 706-709.

SCHER, H. B., RODSON, M. & LEE, K. S. 1998. Microencapsulation of pesticides by interfacial polymerization utilizing isocyanate or aminoplast chemistry. *Pesticide Science,* 54**,** 394-400.

SCHLESINGER, M. & PAUNOVIC, M. 2011. Electroless deposition of nickel. *Modern Electroplating.* Wiley.

SHI, X. Y. & CARUSO, F. 2001. Release behavior of thin-walled microcapsules composed of polyelectrolyte multilayers. *Langmuir,* 17**,** 2036-2042.

SOMMER, F., DUC, T. M., PIRRI, R., MEUNIER, G. & QUET, C. 1995. SURFACE-MORPHOLOGY OF POLY(BUTYL ACRYLATE) POLY(METHYL METHACRYLATE) CORE-SHELL LATEX BY ATOMIC-FORCE MICROSCOPY. *Langmuir,* 11**,** 440-448.

SONG, H., RIOUX, R. M., HOEFELMEYER, J. D., KOMOR, R., NIESZ, K., GRASS, M., YANG, P. D. & SOMORJAI, G. A. 2006. Hydrothermal

growth of mesoporous SBA-15 silica in the presence of PVP-stabilized Pt nanoparticles: Synthesis, characterization, and catalytic properties. *Journal of the American Chemical Society,* 128**,** 3027-3037.

SPECOS, M. M. M., ESCOBAR, G., MARINO, P., PUGGIA, C., TESORIERO, M. V. D. & HERMIDA, L. 2010. Aroma Finishing of Cotton Fabrics by Means of Microencapsulation Techniques. *Journal of Industrial Textiles,* 40**,** 13-32.

SUKHORUKOV, G. B., ANTIPOV, A. A., VOIGT, A., DONATH, E. & MOHWALD, H. 2001. pH-controlled macromolecule encapsulation in and release from polyelectrolyte multilayer nanocapsules. *Macromolecular Rapid Communications,* 22**,** 44-46.

SUKHORUKOV, G. B., DONATH, E., MOYA, S., SUSHA, A. S., VOIGT, A., HARTMANN, J. & MOHWALD, H. 2000. Microencapsulation by means of step-wise adsorption of polyelectrolytes. *Journal of Microencapsulation,* 17**,** 177-185.

SUN, G. & ZHANG, Z. 2002. Mechanical strength of microcapsules made of different wall materials. *International Journal of Pharmaceutics,* 242**,** 307-311.

SUN, Y. G. & XIA, Y. N. 2004. Mechanistic study on the replacement reaction between silver nanostructures and chloroauric acid in aqueous medium. *Journal of the American Chemical Society,* 126**,** 3892-3901.

TAGUCHI, Y. & TANAKA, M. 2001. Preparation of microcapsules composed of waste-expanded polystyrene and paper fiber by semichemical recycle. *Journal of Applied Polymer Science,* 80**,** 2662-2669.

TARN, D., ASHLEY, C. E., XUE, M., CARNES, E. C., ZINK, J. I. & BRINKER, C. J. 2013. Mesoporous Silica Nanoparticle Nanocarriers: Biofunctionality and Biocompatibility. *Accounts of Chemical Research,* 46**,** 792-801.

TASKER, A. L., HITCHCOCK, J. P., HE, L., BAXTER, E. A., BIGGS, S. & CAYRE, O. J. 2016. The effect of surfactant chain length on the morphology of poly(methyl methacrylate) microcapsules for fragrance oil encapsulation. *Journal of Colloid and Interface Science,* 484**,** 10-16.

TEFFT, J. & FRIEND, D. R. 1993. Controlled release herbicide formulations based on polymeric microspheres. *Journal of Controlled Release,* 27**,** 27-35.

THOMAS, J. M. & THOMAS, W. J. 1997. *Principles and Practice of Heterogeneous Catalysis*, Wiley.

TIARKS, F., LANDFESTER, K. & ANTONIETTI, M. 2001. Preparation of polymeric nanocapsules by miniemulsion polymerization. *Langmuir,* 17**,** 908-918.

TIERNO, P. & GOEDEL, W. A. 2006. Using electroless deposition for the preparation of micron sized polymer/metal core/shell particles and hollow metal spheres. *Journal of Physical Chemistry B,* 110**,** 3043-3050.

TORZA, S. & MASON, S. G. 1970. Three-phase interactions in shear and electrical fields. *Journal of Colloid and Interface Science,* 33**,** 67-83.

TSUJI, K. 2001. Microencapsulation of pesticides and their improved handling safety. *Journal of Microencapsulation,* 18**,** 137-147.

TURKEVICH, J., STEVENSON, P. C. & HILLIER, J. 1951. A STUDY OF THE NUCLEATION AND GROWTH PROCESSES IN THE SYNTHESIS OF COLLOIDAL GOLD. *Discussions of the Faraday Society***,** 55-&.

VAKELIS, A. 2006. Electroless plating. *In:* TRACTON, A. A. (ed.) *Coatings Technology Handbook.* 3rd ed. Boca Raton: Taylor & Francis.

VAN RAAMSDONK, J. M. & CHANG, P. L. 2001. Osmotic pressure test: A simple, quantitative method to assess the mechanical stability of alginate microcapsules. *Journal of Biomedical Materials Research,* 54**,** 264-271.

VOLODKIN, D. V., MADABOOSI, N., BLACKLOCK, J., SKIRTACH, A. G. & MOHWALD, H. 2009. Surface-Supported Multilayers Decorated with Bio-active Material Aimed at Light-Triggered Drug Delivery. *Langmuir,* 25**,** 14037-14043.

WAGNER, J., TSHIKHUDO, T. R. & KOEHLER, J. M. 2008. Microfluidic generation of metal nanoparticles by borohydride reduction. *Chemical Engineering Journal,* 135**,** S104-S109.

WANG, W., JIANG, Y., LIAO, Y., TIAN, M., ZOU, H. & ZHANG, L. 2011. Fabrication of silver-coated silica microspheres through mussel-inspired surface functionalization. *Journal of Colloid and Interface Science,* 358**,** 567-574.

WANG, X. J., FENG, Y., QIAN, G., ZHANG, J. C., ZHANG, Q. & DING, F. 2014. A new core-shell Ti3AlC2/Cu composite powder prepared by electroless plating method. *Surface & Coatings Technology,* 240**,** 261-268.

WANG, Z. F., WANG, B., QI, N., ZHANG, H. F. & ZHANG, L. Q. 2005. Influence of fillers on free volume and gas barrier properties in styrene-butadiene rubber studied by positrons. *Polymer,* 46**,** 719-724.

WANG, Z. S., CUI, Y., DAN-OH, Y., KASADA, C., SHINPO, A. & HARA, K. 2008. Molecular Design of Coumarin Dyes for Stable and Efficient Organic Dye-Sensitized Solar Cells. *Journal of Physical Chemistry C,* 112**,** 17011-17017.

WEXLER, P. 2014. *Encyclopedia of Toxicology*, Elsevier Science.

WEXLER, P., ANDERSON, B., DE PEYSTER, A., GAD, S. C., HAKKINEN, P. J. B., KAMRIN, M., LOCEY, B., MEHENDALE, H. M., POPE, C. & SHUGART, L. 2005. *Encyclopedia of Toxicology*, Elsevier Science.

WISCHKE, C. & SCHWENDEMAN, S. P. 2008. Principles of encapsulating hydrophobic drugs in PLA/PLGA microparticles. *International Journal of Pharmaceutics,* 364**,** 298-327.

WONG, M. S., CHA, J. N., CHOI, K. S., DEMING, T. J. & STUCKY, G. D. 2002. Assembly of nanoparticles into hollow spheres using block copolypeptides. *Nano Letters,* 2**,** 583-587.

WU, Z., GE, S., ZHANG, M., LI, W. & TAO, K. 2009a. Synthesis of nickel nanoparticles supported on metal oxides using electroless plating: Controlling the dispersion and size of nickel nanoparticles. *Journal of Colloid and Interface Science,* 330**,** 359-366.

WU, Z. J., GE, S. H., ZHANG, M. H., LI, W. & TAO, K. Y. 2009b. Synthesis of nickel nanoparticles supported on metal oxides using electroless plating: Controlling the dispersion and size of nickel nanoparticles. *Journal of Colloid and Interface Science,* 330**,** 359-366.

YAN, H., XU, N., HUANG, W. Y., HAN, H. M. & XIAO, S. J. 2009. Electroless plating of silver nanoparticles on porous silicon for laser desorption/ionization mass spectrometry. *International Journal of Mass Spectrometry,* 281**,** 1-7.

YANG, Y. Y., CHIA, H. H. & CHUNG, T. S. 2000a. Effect of preparation temperature on the characteristics and release profiles of PLGA microspheres containing protein fabricated by double-emulsion solvent extraction/evaporation method. *Journal of Controlled Release,* 69**,** 81-96.

YANG, Y. Y., CHUNG, T. S., BAI, X. L. & CHAN, W. K. 2000b. Effect of preparation conditions on morphology and release profiles of biodegradable polymeric microspheres containing protein fabricated by double-emulsion method. *Chemical Engineering Science,* 55**,** 2223-2236.

YAP, S. F., ADAMS, M. J., SEVILLE, J. P. K. & ZHANG, Z. B. 2008. Single and bulk compression of pharmaceutical excipients: Evaluation of mechanical properties. *Powder Technology,* 185**,** 1-10.

YE, X. Y., ZHOU, Y. M., CHEN, J., SUN, Y. Q. & WANG, Z. Q. 2008. Coating of ZnO nanorods with nanosized silver particles by electroless plating process. *Materials Letters,* 62**,** 666-669.

YEO, Y., BELLAS, E., FIRESTONE, W., LANGER, R. & KOHANE, D. S. 2005. Complex coacervates for thermally sensitive controlled release of flavor compounds. *Journal of Agricultural and Food Chemistry,* 53**,** 7518-7525.

YOSHIDA, M., MATSUI, T., UEMURA, Y. & HATATE, Y. 2004. Electroselective permeability control of microcapsule immobilized ferroelectric liquid crystals in an external electrical field. *Journal of Chemical Engineering of Japan,* 37**,** 592-596.

YOSHIDA, M., MORI, T., MATSUI, T., UEMURA, Y. & HATATE, Y. 2002. Electro-sensitive microcapsule immobilized ferroelectric liquid crystal. *Journal of Chemical Engineering of Japan,* 35**,** 398-400.

YOW, H. N. & ROUTH, A. F. 2006. Formation of liquid core-polymer shell microcapsules. *Soft Matter,* 2**,** 940-949.

YUAN, L., LIANG, G. Z., XIE, J. Q., LI, L. & GUO, J. 2006. Preparation and characterization of poly(urea-formaldehyde) microcapsules filled with epoxy resins. *Polymer,* 47**,** 5338-5349.

ZHANG, C., LING, G. P. & HE, J. H. 2004. Co–Al2O3 nanocomposites powder prepared by electroless plating. *Materials Letters,* 58**,** 200-204.

ZHANG, G. H., BON, S. A. F. & ZHAO, C. Y. 2012. Synthesis, characterization and thermal properties of novel nanoencapsulated phase change materials for thermal energy storage. *Solar Energy,* 86**,** 1149-1154.

ZHANG, J. H., LIU, H. Y., WANG, Z. L. & MING, N. B. 2007. Preparation and optical properties of silica@Ag-Cu alloy core-shell composite colloids. *Journal of Solid State Chemistry,* 180**,** 1291-1297.

ZHANG, Z., SAUNDERS, R. & THOMAS, C. R. 1999. Mechanical strength of single microcapsules determined by a novel micromanipulation technique. *Journal of Microencapsulation,* 16**,** 117-124.

ZHANG, Z., STENSON, J. D. & THOMAS, C. R. 2009. Micromanipulation in Mechanical Characterisation of Single Particles. *Characterization of Flow, Particles and Interfaces,* 37**,** 29-85.

ZHAO, C. Y. & ZHANG, G. H. 2011. Review on microencapsulated phase change materials (MEPCMs): Fabrication, characterization and applications. *Renewable & Sustainable Energy Reviews,* 15**,** 3813-3832.

ZHAO, Y. J., SHUM, H. C., ADAMS, L. L. A., SUN, B. J., HOLTZE, C., GU, Z. Z. & WEITZ, D. A. 2011. Enhanced Encapsulation of Actives in Self-

Sealing Microcapsules by Precipitation in Capsule Shells. *Langmuir,* 27**,** 13988-13991.

ZHU, G. Z., MALLERY, S. R. & SCHWENDEMAN, S. P. 2000. Stabilization of proteins encapsulated in injectable poly (lactide-co-glycolide). *Nature Biotechnology,* 18**,** 52-57.

ZHU, S. L., TANG, L., CUI, Z. D., WEI, Q. & YANG, X. J. 2011. Preparation of copper-coated β-SiC nanoparticles by electroless plating. *Surface and Coatings Technology,* 205**,** 2985-2988.

ZIMBONE, M., CALCAGNO, L., MESSINA, G., BAERI, P. & COMPAGNINI, G. 2011. Dynamic light scattering and UV–vis spectroscopy of gold nanoparticles solution. *Materials Letters,* 65**,** 2906-2909.

ZUBER, A., PURDEY, M., SCHARTNER, E., FORBES, C., VAN DER HOEK, B., GILES, D., ABELL, A., MONRO, T. & EBENDORFF-HEIDEPRIEM, H. 2016. Detection of gold nanoparticles with different sizes using absorption and fluorescence based method. *Sensors and Actuators B: Chemical,* 227**,** 117-127.

ZYDOWICZ, N., NZIMBA-GANYANAD, E. & ZYDOWICZ, N. 2002. PMMA microcapsules containing water-soluble dyes obtained by double emulsion/solvent evaporation technique. *Polymer Bulletin,* 47**,** 457-463.